

University of Windsor

Scholarship at UWindor

Electronic Theses and Dissertations

Theses, Dissertations, and Major Papers

2002

Development of in-process engine defect detection methods using NVH indicators.

Eric R. Leitzinger
University of Windsor

Follow this and additional works at: <https://scholar.uwindsor.ca/etd>

Recommended Citation

Leitzinger, Eric R., "Development of in-process engine defect detection methods using NVH indicators." (2002). *Electronic Theses and Dissertations*. 1713.
<https://scholar.uwindsor.ca/etd/1713>

This online database contains the full-text of PhD dissertations and Masters' theses of University of Windsor students from 1954 forward. These documents are made available for personal study and research purposes only, in accordance with the Canadian Copyright Act and the Creative Commons license—CC BY-NC-ND (Attribution, Non-Commercial, No Derivative Works). Under this license, works must always be attributed to the copyright holder (original author), cannot be used for any commercial purposes, and may not be altered. Any other use would require the permission of the copyright holder. Students may inquire about withdrawing their dissertation and/or thesis from this database. For additional inquiries, please contact the repository administrator via email (scholarship@uwindsor.ca) or by telephone at 519-253-3000ext. 3208.

INFORMATION TO USERS

This manuscript has been reproduced from the microfilm master. UMI films the text directly from the original or copy submitted. Thus, some thesis and dissertation copies are in typewriter face, while others may be from any type of computer printer.

The quality of this reproduction is dependent upon the quality of the copy submitted. Broken or indistinct print, colored or poor quality illustrations and photographs, print bleedthrough, substandard margins, and improper alignment can adversely affect reproduction.

In the unlikely event that the author did not send UMI a complete manuscript and there are missing pages, these will be noted. Also, if unauthorized copyright material had to be removed, a note will indicate the deletion.

Oversize materials (e.g., maps, drawings, charts) are reproduced by sectioning the original, beginning at the upper left-hand corner and continuing from left to right in equal sections with small overlaps.

**ProQuest Information and Learning
300 North Zeeb Road, Ann Arbor, MI 48106-1346 USA
800-521-0600**

UMI[®]

**DEVELOPMENT OF IN-PROCESS ENGINE DEFECT DETECTION METHODS
USING NVH INDICATORS**

by

ERIC R. LEITZINGER

**A Thesis
Submitted to the Faculty of Graduate Studies and Research
through the Department of Mechanical, Automotive and Materials Engineering
in Partial Fulfillment of the Requirements for
the Degree of Master of Applied Science at the
University of Windsor**

**Windsor, Ontario, Canada
2002**



**National Library
of Canada**

**Acquisitions and
Bibliographic Services**

**395 Wellington Street
Ottawa ON K1A 0N4
Canada**

**Bibliothèque nationale
du Canada**

**Acquisitions et
services bibliographiques**

**395, rue Wellington
Ottawa ON K1A 0N4
Canada**

Your file Votre référence

Our file Notre référence

The author has granted a non-exclusive licence allowing the National Library of Canada to reproduce, loan, distribute or sell copies of this thesis in microform, paper or electronic formats.

The author retains ownership of the copyright in this thesis. Neither the thesis nor substantial extracts from it may be printed or otherwise reproduced without the author's permission.

L'auteur a accordé une licence non exclusive permettant à la Bibliothèque nationale du Canada de reproduire, prêter, distribuer ou vendre des copies de cette thèse sous la forme de microfiche/film, de reproduction sur papier ou sur format électronique.

L'auteur conserve la propriété du droit d'auteur qui protège cette thèse. Ni la thèse ni des extraits substantiels de celle-ci ne doivent être imprimés ou autrement reproduits sans son autorisation.

0-612-75841-9

Canada

© ERIC R. LEITZINGER 2002

ABSTRACT

This study was undertaken to investigate and develop engine defect detection methods using NVH indicators for future implementation into an on-line test system in a production environment. These methods utilized noise and vibration measurements collected from a variety of transducers to successfully detect lower-end engine defects.

The on-line experimental testing of 5.4L V8 engines was conducted at one of the in-process Cold Test stations at the Ford Windsor Engine Plant. Transducers used included accelerometers, microphones, knock sensors and a laser vibrometer. The optimal measurement locations were found to be at each of the 4 locating lugs of the engine.

Baseline measurements were made and based upon these results, control limits were established regarding the acceptable noise and vibration levels an engine can exhibit. A fault diagnosis algorithm that utilized variance analysis and RMS values was developed to detect lower-end engine defects.

The algorithm was successful in identifying defect-free engines as well as detecting lower-end faults such as a non-machined cylinder bore, a cylinder bore containing a deep groove and connecting rod knock.

The transducers found to be most effective in detecting noise and vibration were the accelerometer and the laser vibrometer. The knock sensor and microphone were found to be inconsistent in their ability to detect noise and vibration.

Therefore, it was concluded that the development of an on-line test system that can successfully diagnose engine defects through the use of NVH indicators is feasible and would ultimately reduce the number of defective engines being produced.

DEDICATION

This work is dedicated to my parents, who have always provided me with the love and support necessary to achieve all that I am capable of and to my wife, Jennifer, who is and will always be the inspiration for all that I do in life.

ACKNOWLEDGEMENTS

The author of this thesis would like to express his thanks to Dr. Jimi Tjong and the many members of the Ford Powertrain Research and Development group for their time, assistance and support through the course of this study.

Special thanks go to the Dynamometer Test Analysts and the Major Repair Technicians from the Windsor Engine Plant for their cooperation, knowledgeable insight and technical assistance in conducting all of the engine testing required to complete this study.

The author would also like to extend special thanks to all those who have made a much-appreciated contribution to this project.

TABLE OF CONTENTS

ABSTRACT.....	iv
DEDICATION.....	v
ACKNOWLEDGEMENTS.....	vi
LIST OF TABLES.....	xi
LIST OF FIGURES.....	xii
NOMENCLATURE.....	xvii
CHAPTER 1. INTRODUCTION.....	1
CHAPTER 2. LITERATURE SURVEY.....	4
2.1 Detection Methods and Techniques.....	4
2.1.1 Noise.....	5
2.1.2 Vibration.....	6
2.1.3 Signal Types for Diagnostic Systems.....	7
2.1.4 Transducers.....	8
2.1.4.1 Noise.....	8
2.1.4.2 Vibration.....	8
2.1.5 Data Acquisition Methods.....	9
2.1.5.1 Measurement Location.....	9
2.1.5.2 Operating Conditions.....	10
2.1.5.3 Transducer Selection.....	11
2.2 Data Processing Techniques.....	11
2.2.1 Angle (Position) Domain Signal Analysis.....	12
2.2.2 Time Domain Signal Analysis.....	13
2.2.3 Frequency Domain Signal Analysis.....	14
2.2.3.1 Order Tracking Analysis.....	14
2.2.3.2 Wavelet Analysis.....	15
2.2.4 Acoustic Analysis.....	15
2.2.5 Finite Element Analysis.....	16
2.3 Engine Defect Diagnostics.....	16
2.3.1 Pattern Recognition.....	17
2.3.2 Piston Slap.....	18
2.3.3 Combustion Noise and Vibration.....	19
2.3.4 Valve Train Noise.....	19
2.3.5 Vibration due to Non-cleanup of Cylinder Bores.....	20
2.3.6 Engine Balance.....	20
2.3.7 Overall Engine Sound Quality.....	21

CHAPTER 3. THEORY	22
3.1 Digital Signal Processing.....	22
3.1.1 Analog to Digital Conversion	22
3.1.1.1 Sampling	23
3.1.1.2 Aliasing	24
3.1.1.3 Quantization.....	25
3.1.1.4 Leakage	26
3.1.1.5 Windowing.....	27
3.2 Internal Combustion Engine Theory.....	30
3.2.1 4-Stroke Engine Cycle	30
3.2.2 Engine Operation Fundamentals.....	32
3.2.2.1 Geometrical Properties.....	32
3.2.2.2 Piston Kinematics	33
3.3 Forced Vibration	34
3.4 Noise	36
3.5 Accelerometers.....	37
3.5.1 Piezoelectric Accelerometers	37
3.5.1.1 Piezoelectric Accelerometer Designs.....	38
3.5.1.2 Charge Mode Accelerometers.....	39
3.5.1.3 Internally Amplified Accelerometers.....	39
3.6 Microphones	40
3.6.1 Normal Incidence Microphones.....	40
3.6.2 Random Incidence Microphones	40
3.6.3 Microphone Designs	41
3.6.3.1 Condenser Microphones	41
3.6.3.2 Ceramic-Cartridge Microphones.....	41
3.7 Laser Vibrometers.....	42
3.7.1 Laser Interferometry Measurement Principle.....	42
3.7.2 Laser Doppler Vibrometer Principle of Operation.....	44
 CHAPTER 4. EXPERIMENTAL DETAILS	 46
4.1 Dynamometer Engine Testing.....	47
4.1.1 Dynamometer Test Cell	47
4.1.1.1 Eddy Current Dynamometer	49
4.1.1.2 Data Acquisition System for Operating Parameters	50
4.2 On-line Engine Testing	50
4.2.1 Cold Test.....	51
4.2.1.1 Cold Test Transducer Location.....	52
4.3 Data Acquisition System for NVH Measurements.....	53
4.4 Transducers and Accessories	54
4.4.1 Electro Corporation 58413 Digital-Magnetic Pickup.....	54
4.4.2 Bruel & Kjaer Type 4366 Accelerometer	55
4.4.3 PCB Model 462A Charge Amplifier'	55

4.4.4	PCB Model 359B15 Accelerometer	55
4.4.5	PCB Model 480E09 Sensor Signal Conditioner.....	56
4.4.6	Bruel & Kjaer Type 4294 Calibration Exciter	56
4.4.7	Polytec Laser Vibrometer IVS 200.....	56
4.4.8	TMS Type 130C10 Microphone and Type 130P10 Preamplifier.....	57
4.4.9	Bosch Knock Sensor.....	57
4.4.10	Tektronix Type 2232 Digital Storage Oscilloscope.....	57
 CHAPTER 5. DATA ANALYSIS METHODS		58
5.1	Raw Time/Position Trace Analysis.....	59
5.2	Position/Time Domain Averaging	61
5.3	Variance Analysis	62
5.4	Statistical Indicators.....	65
5.4.1	Mean	65
5.4.2	Standard Deviation.....	66
5.4.3	Root Mean Squared (RMS)	66
5.4.4	RMS Comparison Ratio (CR).....	67
5.5	Frequency Domain Analysis.....	67
5.5.1	Fourier Transform	68
5.5.2	Discrete Fourier Transform.....	69
5.5.3	Fast Fourier Transform	69
5.5.4	Auto Power Spectrum	70
5.5.5	Order Analysis	71
5.6	Mahalanobis-Taguchi System.....	72
 CHAPTER 6. RESULTS AND DISCUSSION.....		74
6.1	Cold Test Transducer Feasibility	74
6.1.1	Accelerometers.....	75
6.1.2	Laser Vibrometer	76
6.1.3	Microphones	78
6.1.4	Pressure Transducers.....	79
6.1.5	Knock Sensor	81
6.1.6	Transducer Locations.....	81
6.2	Triggering Method Validity and Data Positioning.....	82
6.3	Baseline Measurement Results	86
6.3.1	Mahalanobis Distance	86
6.3.2	RMS Comparison Ratio (CR) Results	90
6.4	Fault Diagnosis Using NVH Attributes	91
6.4.1	Variance Signature Analysis.....	93
6.4.2	RMS, CR Threshold Levels.....	94
6.5	Cold Test Fault Diagnosis Results.....	95
6.5.1	Detection of a Non-machined Cylinder Bore.....	96

6.5.2	Detection of a Deep Groove in a Cylinder Bore.....	101
6.5.3	Detection of Connecting Rod Knock.....	107
6.5.4	Detection of Abnormal Engine Noise.....	114
6.5.5	Cold Test Fault Diagnosis Summary.....	118
CHAPTER 7. CONCLUSIONS & RECOMMENDATIONS.....		119
7.1	Conclusions.....	119
7.2	Recommendations.....	120
REFERENCES		122
APPENDICES		126
A.	FAULT DIAGNOSIS FLOWCHART.....	127
B.	EXPERIMENTAL EQUIPMENT SPECIFICATIONS.....	130
C.	MAHALANOBIS DISTANCE METHOD.....	135
VITA AUCTORIS		140

LIST OF TABLES

Table 6.1	Matrix of observations (channel RMS values) for each baseline engine.....	87
Table 6.2	Performance matrix of cylinder non-cleanup detection.....	101
Table 6.3	Performance matrix of deep groove in cylinder detection.....	107
Table 6.4	Performance matrix of connecting rod knock detection.....	114
Table 6.5	Performance matrix of defect detection of engine with reported abnormal noise.....	117
Table 6.6	Overall performance matrix of engine defect detection using NVH indicators... 	118
Table C.1	Original matrix of RMS values.....	136
Table C.2	Standardized matrix [Z].....	136
Table C.3	Correlation matrix [R].....	137
Table C.4	Inverse of the correlation matrix [A].....	137
Table C.5	Standardized matrix [Z] multiplied by inverse of the correlation matrix [A].....	138
Table C.6	Mahalanobis Distances calculated for each of the 30 test engines.....	139

LIST OF FIGURES

Figure 3.1	Difference between proper and improper sampling of a signal [38]	24
Figure 3.2	Example of a low-pass filter showing cutoff and maximum frequency	25
Figure 3.3	Illustrating the concept of quantization of a 4-bit ADC	26
Figure 3.4	Example of leakage over many frequency bins due to non-periodicity of the signal [38].....	27
Figure 3.5	Example of windowing on a non-periodic signal [38]	28
Figure 3.6	Comparison of windowing functions in terms of amplitude and frequency resolution [38]	29
Figure 3.7	Diagram representing the principle of laser interferometry [42].....	43
Figure 3.8	System layout of a laser Doppler vibrometer [42].....	44
Figure 4.1	A top-view schematic diagram of a complete dynamometer test cell.....	48
Figure 4.2	An eddy current dynamometer located behind the NVH test cell	49
Figure 4.3	Cold Test station to be used in the study	51
Figure 4.4	Optimal transducer locations for accelerometer mounting at cold test station.....	53
Figure 5.1	Raw position-based vibration trace collected for 38 engine cycles taken from an accelerometer mounted on the outer cylinder block wall of an engine with a cold knock (piston slap).....	60
Figure 5.2	The same raw position-based vibration trace arranged in 3-D waterfall format for 38 cycles of data. Notice that the spike stands-out over the entire range of engine cycles of data acquired.....	60

Figure 5.3	Averaging of the same raw position-based data over a large number of cycles. The vibration spikes are emphasized and can be linked to specific locations in the engine cycle.....	62
Figure 5.4	Waterfall plot of running variance for 38 cycles of data. The semi-periodic component is easily seen in the figure.....	64
Figure 5.5	Overall variance plot of position-based data. Four spikes are identifiable.....	64
Figure 5.6	An auto power spectrum of block vibration from a "good" engine. There are 3 noticeable frequency components.....	71
Figure 6.1	Accelerometer vibration signal captured from the valley area of a cast iron cylinder block in the detection of a non-machined cylinder bore surface.....	75
Figure 6.2	Accelerometer vibration signal captured from a cam cover bolt head on a 4.6L 4-valve engine to detect a gross valve tick.....	76
Figure 6.3	Laser vibration variance signal captured from the left front locating lug at cold test while detecting a non-machined cylinder bore	77
Figure 6.4	Comparison of noise measurements between engine and plant noise.....	78
Figure 6.5	Vibration signal captured from the knock sensor at cold test.....	81
Figure 6.6	Transducer setup used at cold test as seen from the top view of the engine	82
Figure 6.7	Camshaft identification signal acquired from CID sensor.....	83
Figure 6.8	Comparison of the CID and CPS signals relative positions over one engine cycle.....	84
Figure 6.9	Vibration signature from external triggering method.....	85
Figure 6.10	Vibration signature from adaptive re-sampling method.....	85
Figure 6.11	MD for each of 30 engines tested as part of the baseline "good" group.....	88

Figure 6.12	RMS acceleration values for each transducer for each of 30 baseline engines tested.....	89
Figure 6.13	RMS Comparison Ratio for each of 30 baseline engines tested.....	90
Figure 6.14	An average raw data trace captured by an accelerometer from the lug of a good engine	92
Figure 6.15	An average raw data trace captured by an accelerometer from the lug of a defective engine.....	92
Figure 6.16	Fault diagnosis method that includes 90° bands of data, relative amplitude values and distance between band maximum values	94
Figure 6.17	A 40-cycle average of raw data captured by an accelerometer from the #3 lug.....	97
Figure 6.18	A 40-cycle average of variance data captured by the laser from the #3 lug.....	98
Figure 6.19	A 40-cycle averaged overall level captured by a microphone in the area of the #3 lug.....	98
Figure 6.20	A 40-cycle average of raw data captured by the knock sensor in attempt to detect the non-cleanup of cylinder bore #6	99
Figure 6.21	Diagnosis results from analysis of accelerometer data.....	100
Figure 6.22	Defect report of diagnosis results	100
Figure 6.23	A 40-cycle average of variance data captured by an accelerometer from the #1 lug.....	102
Figure 6.24	A 40-cycle average of variance data captured by an accelerometer from the #4 lug.....	102

Figure 6.25	Waterfall plot for 40-cycles of raw data as collected by the laser vibrometer from lug #1	103
Figure 6.26	Auto-power spectrum of noise data collected from lug #1 of engine with deep groove in cylinder #1 and #8 (frequency shown in orders).....	104
Figure 6.27	Auto-power spectrum of noise data collected from lug #1 of defect-free engine (frequency shown in orders)	104
Figure 6.28	A 40-cycle average of raw data captured by the knock sensor in attempt to detect the deep grooves in cylinder #1 and #8.....	105
Figure 6.29	Diagnosis results from analysis of accelerometer data.....	106
Figure 6.30	Defect reports of diagnosis results.....	106
Figure 6.31	A 40-cycle average of raw data captured by an accelerometer from the #1 lug.....	108
Figure 6.32	A 40-cycle waterfall plot of variance data captured by an accelerometer from the #1 lug	108
Figure 6.33	A 40-cycle average of raw data captured by an accelerometer from the #3 lug.....	109
Figure 6.34	A 40-cycle waterfall plot of variance data captured by an accelerometer from the #3 lug	109
Figure 6.35	An averaged overall level of raw data captured by a microphone from the area of lug #1	111
Figure 6.36	An averaged overall level of raw data captured by a microphone from the area of lug #3	112

Figure 6.37	A 40-cycle average of raw data captured by the laser vibrometer from the #3 lug.....	112
Figure 6.38	A 40-cycle average of raw data captured by the knock sensor.....	113
Figure 6.39	Diagnosis results from analysis of accelerometer data.....	113
Figure 6.40	Defect reports of diagnosis results.....	114
Figure 6.41	A 40-cycle average of raw data captured by an accelerometer from the #1 lug.....	115
Figure 6.42	Auto-power spectrum of noise data collected from lug #1 of engine with reported noise	116
Figure 6.43	Diagnosis results from analysis of accelerometer data.....	117
Figure A.1	Flow chart showing the fault diagnosis methodology used by the algorithm..	128
Figure B.1	Specifications for the Electro Corporation Type 58413 Digital-Magnetic Pickup.....	131
Figure B.2	Specifications for the Bruel & Kjaer Type 4366 Charge Mode Accelerometer	131
Figure B.3	Specifications for the PCB Model 462A Charge Amplifier	132
Figure B.4	Specifications for the Bruel & Kjaer Type 4294 Calibration Exciter.....	132
Figure B.5	Specifications for the PCB Model 359B15 Accelerometer	133
Figure B.6	Specifications for the PCB Model 480E09 Signal Conditioner.....	133
Figure B.7	Specifications for the Polytec Model IVS 200 Laser Doppler Vibrometer	134
Figure B.8	Specifications for the TMS Type 130C10 Microphone.....	134
Figure B.9	Specifications for the Bosch Knock Sensor.....	134

NOMENCLATURE

a	Crankshaft Radius
A	Piston Acceleration
ADC	Analog to Digital Converter
B	Cylinder Bore Diameter
BDC	Bottom Dead Center
CID	Camshaft Identification
CPS	Crankshaft Position Sensor
CR	RMS Comparison Ratio
dB	Decibel
DFT	Discrete Fourier Transform
FFT	Fast Fourier Transform
F_s	Sampling Frequency
f_{max}	Maximum frequency of signal
f_0	Doppler Frequency
i	Sample Index
ICP	Integrated Circuit Piezoelectric
IVS	Industrial Vibration Sensor
j	Cycle Index
l	Connecting Rod Length
L_p	Sound Pressure Level
MD	Mahalanobis Distance
MTS	Mahalanobis Taguchi System
N	Number of Cycles
NCU	Non-cleanup
NVH	Noise, Vibration, Harshness
o	Frequency Order
r_c	Compression Ratio
R	Number of revolutions
RMS	Root Mean Squared
RV	Running Variance
s	Distance between piston pin and crankshaft axis
S	Samples per Cycle
SN	Signal-to-Noise Ratio
TDC	Top Dead Center
V	Piston Velocity
V_c	Clearance Volume
V_d	Displaced (Swept) Volume
\bar{x}	Mean value
y	Location of the piston from TDC
Y_0	Distance from top of block deck to top of piston at TDC
θ	Crankshaft Angle
σ	Standard Deviation

CHAPTER 1.

INTRODUCTION

It is a widely recognized fact that in a production environment, in-process testing of products is far more valuable and efficient than testing of the products upon completion of their assembly. For this reason, a leading automotive engine manufacturing plant relies on this testing procedure to ensure that engines being built are of the best possible quality. By building products with excellent quality, customer satisfaction is increased, which leads to greater sales, a better reputation and a greater profit for the company.

On-line testing is very useful and beneficial when used on an assembly line. By subjecting an engine to rigorous tests at each stage of its assembly life, defects can be detected early on in the process, resulting in a reduction in downtime and repair costs that would be incurred if it were to be disassembled after complete assembly.

Currently, the purpose of on-line testing used in industry is to ensure proper machining of the engine components, assembly of the engine and integrity of all electrical components included on the engine. The testing that is performed on each engine includes monitoring of parameters such as torque, oil/water cavity leak rates, cylinder pressure, crankshaft balance, fuel rail pressure, integrity of the engine harness and all sensors, as well as proper functionality of the electronic control module. As can be seen, there are no on-line tests being performed that monitor engine noise or vibration. In many cases, engines are installed in vehicles and later returned due to excessive noise or vibration from the engine. As well, there are many possible defects that cause noise and vibration in an

engine that cannot be detected by the current testing methods. Thus, it is apparent that there is a need for an on-line detection system that will monitor noise and vibration in order to improve the quality of engines being built and installed in vehicles.

One of the main goals of this study is to investigate the engine diagnostic methods that have previously been used in industry and to use the basis of these methods to develop new techniques for engine fault detection and diagnostics. The techniques under investigation utilize the measurement of engine noise and vibration as the main indicators of overall engine condition and quality. Not only will the measurements allow for detection of faulty engines but will also have the capability to diagnose which component(s) are defective and in turn reduce the amount of time and effort required to manually detect the defect.

There are many applications in industry where noise and vibration measurements are being used for fault detection. However, the majority of these applications involve monitoring of rotating components that have repetitive signals and are generally periodic. Certain analysis techniques such as spectral analysis and time-domain averaging require that the data under consideration is somewhat periodic. For this reason, it is difficult to use standard techniques to analyze measurements from internal combustion engines because these signals have both some periodic components as well as random components that are generated by such items as friction and impact of mechanical components in the engine. As a result, more effective techniques are required in order to better analyze noise and vibration measurements and to more reliably detect engine defects.

The objective of this study is to develop engine defect detection methods using NVH indicators that will assist in reducing the number of defective engines being produced by an automotive engine production facility through the future implementation of an on-line NVH test station that will use these methods to monitor engine condition. In order to successfully meet the objective of this study, there are a number of goals that have to be met and they are:

- 1. To select appropriate transducers for the on-line detection of lower-end engine noise and vibration.**
- 2. To determine optimal measurement locations that exhibit good noise and vibration response characteristics.**
- 3. To use a current on-line test station that allows for additional transducers to be installed and has the capability to drive an engine at an acceptable speed in order to acquire NVH signals.**
- 4. To collect a sufficient amount of data from both normal and abnormal engines and to use a variety of analysis methods to determine which are feasible choices for the detection of the engine defects under consideration.**
- 5. To develop a fault diagnosis algorithm that can successfully diagnose lower-end engine defects using NVH signature analysis.**

CHAPTER 2.

LITERATURE SURVEY

This chapter describes the literature survey that was conducted in the area of noise and vibration fault detection of internal combustion engines in a production environment. A review of basic noise and vibration detection methods is presented, followed by a summary of the various data processing techniques that have been or are currently used in industry, as well as a description of the possible engine defects that can be detected by analyzing an engines noise and vibration signals. Lastly, a summary of the engine fault detection methods that were researched is presented.

2.1 Detection Methods and Techniques

The main objective of this project is to develop engine defect detection methods for a future on-line engine fault detection system using noise and vibration as the primary indicators. This includes determining optimal measurement locations on the engine, usage of the correct transducers and proper mounting of the transducers onto the engine. Tjong [47] used noise and vibration as indicators for engine dynamic signal monitoring and diagnostics. Hulls and Welch [31] describe various diagnostic procedures that should be followed when attempting to detect faults using noise and vibration analysis. In order for the defect detection system to be effective and reliable, the following guidelines should be followed:

1. Ensure the most efficient data acquisition system is in use with the optimal measurement locations and transducers.
2. Apply data processing techniques that will allow for useful representation of the data.
3. Develop algorithms to automate the on-line diagnostics of engine defects.

The goal of this study is to automate the on-line detection of engine faults using noise and vibration analysis and to have this system incorporated into an operational cold test station that will allow for additional transducers to be used in conjunction with the current equipment. Goetz and Meier [27] used a production hot test for engine diagnostic purposes.

2.1.1 Noise

Engine noise is an auditory phenomena that results from the impact of moving mechanical components occurring within an engine or from combustion that occurs due to a chemical reaction occurring within the combustion chamber of an engine.

The condition of an engine can be determined using noise as an indicator. This can be accomplished by positioning microphones at desired locations around the engine. In many cases, it is possible to determine the condition of an engine by analyzing data from a single measurement taken on an engine. Jonuscheit [35] used two over-head microphones to measure the sound pressure of engines in a production environment.

An advantage of using microphones over other conventional contact devices is that they provide non-contact measurements. This is beneficial in maintaining consistent

measurements, increasing the life of the transducer and avoiding any contribution by the transducer to the engine noise.

In general, noise measurements are quite easy to take as long as they are acquired under the proper operating conditions and in a suitable environment. However, in order to capture reliable noise signals in a production environment without the effects of factory noise, it may be required that the engine is enclosed in a chamber that will attenuate the unwanted noise signals. These are issues that will be investigated throughout the course of the project.

2.1.2 Vibration

Engine vibration is a phenomena that results from mechanical impacts occurring within an engine that cause the resulting components to displace due to the nature of the impacts.

Vibration measurements are very useful because they can provide relevant information about specific components of an engine. Moreover, there are no special enclosures that are needed for an engine in a production environment in order to take vibration measurements because transducers are mounted directly onto the engine and the vibration is directly related to mechanical operations within the engine. Ben-Ari et al [8] monitored the vibration levels of a 4-cylinder engine operating with various faults to observe the effect each had on the vibration of the engine.

2.1.3 Signal Types for Diagnostic Systems

The two basic divisions into which it is useful to classify signals that can be used in automatic diagnostic systems are steady state and time varying signals, as described by Hulls and Welch [31]. Steady state signals can be represented by a single value, such as the RMS value of a vibration waveform. A time varying signal, on the other hand, supplies information by indicating the instantaneous value of the variable as a function of time. Time varying signals are useful when diagnosing internal combustion engines because they operate on a cyclical basis and therefore, the amplitude of a signal as a function of time can be correlated to a position in the engine cycle.

Signals can be further classified as stochastic or deterministic. A deterministic signal is defined as one that is repeatable from cycle to cycle, so that it is only necessary to consider one engine cycle to obtain all the information. A stochastic signal, on the other hand, contains statistical variations that can be considered as random noise. Thus, it is necessary to analyze the performance over a number of engine cycles before the full information contained in the signal can be extracted.

Steady state signals are the easiest to interpret, for instance, the RMS vibration amplitude of an engine operating under specific conditions can be measured and if this value exceeds an acceptable limit, it can be assumed that there is some degree of malfunctioning within the engine. However, steady state signals provide the least amount of relevant diagnostic information per signal. Deterministic time varying signals are more difficult to interpret, but generally contain more information than steady state signals. Finally, stochastic time varying signals are the most difficult to analyze.

Without preliminary signal processing, such as noise filtering or statistical averaging, it is not possible for even a skilled operator to interpret them.

2.1.4 Transducers

There are a variety of transducers that exist for the purpose of NVH testing. The most frequently used transducers are discussed in the following sections.

2.1.4.1 Noise

The main transducer used in industry to measure noise is the microphone. For testing purposes, microphones are chosen based on the required frequency response, the environment in which they will be used, the specific sound fields required and their cost. Numerous microphone setups and mounting location specifications are specified by Evenson et al [23].

2.1.4.2 Vibration

The main transducer used for the measurement of vibration is the piezoelectric accelerometer. The theory and applications relating to this type of transducer is described by Bruel & Kjaer [36]. This is the transducer of choice because of its relatively small size, durability, low cost, wide frequency range and good measurement stability. The two types of accelerometers that are most commonly used are the charge output and internally amplified accelerometers as described by PCB [41]. Charge output sensors are high output impedance, piezoelectric sensors (without built-in electronics) that typically require external charge or voltage amplifiers for signal conditioning. ICP (Integrated

Circuit Piezoelectric) sensors are low output impedance sensors that contain built-in integrated circuits and usually only require a constant current power supply.

Another common transducer used for vibration measurements is the laser Doppler vibrometer as described by Polytec [42]. It is an optical instrument using laser technology to measure velocity of points on a vibrating structure. Unlike accelerometers, laser vibrometers are completely non-contact and are not affected by properties of the test surface and environmental conditions such as temperature or pressure. Laser vibrometers can measure over a wide frequency range, a wide range of operating distances and no surface reflective substances are usually required in order to obtain reliable measurements. Aust [2] used laser tomography to perform in-cylinder temperature and pressure measurements. Joerres et al [34] used a laser vibrometer with adjustable mirrors to measure vibration in a number of locations in order to detect defects on-line.

2.1.5 Data Acquisition Methods

There are endless methods of taking noise and vibration measurements on an internal combustion engine depending on the desired measurement locations, engine operating conditions and transducer type used. The following sections discuss some common methods that have been used previously.

2.1.5.1 Measurement Location

Effective measurement locations for detection of engine vibration are discussed by Hulls and Welch [31]. Vibration signals are difficult to analyze because a vibration sensor placed at any point on the engine is likely to receive signals from every other moving

component. Therefore, the signal from one mechanical component may become the noise when studying a different component.

In mounting vibration sensors, the object is to maximize the pickup of the signal of interest and to attempt, by proper location of the sensor, to minimize the pickup of unwanted signals. This is done in many cases by mounting an accelerometer on the cylinder block wall of each cylinder and thus, capturing the vibration signal from each individual cylinder of the engine. This method was utilized by Ghosh and Vora [26] in the detection of piston slap and combustion knock.

2.1.5.2 Operating Conditions

Many factors contribute to engine vibration such as engine speed, load, temperature, relative humidity, etc. The effect of varying loads and engine speed was studied by Ben-Ari et al [9].

It is known that mechanical components resonate when excited at certain frequencies. Therefore, by running the engines at certain speeds and loads, it is possible for the resonant frequencies of various components to come into step with the operating frequency of the engine and in turn cause vibration.

Temperature is also an important factor in measuring engine vibration because different components of the engine tend to distort, warp, expand or contract depending on the operating temperature of the engine. This may result in insufficient or excessive clearances that in turn could cause vibration.

2.1.5.3 Transducer Selection

There are many transducers that exhibit different characteristics and are more or less sensitive to noise and vibration. For this reason, different transducers are selected for different applications. PCB [41] describes the advantage of using charge output sensors over ICP sensors for high temperature applications. However, due to the sensitivity to environmental factors of the output signals from charge output sensors, low noise cabling is required to ensure no signal quality is lost when transmitted through the cables. In contrast, due to the low impedance of ICP sensors, output signals can be transmitted over long cables through harsh environments with virtually no loss in signal quality.

For noise measurements, it is frequently desired to measure a general area of an engine or the ambient noise present instead of measuring a specific location. In cases like these, it is more desirable to use a random incidence microphone that can pickup noise in a spherical region around the microphone as opposed to a free-field microphone that would only pickup noise directly in front of it.

2.2 Data Processing Techniques

Engine noise and vibration arise from various phenomena occurring within the engine.

The most common forms of noise and vibration are due to the following:

1. Unbalance of rotating and reciprocating components such as the crankshaft, camshaft, balance shaft, etc.
2. Mechanical impacts of various components due to insufficient or excessive clearances.
3. Abnormal combustion due to incorrect timing, incorrect valve timing, etc.

Due to the numerous combinations of noise and vibration that can be generated in an engine, it is apparent that the signals produced by the noise and vibration will be quite complex. Therefore, conventional data processing techniques are not sufficient in properly analyzing these signals and more advanced techniques must be used. In doing so, the desired signal information may be extracted without including that portion of the signal that does not provide any useful information and will only attenuate the effects of the faults present.

2.2.1 Angle (Position) Domain Signal Analysis

Internal combustion engines operate on a cyclical basis, therefore, all of the events that occur can be matched to a position in the cycle. The crankshaft angle is the most commonly used position reference for engines because most events are specified with respect to this location. For this reason, it is beneficial to collect data based upon crankshaft angle by using an encoder that samples at known points in the engine cycle. This makes diagnosis of engine faults much easier because noise and vibration signals can be linked to a specific engine event. Goetz and Meier [27] sampled vibration data based upon the engine's flywheel teeth in order to correlate vibration measurements to the crankshaft angle.

A useful method to process and analyze noise and vibration measurements sampled based upon position is the variance analysis method as was used by Tjong [47]. This method is useful in separating the random components of the vibration signal from the repeatable portion of the signal and allows for the vibration pulses to greatly stand out from the rest of the signal. The benefit of using this method is that vibration pulses can

be matched to exact locations in the engine cycle, and in turn to specific events occurring at that position.

Measurements taken based upon time for fixed conditions (i.e. RPM) can also be matched to position by re-sampling of the data using numerical integration. This method is not advised due to the numerous errors involved in using numerical techniques to perform integration. However, algorithms to transform time-based data into the angle domain are available if both the Crank Position Sensor and Camshaft Identification Sensor signals are acquired along with the data.

2.2.2 Time Domain Signal Analysis

It is uncommon for analysis of engine noise and vibration to be conducted using raw time data, because in many cases the raw data is difficult to comprehend and seems to provide no useful information. Therefore, in almost all cases, post-processing of the raw data is performed in order to present the data in a form that will provide useful information regarding frequencies, amplitudes, etc. Some typical processing methods that may be performed in the time domain are time domain averaging or calculation of the RMS noise and vibration amplitudes as described by Bruel & Kjaer [14]. These values will give an indication of the noise or vibration present based solely on one value and can only determine whether the signal has exceeded some threshold value. Therefore, these methods possess only minimal diagnostic capabilities needed for on-line detection of engine defects.

2.2.3 Frequency Domain Signal Analysis

The decomposition of noise and vibration signals into their frequency components has proven to be an effective method of diagnosing engine defects. This is because most engine faults are characterized by certain impulses that occur at particular frequencies or have components at known harmonics.

The most commonly used frequency domain analysis method is the Fourier Transform. This transform decomposes a time-based signal into a series of sine waves composed of various frequencies. Therefore, frequency content information of the signal is available, thus, providing a better indication of the events occurring at certain frequencies. However, these transforms are more suitable to stationary signals that are somewhat periodic than to time varying signals similar to those generated by internal combustion engines.

Ghosh and Vora [26] used FFT techniques to diagnose piston slap and combustion knock in gasoline and diesel engines. Vibration measurements were taken in a production environment and FFT methods were used as engine defect diagnostic tools as described by Goetz and Meier [27].

2.2.3.1 Order Tracking Analysis

Order tracking is a useful tool to use in the analysis of engine noise and vibration, where the primary interest is the behaviour of harmonic orders of the crankshaft speed as described by Bruel and Kjaer [43]. This method is particularly useful when taking measurements over a range of engine speeds in order to analyze the vibration characteristics of an engine as was discussed by Mercer [39]. Moreover, the strengths

and weaknesses of various order tracking analysis methods were presented by Blough and Gwaltney [12].

2.2.3.2 Wavelet Analysis

Wavelet analysis is a relatively new method of noise and vibration analysis somewhat similar to Fourier analysis. The main difference that exists between these two methods is that wavelets are functions that better suit certain responses that cannot properly be fitted by a series of sine or cosine waves. Wavelet analysis allows for the decomposition of the signal into different levels in order to observe the effect of the various frequency components contained in the signal. Blough et al [11] used wavelets to extract and filter transients embedded in stationary signals. Cheng [16] used wavelets to analyze responses due to automobile crashes. A wavelet based technique for bearing diagnostics was developed by Discenzo et al [19].

2.2.4 Acoustic Analysis

Engine noise can be analyzed using many different techniques that each provides a particular piece of information regarding the engine sound levels. It is common to analyze the time-averaged A-weighted overall levels and respective spectral maps for measurements that are taken while the engine speed is varying. This will enable one to observe the frequency content and amplitude over a range of engine speeds.

Noise measurements can also be decomposed into their frequency components and represented in 1/3, 1/6, 1/12 octave bands. This technique is useful when analyzing data that was collected from engines operating at a somewhat constant speed.

Gerges et al [24] used acoustic intensity analysis to measure the frequency response of an engine block and compared the results with those found from the classical modal analysis method.

2.2.5 Finite Element Analysis

A common analysis tool that is used to predict the noise and vibration of an engine is the finite element analysis (FEA) method. With the current computing power available, it is not difficult to perform simulations of complex engine models for the prediction of engine vibration.

Nefske and Sung [40] used FEA to identify the resonant frequencies, global modes and local surface vibrations for a particular operating load of a modeled engine. Iwahara et al describe a FEA method to effectively reduce the idling vibration of heavy-duty trucks using a full vehicle model comprised of finite elements.

2.3 Engine Defect Diagnostics

Once a noise or vibration signature for an engine with a faulty component is collected, processed and categorized, it is possible to use this signature to identify defects of the same nature on other engines. These signatures will exhibit specific characteristics, based on particular defects that will not be present in the signatures of "good" engines. This method of signature analysis is currently used in many production environments in which engine test signatures are compared to baseline signatures and limits are set as to the degree of allowable deviation between them. More in depth algorithms are also used in production environments where various characteristics and signatures are compared to

baseline signatures and a logic-based decision is made depending on the result of the signature comparisons.

The objective of this study is to acquire more advanced noise and vibration analysis techniques to be used for the detection of engine defects. Thus, it is necessary to be aware of the possible engine defects that can be detected by using noise and vibration as the primary indicators. The following sections describe procedures that should be followed in proper diagnosis of engine defects as well as a summary of the common engine defects that produce noise and vibration and that are capable of being detected by using diagnostic methods.

2.3.1 Pattern Recognition

Pattern recognition is any technique that processes information from a set of signatures or measurements so that decisions can be made regarding some underlying phenomena associated with the signatures or measurements. Hulls and Welch [31] have concluded that in order to implement any kind of pattern recognition system, the steps that must be followed are as follows:

1. Make a decision on the states of the system (features) that are to be recognized.
2. Choose a set of measurements from which the classifications can be made.
3. Use a processing or feature extraction technique to present the measurements in a form that will be most useful for the comparison task.
4. Use a logical design or a well-defined statistical algorithm to devise a system for making the desired classification.

5. **Implement the system and test its effectiveness on a set of samples that are different from the samples used in the design of the system.**

In general, there are three possible ways of limiting the signal information to better detect a specific engine defect. They include comparing the signal to the engine cycle in order to relate specific faults to a particular occurrence within the engine, choose the sensor location so that it only receives information from a particular part of the engine and use filtering or statistical averaging in order to accentuate the characteristics of the signal that are associated with specific faults.

2.3.2 Piston Slap

Piston slap is the phenomenon that occurs when the piston bounces from one side of the cylinder wall to the other. These impacts can occur in any engine or slider-crank mechanism with clearance between the bore and piston. Vibration due to piston slap is analyzed with reference to the major-minor thrust relationship, cylinder-to-cylinder variation, piston slap force diagrams and vibration-frequency curves. Piston slap generally occurs due to the following reasons:

1. The force holding the piston against the cylinder wall changes direction as the connecting rod moves from one side of the centerline to the other at top dead center (TDC) and bottom dead center (BDC) of the cylinder.
2. The piston is first accelerated and then decelerated along the stroke.
3. The piston does not move with its axis always parallel to the axis of the cylinder due to tilting from the drag force at the pin and moments that are generated between the center of gravity and center of rotation of the piston.

Ghosh and Vora [26] determined that piston slap could be reduced considerably by offsetting the pin axis towards the side of maximum piston thrust. Gerges et al [25] developed a mathematical model for piston slap force level prediction by considering the role of oil film in the bore on the impact behaviour of the piston.

2.3.3 Combustion Noise and Vibration

The combustion process itself provides a major contribution to the overall noise and vibration present in an engine. Ghosh and Vora [26] conducted experiments regarding the effect of engine speed and load on combustion noise and vibration. They concluded that vibration due to combustion is highly influenced by changes in engine speed in that as the engine speed increases, so does the vibration levels. However, vibration due to combustion at a particular engine speed is nearly independent of load.

Another form of vibration occurring as a result of combustion is combustion (spark) knock, which is due to abnormal combustion that produces very large pressure pulses in the combustion chamber. Factors affecting the presence of spark knock include spark timing, octane rating of the fuel, spark plug location and valve placement. Tomota and Zhang [48] analyzed the pressure signals in a spark ignition engine and the vibration of the engine block under knocking conditions. They proposed a knocking detection method based on the frequency characteristics of the engine block vibration signal.

2.3.4 Valve Train Noise

Valve train noise is developed in an engine by a number of contributing factors that include such items as valve lift, valve bounce, valve seat distortion and valve train

unbalance. Stout [45] used an analytical approach to determine the effects of valve train unbalance on engine noise and vibration levels.

Valve train noise is a result of impacts occurring within the engine and the resultant sound level increases as the impact speed increases. Follower noise is caused by frictional vibration due to insufficient lubrication between metal on metal contact points. Eovaldi et al [22] investigated the effect of operating speed on the vibration characteristics of the valve train. They found that the most effective way to analyze the dynamic behaviour of the valve train is by acceleration measurements followed with analysis in both the time and frequency domains.

2.3.5 Vibration due to Non-Cleanup of Cylinder Bores

Engine cylinder bores require a polished surface in order to ensure a smooth operation and to reduce the frictional effects that exist between the cylinder wall and piston. In some cases, a cylinder bore may be machined improperly and will cause areas of the cylinder wall to be somewhat rough. In cases like these, vibration will be present as a result of the piston rings coming into contact with the rough surface of the bore. The noise and vibration due to the impacts are usually large enough to be detected using the accelerometers mounted on the cylinder block walls.

2.3.6 Engine Balance

Another source of noise and vibration results from the unbalance of rotating and reciprocating components of an engine. Unbalanced forces in the engine include static

and dynamic unbalance of rotating parts such as the crankshaft, piston unbalance and piston inertia torque as described by Summers [46].

2.3.7 Overall Engine Sound Quality

Automotive companies strive to make the quietest engines possible in order to satisfy customer's desires to have a comfortable and quiet vehicle. Beidl et al [5] used both simulation and experimental analysis to attempt to reduce noise emissions from an internal combustion engine by 3 dB in order to meet 2004 automotive standards. Bernard et al [10] simulated the structure and air-born noise behaviour of engines under particular operating conditions in order to develop methods to reduce noise and vibration levels.

CHAPTER 3.

THEORY

This chapter discusses the theoretical aspects involved in measuring engine noise and vibration, processing this information and understanding the phenomenon that causes it. The topics to be covered include basic engine theory, equations pertaining to noise and vibration calculations, the fundamentals of digital signal processing, aspects associated with accelerometers, lasers and microphones and processing techniques such as the Fast Fourier Transform and variance analysis.

3.1 Digital Signal Processing

In almost all cases, after noise and vibration signals are acquired through a data acquisition system, further processing is required in order to extract important information regarding the signals captured. The following sections describe the most commonly applied techniques that are used to acquire, process and analyze digital signals.

3.1.1 Analog to Digital Conversion

In order to perform any type of digital post-processing, a digital signal must first be acquired. Any measurement taken from a real-world component will exist in an analog, continuous form. The transducer being used to measure the signal converts a physical event into a continuous time varying voltage. This continuous signal must be then converted into a digital form by the process of sampling and quantization using an analog

to digital converter (ADC). Sampling is the process by which an analog signal is converted into digital form by capturing discrete data points at equal time intervals. The result is a discrete time history. Quantization refers to the precision of amplitude conversion from analog to digital form.

3.1.1.1 Sampling

Sampling can be represented as a process where the continuous analog signal is multiplied by a unity amplitude discrete valued sampling function resulting in a discrete time signal with amplitude values equally spaced in time. The sampling frequency is represented by F_s and is determined as follows:

$$F_s = \frac{1}{\Delta t} \quad (3.1)$$

where Δt represents the time between samples.

In order to extract valid frequency information, digitization of the analog signal must occur at a certain rate that will allow for the analog signal to be recreated properly. This is the basis for Shannon's Sampling Theorem, which states that the sampling frequency must be at least twice the maximum frequency of the analog signal.

$$F_s > 2f_{\max} \quad (3.2)$$

If the sampling frequency is not at least twice the maximum frequency of the signal, there will be errors in the resulting digital signal. Frequency components that occur at a frequency greater than $\frac{1}{2}$ the sampling frequency in the analog time domain will cause amplitude and frequency errors in the computed frequency domain. These errors are referred to as aliasing.

3.1.1.2 Aliasing

A frequency that occurs above f_{max} in the analog time history will be shown as a frequency that is lower than f_{max} if the signal is not sampled correctly. The conversion from the time to frequency domain cannot distinguish between proper and improperly sampled data. The figure below shows the difference between proper and improper sampling of a signal.

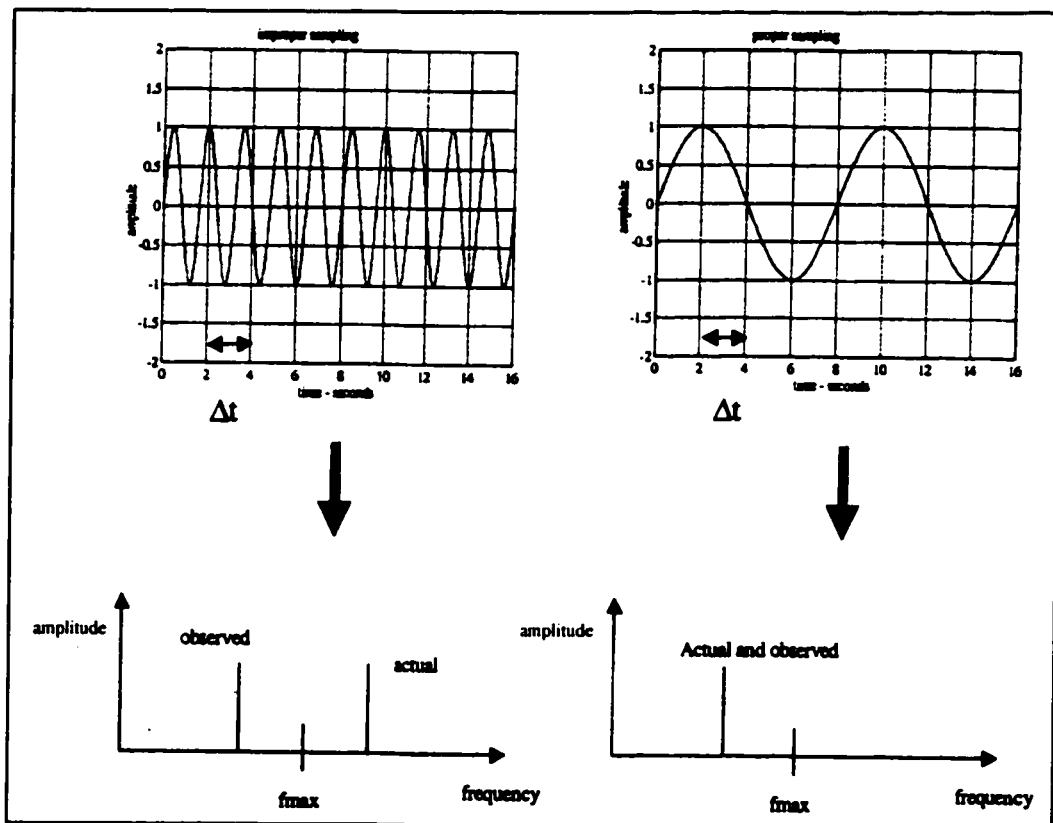


Figure 3.1 Difference between proper and improper sampling of a signal [38].

When aliasing occurs, frequencies that are greater than the maximum frequency get "folded back" at an equal distance from f_{max} and appear to be lower in the frequency spectrum.

Incorporating a low pass filter to the analog signal prior to digital conversion usually prevents aliasing. Low pass filters are used to attenuate any portion of the analog signal that could potentially appear as an alias based on the sampling frequency of the ADC.

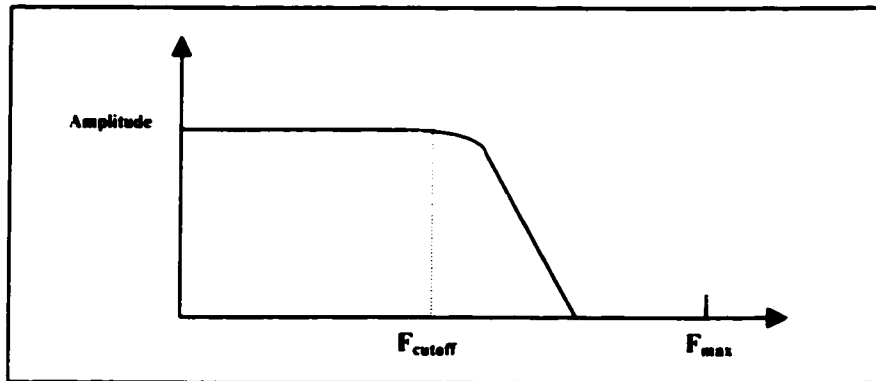


Figure 3.2 Example of a low-pass filter showing cutoff and maximum frequency.

3.1.1.3 Quantization

An equally important aspect of analog to digital conversion is the representation of the analog amplitude in a digital form. The process of converting the continuous analog voltage level to a discrete digital level is known as quantization. This is done by dividing up the amplitude range into discrete levels as determined by the specifications of the ADC, in particular, the number of bits of resolution in the ADC. For instance, an N-bit ADC would allow for 2^N quantization levels to be used in the conversion. A 12 Bit ADC would be broken down as follows.

$$12 \text{ Bit ADC} = 000\ 000\ 000\ 000 = 2^{11} + 2^{10} + 2^9 + \dots + 2^1 + 2^0 = 4096 \text{ levels}$$

The following figure illustrates the concept of quantization for a 4 Bit ADC. Notice that the amplitude range is broken down into 16 levels.

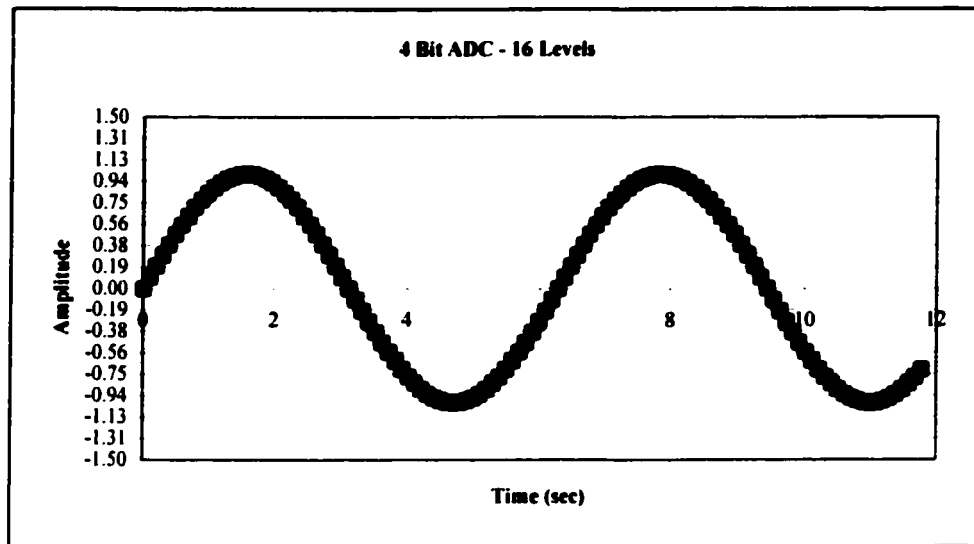


Figure 3.3 Illustrating the concept of quantization of a 4-bit ADC.

In order to most effectively convert the analog amplitude into a digital level, the ADC range should be set so that the full precision (all bits) is used. However, most converters allocate a portion of the range to headroom in case of any large transients present in the data, therefore reducing the range. Some possible quantization errors include over-ranging, where too much of the range is used and clipping of the data occurs and under-ranging, where only a small portion of the range is being utilized therefore reducing the amplitude resolution. Most analog to digital converters use auto-ranging, which allows for the optimization of the ADC range to be used when acquiring data.

3.1.1.4 Leakage

In order to compute an FFT correctly, the signal should be periodic and contain frequency content at integer multiples of Δf . For the case of non-periodic signals, the frequency content will usually fall between integer multiples of Δf . Computing an FFT

on such data will be possible but will lead to erroneous results as can be seen in the following figure.

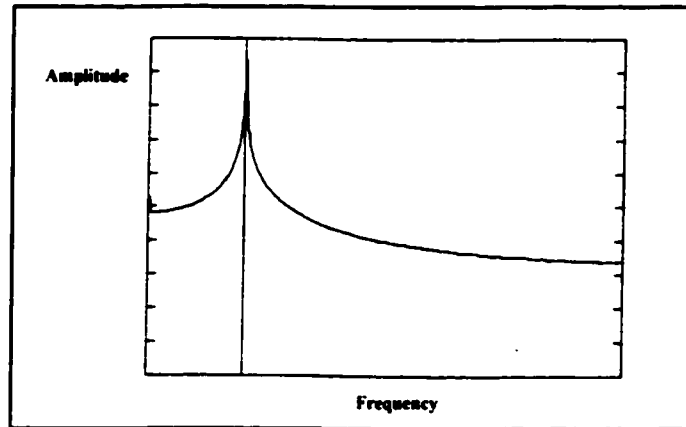


Figure 3.4 Example of leakage over many frequency bins due to non-periodicity of the signal [38].

This effect is called leakage. It is probably the most common and most serious digital signal processing error. Leakage cannot be eliminated completely, only reduced by using averaging techniques, increased frequency resolution or the use of windowing functions.

3.1.1.5 Windowing

In almost all cases involving data acquisition of noise and vibration, the signals captured are generally non-periodic. They are usually time varying, stochastic signals that contain random components. As a result, an FFT cannot be directly computed on the raw data acquired without some type of manipulation. Therefore, a time domain weighting function is required prior to the FFT in order to reduce the data into a periodic form. This weighting function is called a window.

A window is simply a function that is multiplied by the data signal in the time domain to ensure periodicity within the measurement period. This is possible because the windowing function is zero at either end of the windowing period. This concept is shown in the following figure.

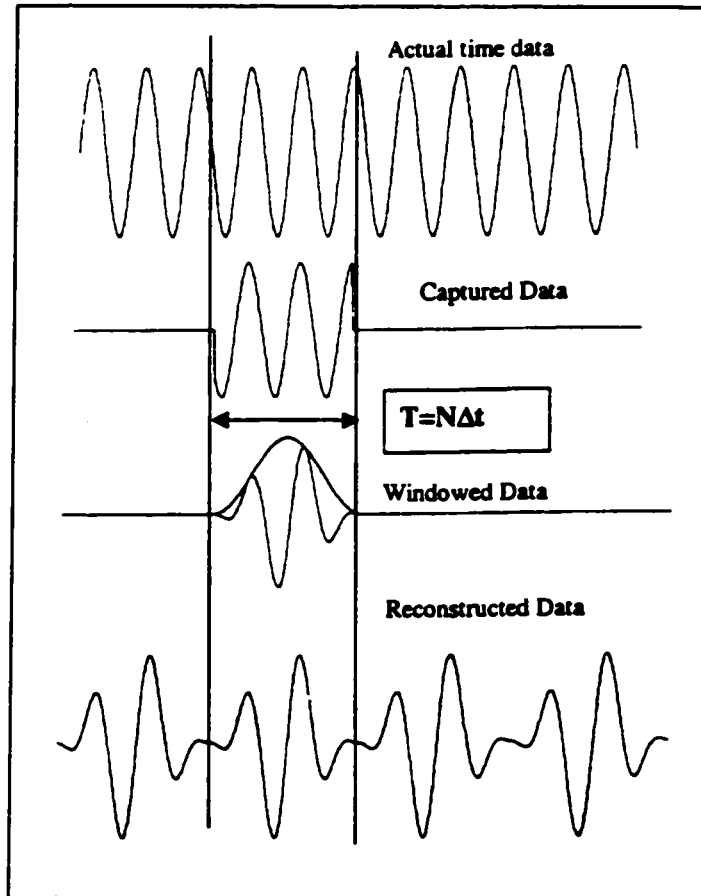


Figure 3.5 Example of windowing on a non-periodic signal [38].

There exist many types of windowing functions that help in achieving a high frequency or amplitude resolution, depending on which ever is desired for the data under consideration. The most commonly used windows are the Rectangular, Hanning and Flat Top windows. Each of these windows has their own beneficial characteristics depending

on what is desired in the analysis. Their time and frequency domain representations are shown in Figure 3.6.

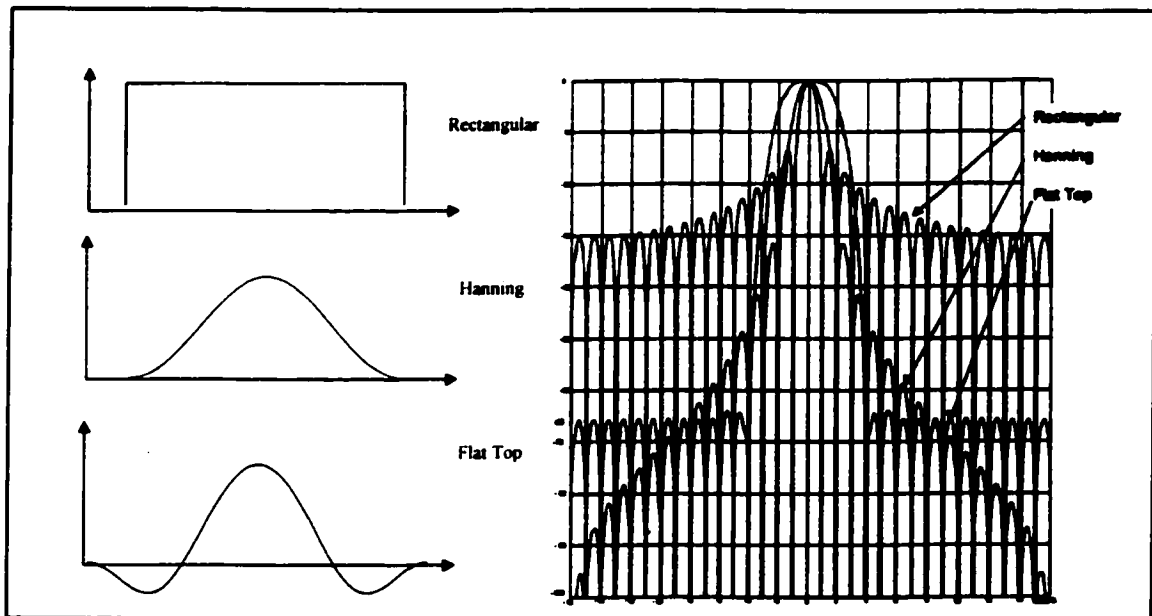


Figure 3.6 Comparison of windowing functions in terms of amplitude and frequency resolution [38].

The Rectangular (uniform) window provides very good frequency resolution since the main frequency lobe is quite narrow, however, the side lobes are quite large and roll off slowly. The main lobe is also quite rounded and thus, can introduce large amplitude errors as large as 36 %.

The Hanning window does not provide as good of a frequency resolution as does the uniform window. However, the amplitude resolution is better and does not usually exceed 16 %. This is due to the quicker roll-off of the smaller side lobes. In general, a Hanning window is the preferred choice for the best compromise between amplitude and frequency resolution.

The Flat Top window provides the best amplitude resolution with a margin of error of only about 0.1 %. Due to the main lobe spreading over several frequency bins, this

window provides very poor frequency resolution. Therefore, it should only be used in cases where the frequency resolution is not being considered and only amplitude resolution is the desired factor.

3.2 Internal Combustion Engine Theory

In order to use vibration and noise measurements as a diagnostic tool for engine defect detection, it is necessary to understand the fundamentals behind the operation of the internal combustion engine. In order to correlate certain vibration or noise signals to specific engine events, it must be known at what point in the engine cycle the events are occurring. Therefore, the fundamentals of the 4-stroke engine cycle will be explained as well as aspects associated with the combustion process, valve train operation and piston dynamics. The engines to be used in the study are spark-ignition engines that operate on a 4-stroke cycle, thus, the following information presented will be limited to this type of engine only.

3.2.1 4-Stroke Engine Cycle

The most common form of reciprocating engine operates on a 4-stroke cycle. A single cycle consists of 2 crankshaft revolutions and 4 strokes of the piston for each cylinder in order to produce one power stroke. There are 4 main processes that occur within one engine cycle, an intake, compression, power and exhaust stroke. With reference to Heywood [30], page 10, the 4-stroke engine cycle is explained below.

Intake Stroke: The cycle begins with the piston at top-dead-center (TDC), which then travels down the cylinder to bottom-dead-center (BDC) while drawing in a fresh air-fuel

mixture through the inlet opening. The inlet valve opens prior to the beginning of the stroke (before the piston reaches TDC) and closes shortly after the stroke ends (after the piston reaches BDC) in order to increase the amount of fresh mixture ingested into the cylinder.

Compression Stroke: The cycle continues with the piston traveling upwards to TDC from BDC while both the inlet and exhaust valves are closed. As a result, the volume decreases and the mixture is being compressed as the piston moves upward. Prior to the piston reaching TDC, combustion is initiated through the use of a spark plug that generates a spark and ignites the mixture.

Power Stroke: With both valves still closed, the piston reaches TDC and once again travels downward. Due to the high pressures and temperatures that result from the combustion process, the piston is pushed down the cylinder with a great amount of force. As a result, the work delivered to the crankshaft is much greater than the work required for the piston to compress the mixture and this is how the engine is able to continuously get power and run. Prior to the piston reaching BDC, the exhaust valve opens in order to reduce the in-cylinder pressure and to initiate the exhaust process.

Exhaust Stroke: With the exhaust valve open, the piston travels upward once again and pushes the burned gases out through the exhaust opening. Also, when the cylinder pressure is greater than the exhaust pressure, this also aids in expelling the remaining burned gases. Prior to the piston reaching TDC, the inlet valve opens once again and the exhaust valve closes shortly after TDC, therefore, re-initiating the engine cycle.

3.2.2 Engine Operation Fundamentals

Many phenomena that will be investigated in the study will relate to the vibration and noise generated by the impacts of the piston on the cylinder as well as impacts involving the connecting rod and crankshaft. For this reason, it is beneficial to understand the relationships that exist between the crankshaft, connecting rod, piston and cylinder. However, since the study will involve more of an experimental approach, only fundamental analytical relationships will be derived in the following sections in order to help understand the basic concepts relating to engine operation.

3.2.2.1 Geometrical Properties

The fundamental relationships that exist in an internal combustion engine will be derived for the case of one cylinder only, but are equivalent for all other cylinders as well. A typical piston-slider model of the cylinder, piston, connecting rod and crankshaft can be found in Heywood [30], page 44 and is referred to in the following derivation.

An important parameter in the design and performance of any internal combustion engine is the compression ratio r_c , which is defined below.

$$r_c = \frac{\text{Maximum Cylinder Volume}}{\text{Minimum Cylinder Volume}} = \frac{V_d + V_c}{V_c} \quad (3.3)$$

where V_d is the displaced (swept) volume and V_c is the clearance volume. Typical compression ratio values for spark ignition (SI) engines usually fall in the range of 8-12.

It is also important to be able to determine the volume at any piston location along the stroke. The cylinder volume V at any crankshaft position θ is determined by the following relationship.

$$V = V_c + \frac{\pi B^2}{4}(l + a - s) \quad (3.4)$$

where B is the bore diameter, l is the connecting rod length, a is the crank radius and s is the distance between the piston pin axis and the crankshaft axis and is found using

$$s = a \cos \theta + (l^2 - a^2 \sin^2 \theta)^{1/2} \quad (3.5)$$

3.2.2.2 Piston Kinematics

The displacement of the piston can be determined by the following equation.

$$y = Y_0 + a(1 - \cos \theta) + l \left[1 - \sqrt{1 - \left(\frac{a}{l}\right)^2 \sin^2 \theta} \right] \quad (3.6)$$

where y is the location of the piston from TDC and Y_0 is the distance from the top of the block deck to the top of the piston at TDC.

If the ratio of the crank radius a to the connecting rod length l is defined as λ as follows:

$$\lambda = \frac{a}{l} \quad (3.7)$$

and ϕ is defined as

$$\phi = \sqrt{1 - \left(\frac{a}{l}\right)^2 \sin^2 \theta} = \sqrt{1 - \lambda^2 \sin^2 \theta} \quad (3.8)$$

By combining these equations, the piston displacement can be simplified to the following form.

$$y = Y_0 + a(1 - \cos \theta) + l(1 - \phi) \quad (3.9)$$

It is well known that the velocity and acceleration of the piston can be found by taking the first and second derivatives, respectively, of the equation for piston displacement.

The resulting equations for each of these are shown below.

$$V = \dot{y} = a\omega \sin\theta \left(1 + \frac{\lambda \cos\theta}{\phi} \right), \quad A = y = a\omega^2 \left[\cos\theta + \frac{\lambda(\cos 2\theta + \lambda^2 \sin^4 \theta)}{\phi^3} \right] \quad (3.10)$$

In most modern and practical engine designs, the piston pin axis is offset from the centerline of the bore, in which case the formulas shown above would have to be altered in order to take into consideration the offset. However, for the purpose of this study, the derivation of piston displacement, velocity and acceleration with no offset will be sufficient in providing a general description of how these values would be calculated analytically.

3.3 Forced Vibration

The vibration signals generated within an internal combustion engine due to the combustion process and/or by mechanical impacts can be classified as forced vibrations. Due to the complex nature of an internal combustion engine, it is quite difficult to use analytical methods to determine the forced response of the engine block or other components. Therefore, it is quite uncommon to use an analytical approach that generalizes the vibratory response of an IC engine to determine the expected response. However, for the purpose of the study, the equations of motion for a 1-degree of freedom system subjected to a harmonically excited force will be presented in order to provide the reader with a fundamental view of the topic.

If a mass m , with a stiffness k and a damping coefficient c , is acted upon by a harmonic force $F(t)$, the summation of the forces in the x-direction will be

$$m \ddot{x} + c \dot{x} + kx = F(t) = F_0 \cos \omega_d t \quad (3.11)$$

and if both sides of the equation are divided by the mass m :

$$\ddot{x} + 2\zeta\omega \dot{x} + \omega^2 x = f_0 \cos \omega_{dr} t \quad (3.12)$$

where

$$\omega = \sqrt{\frac{k}{m}}, \zeta = \frac{c}{2m\omega}, f_0 = \frac{F_0}{m} \quad (3.13)$$

It is known that the forced response of a damped system will be of a harmonic form of the same frequency as the driving force, but with a different amplitude and phase. After applying the rules of differential equations, the particular solution is determined to be:

$$x_p(t) = \frac{f_0}{\sqrt{(\omega^2 - \omega_{dr}^2)^2 + (2\zeta\omega\omega_{dr})^2}} \cos(\omega_{dr}t - \tan^{-1} \frac{2\zeta\omega\omega_{dr}}{\omega^2 - \omega_{dr}^2}) \quad (3.14)$$

The total solution consisting of both the homogeneous (transient) and particular (steady state) solutions can be represented as follows.

$$x(t) = Ae^{-\zeta\omega t} \sin(\omega_d t + \theta) + A_0 \cos(\omega_{dr} t - \mathcal{G}) \quad (3.15)$$

where

$$\omega_d = \omega\sqrt{1-\zeta^2}, A = \sqrt{x_0^2 + \left(\frac{v_0 + \zeta\omega x_0}{\omega_d}\right)^2}, \theta = \tan^{-1} \frac{x_0\omega_d}{v_0 + \zeta\omega x_0} \quad (3.16)$$

and

$$A_0 = \frac{f_0}{\sqrt{(\omega^2 - \omega_{dr}^2)^2 + (2\zeta\omega\omega_{dr})^2}}, \mathcal{G} = \tan^{-1} \frac{2\zeta\omega\omega_{dr}}{\omega^2 - \omega_{dr}^2} \quad (3.17)$$

After some manipulation, the above expressions can be rewritten as:

$$\frac{A_0\omega^2}{f_0} = \frac{1}{\sqrt{(1-r^2)^2 + (2\zeta r)^2}}, \mathcal{G} = \tan^{-1} \frac{2\zeta r}{1-r^2} \quad (3.18)$$

where $r = \omega_{dr} / \omega$ is called the frequency ratio.

If the above expressions for magnitude and phase are plotted against the frequency ratio r for various damping ratio ζ values, the graphs appear as shown in Inman [32], inside cover.

It can be seen that as the frequency ratio approaches a value of 1, implying that the driving frequency and undamped natural frequency come into step, the curves corresponding to low damping ($\zeta < 0.1$) have their highest magnitude at this point. Moreover, at this point a phase shift of 90° occurs. When these conditions are present, this defines the phenomena of resonance for a system with damping.

The derivation shown above corresponds to only a single degree of freedom system, however, these same fundamentals can be applied to much larger and more complicated systems in order to determine the forced response of the system. In these cases, different techniques must be applied in order to determine the forced vibration response of such systems.

3.4 Noise

The effective sound pressure commonly used in all noise calculations is the RMS sound pressure that can be calculated given the sound pressure amplitude. More importantly, one of the most common forms of noise indicators is termed the sound pressure level, L_p and is calculated as

$$L_p = 20 \log P_{RMS} + 94 \quad (3.19)$$

Sound pressure level is measured in units of decibels, dB.

3.5 Accelerometers

The most commonly used transducer for engine vibration measurements is the accelerometer. In particular, the piezoelectric accelerometer, which is generally accepted as the best available transducer for vibration measurements because of its wide frequency operating range, excellent linearity and its robustness in harsh conditions. Some other common vibration transducers include piezoresistive, variable capacitance and servo force rebalance accelerometers. The piezoelectric accelerometer will be the main transducer used in the study and is therefore the focus of the following sections.

3.5.1 Piezoelectric Accelerometers

The main composition of a piezoelectric accelerometer consists of the accelerometer base, the piezoelectric elements and a series of seismic masses. A general representation of a piezoelectric accelerometer can be found in Licht et al [36], page 13.

The piezoelectric elements act as springs connecting the base of the accelerometer to the seismic masses by means of the center post. When the accelerometer is subjected to a vibration, the seismic masses exert a force that is equal to the product of their mass and acceleration on the piezoelectric elements. The elements then produce a charge that is proportional to the force exerted upon them, and since the masses are constant, the charge is proportional to the acceleration of the seismic masses. Furthermore, as the seismic masses vibrate with the same magnitude and phase as the accelerometer base, the output of the accelerometer is proportional to the base acceleration and thus, the acceleration of the surface of the component being measured.

3.5.1.1 Piezoelectric Accelerometer Designs

Piezoelectric accelerometers are available in a variety of designs that incorporate different arrangements of the components as well as a different form of vibration detection method. The most common designs are the Delta Shear, Planar Shear and Center Mounted Compression Design.

The Delta Shear design consists of three piezoelectric elements and three masses arranged in a triangular configuration around a triangular center post. These components are held securely in place by a high tensile clamping ring. When the accelerometer is subject to vibration, the seismic masses apply a shear force on the elements and a charge is generated. The charge is then collected between the accelerometer housing and the clamping ring. This design gives a high sensitivity-to-mass ratio, has a relatively high resonant frequency and is not greatly affected by large temperature transients.

The Planar Shear design also uses the shear deformation of the element to generate the charge but the number and orientation of the components are different. This design has two piezoelectric elements that are arranged around a rectangular center post. The seismic masses are placed around each element and the entire arrangement is kept together using a high tensile clamping ring. These accelerometers are also not greatly affected by temperature fluctuations because the elements are essentially isolated from the base.

The Center Mounted Compression design uses a piezoelectric element-mass-spring combination that is mounted on a cylindrical center post attached to the base of the accelerometer. The base and center post effectively act as a spring in parallel with the piezoelectric elements and thus, any dynamic changes in the base will cause stresses in

the piezoelectric elements and lead to erroneous outputs. These types of accelerometers are generally used in cases where the amplitudes are extremely high, in which case the erroneous effects are small compared to the measurements.

3.5.1.2 Charge Mode Accelerometers

All of the accelerometers mentioned up to this point have been of the charge mode type. These accelerometers contain no circuitry in the housing itself, but rather send a high impedance output through a cable into a charge amplifier that produces an output voltage proportional to the input charge. Due to the high impedance output from the accelerometer, a low noise cable should always be used in order to maintain a good signal. Due to the lack of circuitry in these accelerometers, they can withstand high temperatures and amplitudes, which makes them beneficial for applications such as engine monitoring.

3.5.1.3 Internally Amplified Accelerometers

These types of accelerometers are often referred to as line-drive or ICP accelerometers. They contain a built in amplifier that produces a low impedance output. For this reason, low noise cabling is not necessary to ensure good signal quality. However, due to the complex circuitry contained in the accelerometers, they are quite sensitive to temperature effects as well as high amplitude measurements. Internally amplified accelerometers require the use of a power supply in order to supply a constant voltage to the amplifier, which then transmits a current back to the external supply.

3.6 Microphones

The most commonly used transducer for acoustic measurements is the microphone. A microphone converts small-amplitude pressure variations (sound waves) into corresponding voltages. All microphones are designed for optimum frequency response in specific sound fields. There exist two main designations for microphones, normal incidence (free-field) and random incidence (pressure, diffuse). The two main design types of microphones used in industry are the condenser and ceramic-cartridge microphones. For this study, the condenser-type microphone will be used but the operation of both types will be explained below.

3.6.1 Normal Incidence Microphones

These microphones are generally referred to as free-field microphones. This style of microphone gives the best frequency response for sound waves arriving at normal incidence (perpendicular) to the microphone. For this reason, these microphones are commonly referred to as directional and should be pointed toward the source of sound.

3.6.2 Random Incidence Microphones

Unlike normal incidence microphones, this style of microphone has optimum frequency response when sound waves arrive simultaneously from all angles of incidence, as in a reverberant sound field. These microphones are commonly referred to as pressure or diffuse-field microphones and are the preferred choices when taking acoustic measurements of factory noise or moving sound sources.

3.6.3 Microphone Designs

Similar to accelerometers, microphones are based upon different design techniques that each has their own advantages over other designs. The two main design types currently used are the condenser and ceramic-cartridge type microphones. Each of these design methods is described in the following sections.

3.6.3.1 Condenser Microphones

This type of microphone consists of two plates separated by a small distance. The outer plate, which is known as the diaphragm, is very thin and deflects slightly when subjected to sound waves resulting in a change in capacitance. Opposite charges are formed on the plates due to a polarization voltage or by permanently embedding the charges on each surface during the manufacturing process. Microphones of these types are usually ½" or 1" in diameter and are widely used because of their combination of high sensitivity and good dynamic range (20-140 dB) with good frequency response (20 Hz to 15 kHz). The lower limit is determined by a small bleed hole located behind the diaphragm to provide static-pressure equalization and the upper limit is determined by the microphone diameter.

3.6.3.2 Ceramic-Cartridge Microphones

The composition of a ceramic-cartridge type microphone is somewhat similar to that of the condenser microphone, however, this design also encompasses the use of a piezoelectric crystal. The ceramic type usually has a diameter of 1" and is more rugged

and less sensitive to humidity variations than the condenser type. However, it has less sensitivity and a narrower range of frequency response.

The manner in which this type of microphone functions involves the slight deformation of the piezoelectric crystal due to impinging sound waves on the diaphragm. A charge proportional to the acoustic pressure is developed and output to an amplifier, which then converts the signal into a voltage that can be input into a data acquisition system for analysis.

3.7 Laser Vibrometers

Laser Doppler vibrometers are optical measurement devices that use laser technology to measure velocity from points on a vibrating structure. Unlike conventional transducers such as accelerometers, laser vibrometers are completely non-contact and are not affected by properties of the test surface and environmental conditions such as temperature or pressure.

A typical laser vibrometer system comprises of an optical interferometric sensor head and an electronic controller that demodulates the signal from the optical head and provides an analog voltage proportional to the velocity of the surface that is then digitally sampled and differentiated to obtain the acceleration signal from the laser. This is done so that laser measurements can be compared to those acquired from an accelerometer.

3.7.1 Laser Interferometry Measurement Principle

In a laser interferometer, a laser beam is divided into object and reference beams by a beam splitter, BS. The object beam strikes a point on the moving object and light

reflected from that point travels back to the beam splitter and interferes with the reference beam. If the object is moving, this interference process produces an intensity fluctuation in the light. Whenever the object has moved by half the laser wavelength, $\lambda/2$, the intensity has gone through a complete dark-bright-dark cycle. A detector then converts this signal into a voltage fluctuation. This concept is shown below.

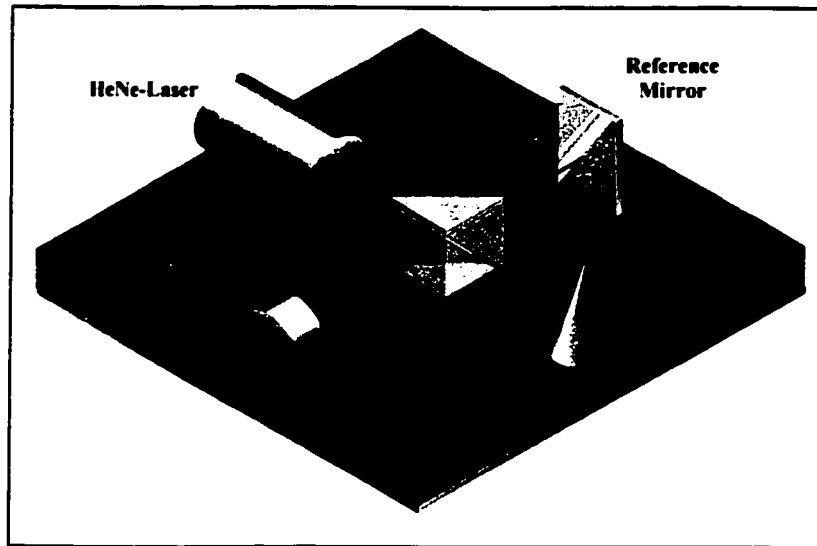


Figure 3.7 Diagram representing the principle of laser interferometry [42].

The frequency f_0 , which is known as the Doppler frequency, of the produced sinusoidal cycle is proportional to the velocity v of the object according to the formula:

$$f_0 = \frac{2v}{\lambda} \quad (3.20)$$

The problem with a conventional laser interferometer is that the Doppler frequency f_0 is independent of the motion's direction. In order to overcome this issue, many laser vibrometers use acousto-optic modulators (Bragg cells) to frequency shift the reference

beam in order to distinguish between movement towards and away from the interferometer.

3.7.2 Laser Doppler Vibrometer Principle of Operation

Standard laser vibrometer heads operate according to the principle of laser interferometry as mentioned previously. They use a visible, safe, low power Helium Neon (HeNe) laser source, highest quality optical components and a Bragg cell, which is known to be the most reliable, stable and accurate means for frequency shifting of a laser beam. The layout of this system is shown in Figure 3.8.

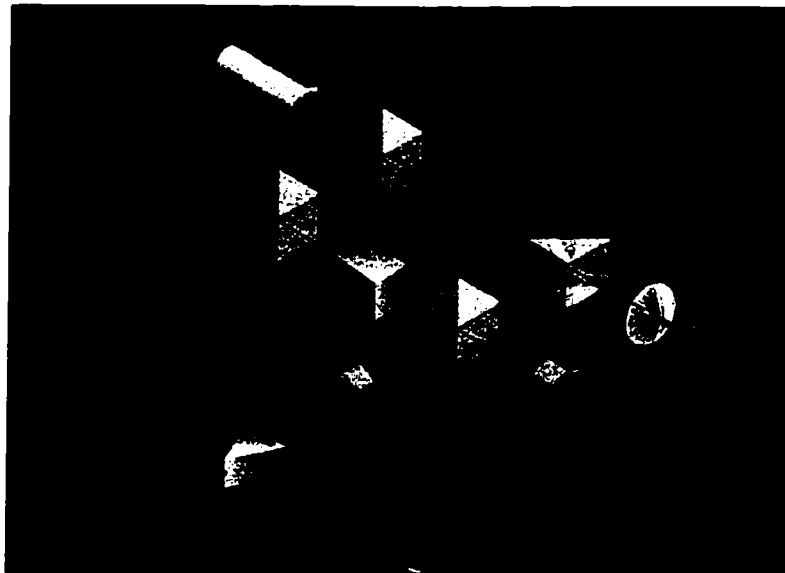


Figure 3.8 System layout of a laser Doppler vibrometer [42].

As can be seen from the figure, the light from the laser is split into a reference beam and an object beam by beam splitter BS1. The object beam then passes through beam splitter BS2 and is focused to a point on the surface of the object being measured by a high precision lens assembly. The same lens system collects some of the back-scattered light,

which is then diverted to beam splitter BS3 at which point it interferes with the reference beam. The light scattered from the vibrating object experiences a Doppler frequency shift that is proportional to the instantaneous velocity of the object in the direction of the laser beam.

The frequency difference between object beam and reference beam shows up as a light intensity modulation, which is converted to an electronic signal by detectors D1 and D2.

Two detectors are utilized to minimize noise and drift.

In order to distinguish between motion toward and away from the optical head, the Bragg cell is used to introduce a static frequency shift onto the reference beam. This is the basic operation for a standard optic vibrometer.

CHAPTER 4.

EXPERIMENTAL DETAILS

The preliminary experimental testing was conducted on numerous V8 5.4 L engines operating under various conditions in a dynamometer test cell, whereas the main experimental testing was conducted on-line.

The test parameters being measured were engine noise and vibration and therefore were used as the primary indicators for engine fault detection.

In order to establish an effective technique of detecting engine defects, a variety of operating conditions, measurement locations and transducers were used. The main operating conditions that were varied included:

1. Engine speed
2. Engine load
3. Coolant Temperature

Moreover, to observe the effect of combustion on engine vibration, measurements were taken using both a "hot" and "cold" test technique. A "hot" test refers to the running of an engine on a dynamometer test stand using combustion as the source of power for the engine, while monitoring various parameters such as noise and vibration. A "cold" test also refers to the running of an engine on a dynamometer test stand, but uses the dynamometer drive shaft to manually turn the engine without the use of combustion (i.e. no fuel, no spark).

The following sections describe the experimental setup, the measurement locations, the measurement procedures and the test equipment that was used in the study.

4.1 Dynamometer Engine Testing

At many automotive facilities, dynamometer testing is performed to establish engine performance, estimated lifetime of an engine and general integrity of all components of the engine, as well as to validate all design specifications related to the performance of the engine. This is accomplished by subjecting an engine to rigorous tests that monitor the durability and endurance of an engine, as well as the engine's ability to withstand thermal shock. The general test apparatus and procedures will be discussed in the following sections.

4.1.1 Dynamometer Test Cell

A dynamometer test cell was the primary test facility used for all of the preliminary experimental tests conducted in the study. An engine test stand generally consists of the following components:

1. Dynamometer
2. Drive shaft
3. Engine and engine mounts
4. Base plate on an isolated foundation
5. Test stand control and data acquisition system

A top-view schematic diagram of a complete dynamometer test cell is shown in Figure 4.1. When running an engine in a test cell, the engine, which is supported by engine

mounts that are located on a base plate isolated from the dynamometer, is attached to the dynamometer through the use of a drive shaft. An operator, through the use of a test stand control system controls the engine speed and load while the engine operating parameters are monitored and stored using a data acquisition system.

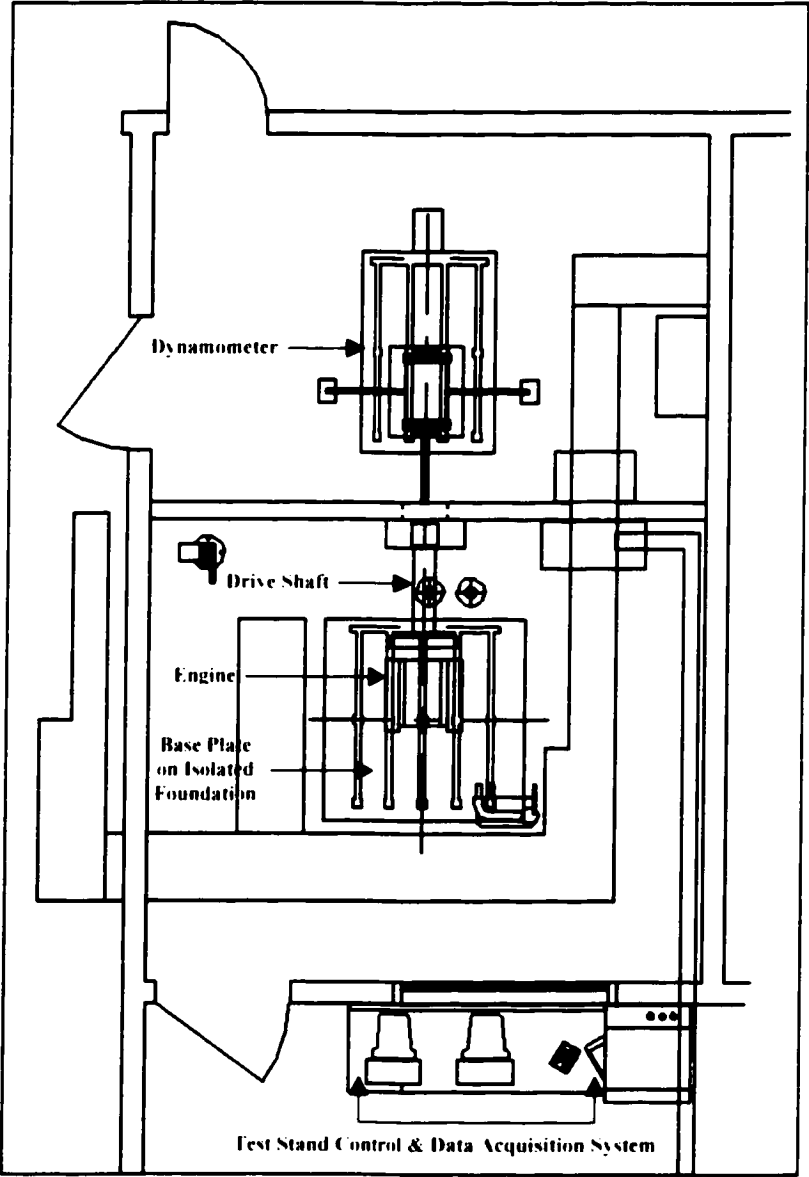


Figure 4.1 A top-view schematic diagram of a complete dynamometer test cell.

4.1.1.1 Eddy Current Dynamometer

The majority of the preliminary tests performed were conducted in cells utilizing an Eddy Current dynamometer. These types of dynamometers measure the engine speed and torque and are composed of an assembly of 4 main components including a rotating eddy current machine, cradle, torque measurement equipment and speed measuring equipment. The dynamometers used in the study can turn at a maximum speed of 6000 RPM with a maximum load output of approximately 400 ftlb. Therefore, the dynamometer specifications are sufficient in meeting the requirements established for the study and present no problems in the data collection process. With this in mind, the advantages of using an eddy current dynamometer include its high speed and load capabilities, its high power absorption and relatively low cost. An eddy current dynamometer is shown in the following figure.

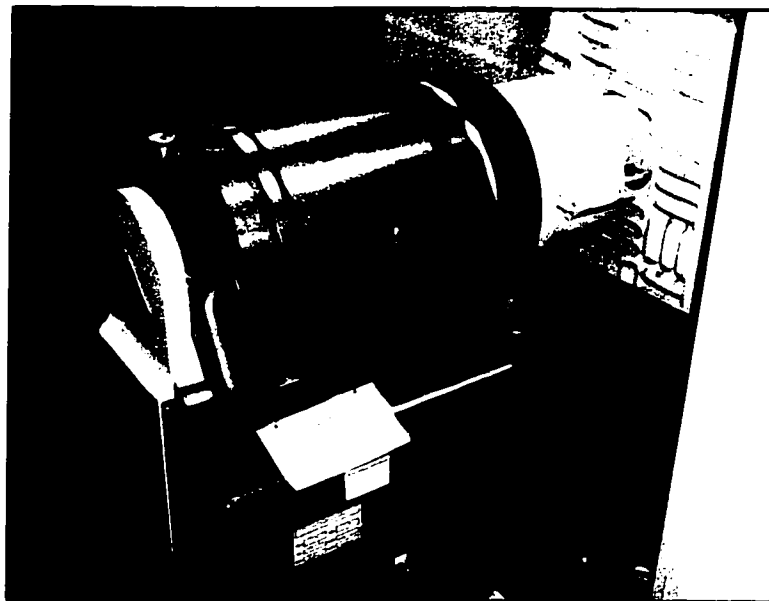


Figure 4.2 An eddy current dynamometer located behind the NVH test cell.

4.1.1.2 Data Acquisition System for Operating Parameters

Each test cell has an accompanying test control and data acquisition system. These are generally HP Workstations that are UNIX based. Engine speed and load are both controllable from the workstation and parameters such as oil pressure, coolant temperature, manifold pressure and throttle angle can all be monitored from the workstation. Important data such as fuel-flow, spark advance, exhaust temperatures, horsepower and torque are acquired and eventually used in generating baseline horsepower and torque curves.

4.2 On-line Engine Testing

Due to the number of constraints present in an engine assembly process, the test systems that are used to identify incorrect assemblies or general engine faults are limited to only capturing a certain amount of data taken at feasible locations allowed by the test station. These tests monitor items such as running torque, breakaway torque, running velocity, oil-gallery pressure, cylinder pressures, sensor integrity, etc. Currently, none of the on-line test stations that are in use at the automotive production facility under consideration in the study use noise or vibration as an indicator for engine defects. For this reason, an on-line test station will be modified into one that will operate as before plus have additional transducers installed in order to use noise and vibration signals as indicators of engine faults. The desired station will allow for the addition of transducers and will operate at a level where noise and vibration signals will be good indicators of engine condition. The on-line test station that is most suitable for this application is the Cold Test station and is described in the following section.

4.2.1 Cold Test

Cold Test is the most in-depth in-process test currently being used at the production facility under investigation. This is because this test is performed on fully assembled engines at the end of the assembly line and is used on 100% of the engines produced. The test monitors engine parameters such as running torque, running velocity, fuel rail supply pressure, fuel rail leak rate, vacuum leak rate, integrity of the wire harness and all sensors, injector and coil integrity as well as a variety of other parameters. Figure 4.3 below shows the Cold Test station that will be used in the study.

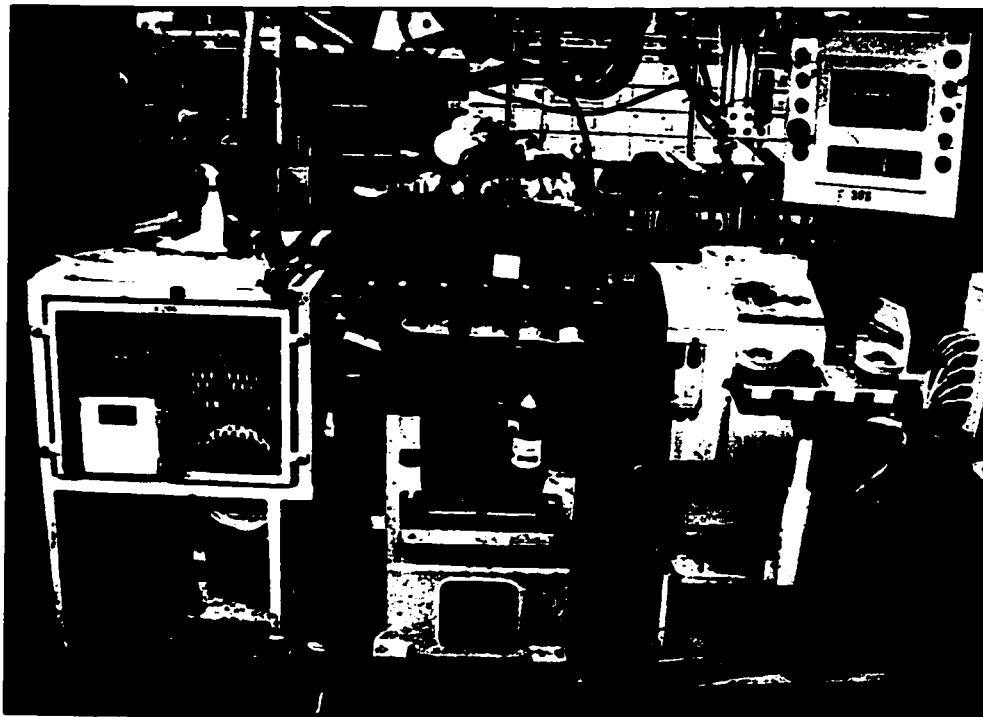


Figure 4.3 Cold Test station to be used in the study.

The test station motors the engine (i.e. no combustion) at an operating speed of 600 RPM while monitoring the parameters mentioned above. Since most noise and vibration issues

are more noticeable at higher engine speeds, the Cold Test station was chosen since its operating speed will be sufficient in detecting noise and vibration.

4.2.1.1 Cold Test Transducer Location

Due to constraints imposed by the test station itself, transducer selection will be made in areas that are easily accessible by advancing mechanisms on the test station as well as those areas that will meet safety regulations of the plant. The possible areas include the external cylinder block walls, the camshaft covers, the front cover and the locating lugs of the engine. However, since the main focus of this study is to detect faults related to the vibration of lower-end components (i.e. cylinder block, connecting rod, crankshaft, pistons), transducer locations such as the cylinder head, camshaft cover and front cover will not be used.

Locating the transducers on to the cylinder block walls of the engine is a difficult process. This is because there are components that are directly in the way of feasible measurement locations. As a result, it would only be possible to have 2 or 3 possible measurement locations on the block, which would be an insufficient amount of measurements.

A solution to this dilemma lies in the fact that every engine has 4 locating lugs found on the cylinder block. These are located at the front and rear of the block wall for both the right and left side of the engine. Previous experimentation has shown that these locations are excellent for picking up vibration related to lower-end components and due to their locations on the engine, pin-pointing which area of the engine the vibration is emanating from is not a difficult task.

For this reason, the locating lugs have been chosen as the optimal mounting transducer locations to detect defects occurring in the vicinity of the lower-end of the engine. The following figure shows the location of the lugs on the engine.

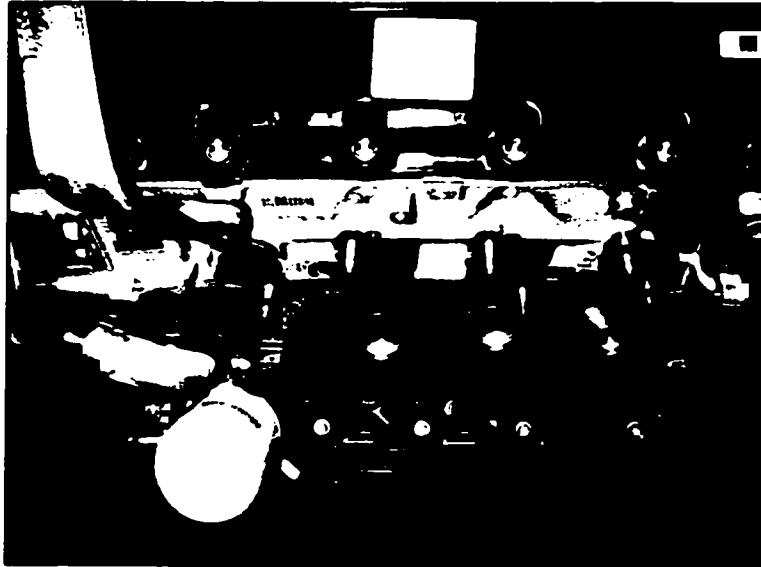


Figure 4.4 Optimal transducer locations for accelerometer mounting at cold test station.

4.3 Data Acquisition System for NVH Measurements

The main data acquisition system used in all of the baseline testing was a stand-alone system developed by Checksum Inc. This system uses a Datel PCI-416 data acquisition card that can support A/D sample rates up to 300 kHz (all channels sampled), 16-channel simultaneous sampling with an input range of ± 10 VDC, 12-bit A/D resolution and pre/post triggering capabilities. The system also consists of a Checksum interface card that provides external power, external source input, such as an encoder input and an A/D sample clock as well as two analog buffers/voltage limiters that use PC ± 5 VDC and ± 12 VDC. There is also an Alligator Technologies AAF-16 filter card that is accessed

through the ISA slot. However, since most filtering is done in the analysis process, this card is not currently used. These components are used in conjunction with a Dolch FlexPac personal computer running Windows 98 with all software components integrated by a custom Visual Basic software interface.

4.4 Transducers and Accessories

There were a variety of transducers used in the study to detect engine vibration. In addition, many of these transducers required various accessories in order to function properly or at all. Therefore, the following sections will give a detailed description of the transducers and accessories used in the study. A listing of all transducer specifications is listed in Appendix B.

4.4.1 Electro Corporation 58413 Digital-Magnetic Pickup

The digital-magnetic pickup provides a digital pulse (square wave) output whenever there is an abrupt change from non-magnetic to magnetic material moving past the pole piece in the pickup. The rise-fall times and amplitude of the output pulse are independent of the characteristics and speed of the magnetic discontinuity.

The digital-magnetic (di-mag) pickup was used as an encoder in many of the NVH tests conducted. By detecting the rise and fall of every tooth attached to the custom built flywheel with 360 equally spaced teeth attached to the crankshaft of the engine, the pickup created a pulse for each of these events and thus created a square wave signal. This signal was input into the data acquisition system and a sample clock was created based on a threshold value of the rise and fall of each tooth. Thus, true position-based

samples were taken at known angles in the engine cycle resulting in a resolution of 0.5 degrees/sample.

4.4.2 Bruel & Kjaer Type 4366 Accelerometer

This is a charge mode, delta-shear type piezoelectric accelerometer requiring the use of a charge amplifier. It is composed of a base that transmits vibration to a series of seismic masses that are in contact with piezoelectric elements and is held together by a clamping ring. It can withstand high temperatures and is quite durable and robust under harsh conditions, but requires low-noise cabling due to its high impedance output.

4.4.3 PCB Model 462A Charge Amplifier

This type of charge amplifier is a wide frequency range charge amplifier for use with piezoelectric charge mode accelerometers. It converts an input charge signal from the accelerometer into an output voltage signal to be sent to a data acquisition system. The amplifier allows for direct dial-in of transducer sensitivity in the range of 0.1-1.1 pC/unit.

4.4.4 PCB Model 359B15 Accelerometer

This is a miniature Integrated Circuit Piezoelectric (ICP) type accelerometer that is used for moderate temperature range applications. Due to the microelectronics built into the accelerometer itself, it is unable to withstand high temperatures. However, due to its low impedance output, low-noise cabling is not a necessity in order to obtain clean signals. Its sensitivity of 10 mV/g and wide frequency range of 1 to 10 000 Hz ($\pm 5\%$) suits most

applications, such as NVH testing, gear mesh, and other general-purpose vibration measurements.

4.4.5 PCB Model 480E09 Sensor Signal Conditioner

This sensor signal conditioner (power supply) is a portable, compact means for powering sensors that contain built-in microelectronics (i.e. ICP accelerometers) or in-line charge converters. Some of the capabilities of the power supply include eliminating an accelerometer's bias voltage, outputting an AC coupled signal and performing a self test to detect cable faults. The power supply also provides adjustable gain settings that range from 1 to 100 times the input signal.

4.4.6 Bruel & Kjaer Type 4294 Calibration Exciter

This accelerometer calibrator is a compact, self-contained vibration reference source that is generally used in a test laboratory environment. It is intended for rapid calibration and checking of vibration measurement, monitoring and recording systems. The calibrator produces a reference sinusoidal acceleration of 10 m/s^2 rms at a frequency of 1000 rad/s (159.2 Hz). Accelerometers are threaded onto the calibrator, attached magnetically or held onto the calibrator using wax.

4.4.7 Polytec Laser Vibrometer IVS 200

The Industrial Vibration Sensor (IVS) is generally used for non-contact measurements of surface vibrational velocity. It is designed as an optical vibration sensor for applications in industrial processes, such as an automotive assembly line. The robust industrial housing is suitable for harsh ambient conditions and reflective paint or tape is not

required on the measurement surface. It has variable optimal stand-off distance capability and a sensitivity of 25 (mm/s)/V over an operating range of 0.5 to 25,000 Hz.

4.4.8 TMS Type 130C10 Microphone and Type 130P10 Preamplifier

The 130C10 is a free-field (directional) ICP microphone with a ¼" diameter that is housed in a stainless steel case and has a high sensitivity and low inherent noise. The microphone mates with the 130P10 preamplifier that is then output to an ICP power supply. The 130C10 has a sensitivity of 25 mV/Pa and a frequency range of 10 to 15,000 Hz.

4.4.9 Bosch Knock Sensor

The Bosch Knock Sensor is simply a lower-end accelerometer that is used in all production engines to monitor vibration of the engine due to combustion (spark) knock. Its use in this study will be to monitor lower-end engine vibration in order to test its validity as a possible transducer that can be used to detect engine defects on-line. Its maximum operating frequency is 18 kHz and its sensitivity is 30 mV/g.

4.4.10 Tektronix Type 2232 Digital Storage Oscilloscope

The Tektronix 2232 oscilloscope is a reliable piece of equipment used for displaying, measuring and saving waveforms. It is a two-channel, combination analog and digital oscilloscope with a maximum 100 MHz analog bandwidth and has a sample rate of 100 Megasamples/sec. It is an excellent tool for verification of signals while performing vibration analysis using various transducers.

CHAPTER 5.

DATA ANALYSIS METHODS

When attempting to detect engine defects through the use of NVH measurements, there are a variety of data analysis techniques available to help in identifying particular defects. This study attempts to use many of these techniques in diagnosing engine defects related to mechanical impacts.

The main indicators that are used to detect abnormal mechanical impacts occurring in an engine or from the combustion process itself include vibration signals, noise signals and pressure signals that are all time-varying and semi-deterministic in nature. Vibration signals are generally in the form of surface borne acceleration or velocity that can be detected using accelerometers and lasers, respectively. Noise signals are captured using microphones or sound intensity equipment. Pressure measurements are generally taken using pressure transducers in the vicinity of the combustion chamber to detect vibration due to combustion. For this study, the main indicator used in the detection of engine defects was vibration using both accelerometer and laser measurement data.

With regards to data analysis methods used in the study, they included the following:

- 1. The simple analysis of observing the raw time/position domain traces to observe any inconsistencies between the test signals and the known baseline signal, as well as to observe any spikes that stand out from the rest of the data.**
- 2. Cyclic averaging of the time/position domain signals into one overall average cycle representation of the engine noise or vibration.**

3. A variance analysis of the data that clearly shows any deviations in the data from the average value. This method is very useful in extracting vibration signals from mechanical impacts occurring in an engine.
4. Many useful statistical parameters were also determined including the overall mean, standard deviation and rms values of the collected noise or vibration data.
5. Frequency analysis methods such as the Discrete Fourier Transform (DFT) and Auto Power Spectrum were used in relating defects to particular frequencies or orders.

5.1 Raw Time/Position Trace Analysis

This analysis method involves observing the acquired raw data trace as is, prior to any filtering or manipulation of the data. It may consist of simply analyzing the raw time trace for any items that appear to be abnormal or that stand out from the rest of the data. It can also consist of arranging raw position based data into cycles to observe any large spikes or any cycle-to-cycle variations that may be present. Figure 5.1 shows a raw position domain trace collected over 38 engine cycles. Figure 5.2 shows the 3-dimensional view of the same data in a waterfall plot. In both plots a vibration spike can be seen from cycle to cycle. However, in many cases vibration spikes may not be easily detected in observing the raw data. This may be due to a low signal-to-noise ratio, low vibration amplitudes or random occurrences that may not appear to be semi-periodic. This is the main reason why data manipulation such as filtering is required in order to utilize the data more efficiently.

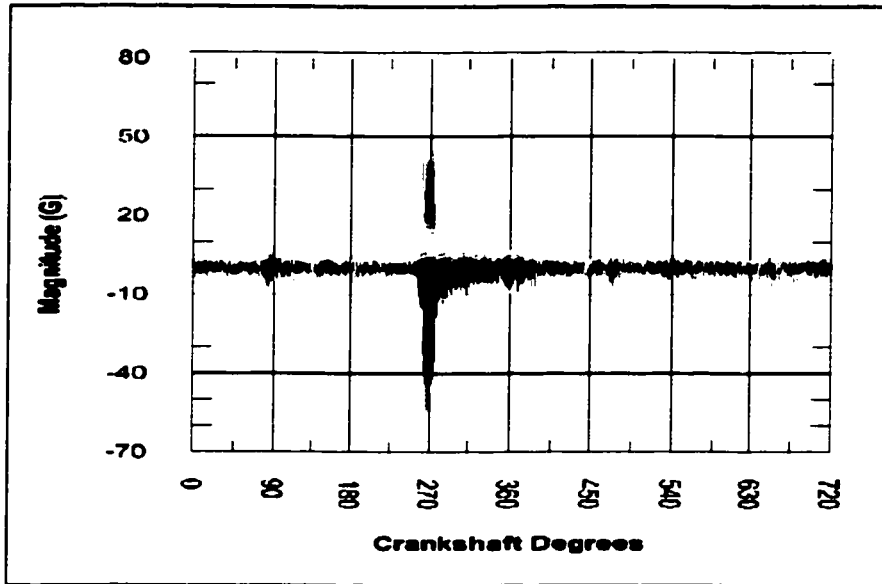


Figure 5.1 Raw position-based vibration trace collected for 38 engine cycles taken from an accelerometer mounted on the outer cylinder block wall of an engine with a cold knock (piston slap).

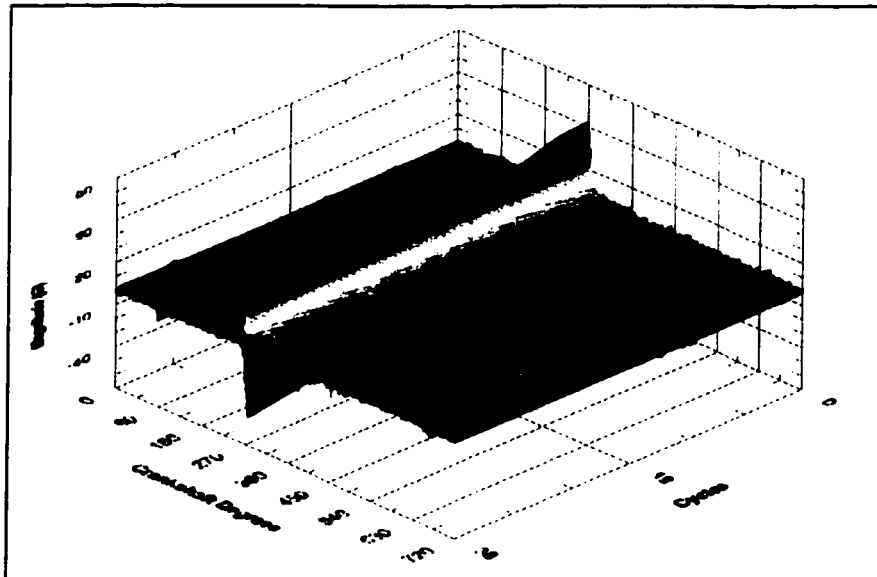


Figure 5.2 The same raw position-based vibration trace arranged in 3-D waterfall format for 38 cycles of data. Notice that the spike stands-out over the entire range of engine cycles of data acquired.

5.2 Position/Time Domain Averaging

Averaging in either the position or time domain is accomplished by simply averaging respective points from each cycle once the data has been arranged into a number of cycles or desired data segments. The result is one averaged cycle of data that gives a general representation of the noise or vibration present in one cycle (segment). This method is also useful for extracting periodic or regularly occurring events in the collected data. However, for transient or randomly occurring events, this method is not beneficial since the impact of these events may be dissolved once they are averaged over a number of cycles. The general formula for position/time based averaging of a signal over a number of cycles is

$$\bar{x}_i = \frac{1}{N} \sum_{j=1}^N x_{ij}, \quad i = 1, 2, 3, \dots, S \quad (5.1)$$

where \bar{x}_i = i_{th} Average value, i = Sample Index, j = Cycle Index, S = Samples/Cycle and N = Number of Cycles.

The following figure displays the result of averaging the position-based data from figures 5.1 and 5.2 over a large number of cycles. A benefit of using position-based sampling to collect data is that each sample can be related to an event in the engine cycle once a reference point is determined. In most cases, the camshaft identification (CID) signal is used to specify the location of top-dead-center of cylinder #1 on the power stroke. Once this position is known, the remainder of the data can be offset to this known reference position. The use of the CID signal will be described later in the study.

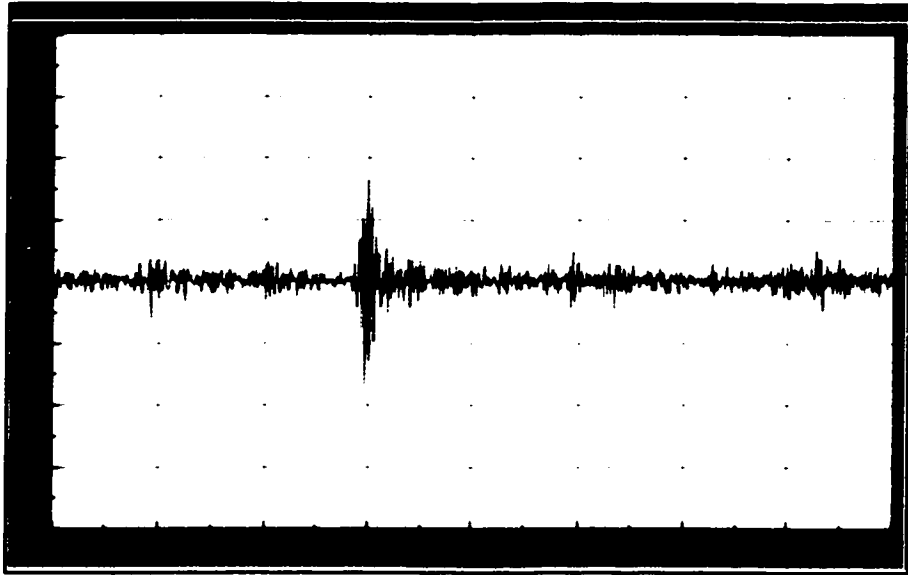


Figure 5.3 Averaging of the same raw position-based data over a large number of cycles. The vibration spikes are emphasized and can be linked to specific locations in the engine cycle.

5.3 Variance Analysis

Variance analysis is a preferred analysis tool to use when attempting to observe deviation of data from the mean value. In many cases, vibration spikes occur at specific positions of the engine cycle, but are not always present in every cycle of collected data. The vibration spikes that occur in such a manner are termed semi-periodic components. As described above, time/position domain averaging is not always beneficial for this type of data since the semi-periodic components may get attenuated once averaged over many cycles of data. To overcome this, the statistical indicator of variance is used in order to observe the effect of semi-periodic components occurring in the data.

In performing a variance analysis, the collected data is organized into cycles so that there are an equal number of samples per cycle. An overall average cycle is calculated as in the time/position domain averaging calculation, which is referred to as an ensemble average. For each sample index of each cycle, the sampled value is subtracted from the

corresponding indexed average value and then squared. The resulting sets of values are termed the running variance values. Furthermore, if these values are averaged into one cycle, these values are the true overall variance values. The following equations provide a mathematical representation of the variance analysis method used in the study.

The ensemble-averaged values are found using equation (5.1) as shown below:

$$\bar{x}_i = \frac{1}{N} \sum_{j=1}^N x_{j,i}, \quad i = 1, 2, 3, \dots, S \quad (5.1)$$

Therefore, in order to determine the running variance values, the following equation is used:

$$RV_{j,i} = (x_{j,i} - \bar{x}_i)^2, \quad j = 1, 2, \dots, N \quad i = 1, 2, \dots, S \quad (5.2)$$

In order to acquire the overall variance levels for one cycle, the following equation is used:

$$V_i = \frac{1}{N} \sum_{j=1}^N RV_{j,i}, \quad i = 1, 2, 3, \dots, S \quad (5.3)$$

The variance analysis method is a valuable tool when detecting mechanical impact events such as piston slap, connecting rod knock and others. The method allows for semi-periodic components to be identified through the process of squaring their deviation from the mean, which exaggerates their overall effect. It also takes repeatable components and items such as noise and averages them out to constant value over the entire cycle range. In addition, when performing a variance analysis on position-based data, the semi-periodic components can be associated with a particular crankshaft location and therefore, to a particular engine event. The following figures show both a waterfall plot of running variance values and an overall cycle variance plot of data taken from vibration tests conducted in a dynamometer cell.

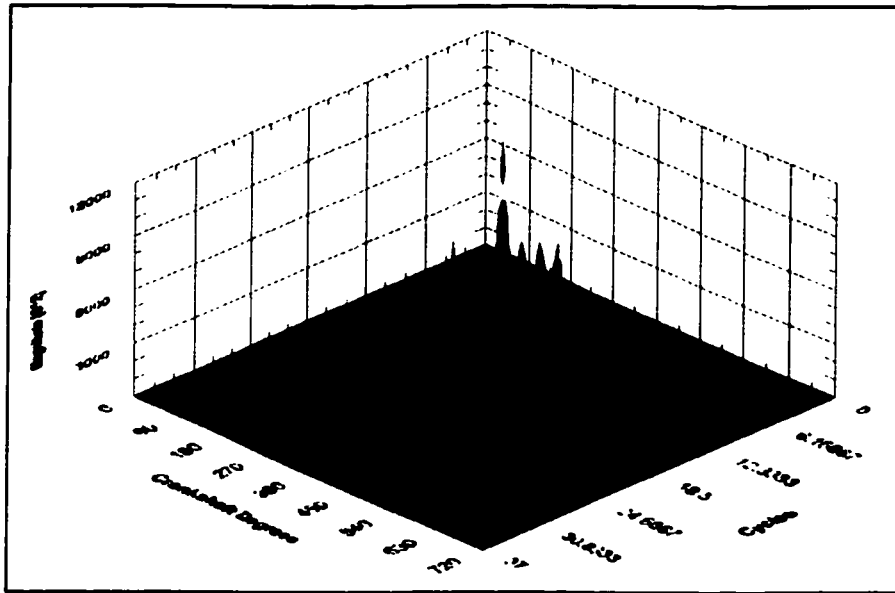


Figure 5.4 Waterfall plot of running variance for 38 cycles of data. The semi-periodic component is easily seen in the figure.

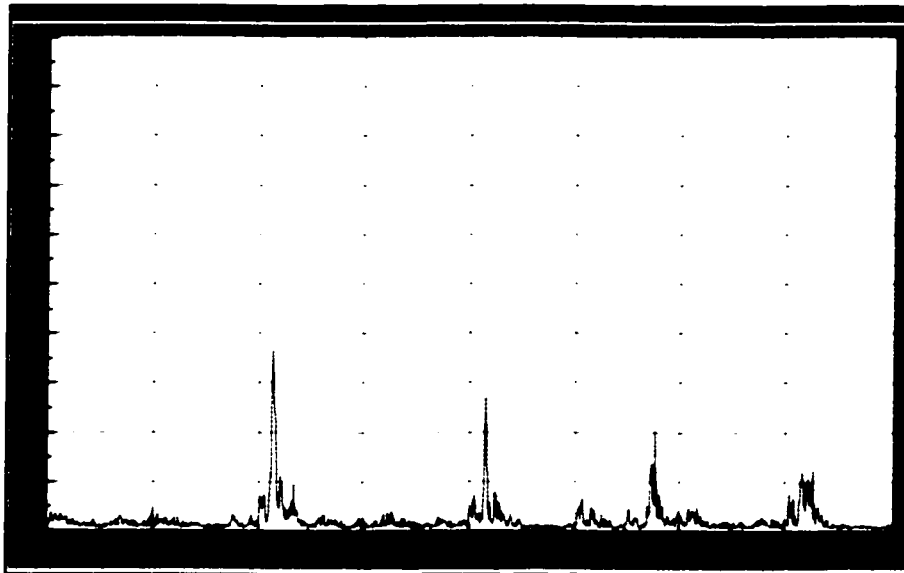


Figure 5.5 Overall variance plot of position-based data. Four spikes are identifiable.

5.4 Statistical Indicators

There are many other statistical parameters in addition to variance that can be calculated given a set of data. However, for the case of engine vibration data, not all of these parameters provide any useful information. For this reason, only a number of statistical parameters will be used in the study to assist in identifying engine vibration. Such parameters include the mean, standard deviation and root mean squared (RMS) of the collected data.

5.4.1 Mean

The overall mean of a specific channel of data is an indicator that provides only a minimal amount of information regarding the signal. This is because most vibration signals contain data spikes that occur in a peak-to-peak manner symmetric about the time/position axis and when averaged, converge to zero or some small value. However, all vibration signals are semi-periodic and aren't perfectly symmetric in the vertical direction, therefore, in many cases the amplitudes in a certain direction of motion will be greater than others. For this reason, it is possible to compare the overall mean to a pre-determined threshold value in a defect detection process.

Due to the randomness of vibration signals and the minimal amount of useful data provided by the mean, it will only be used as an observatory indicator in the study and pass/fail decisions will not be based upon it. The equation for determining the overall mean of a segment of data is shown below.

$$\bar{x} = \frac{1}{S^*} \sum_{i=1}^{S^*} x_i \quad (5.4)$$

Where S^* is the total number of samples per segment (or channel).

5.4.2 Standard Deviation

Another statistical parameter that measures deviation from the average value in a set of data is called the standard deviation. It is derived by taking the square root of the calculated variance. However, its use in this study is not derived from the variance that was used to observe deviations from cycle to cycle described earlier, but rather from a variance calculation performed on an entire channel of data. Therefore, the standard deviation calculated will show the general deviation of the data from the overall channel average value, rather than the ensemble average. It is calculated using the following equation:

$$\sigma = \sqrt{\frac{1}{S^*} \sum_{i=1}^{S^*} (x_i - \bar{x})^2} \quad (5.5)$$

where S^* is the total number of samples per segment (or channel).

5.4.3 Root Mean Squared (RMS)

The root-mean-squared (RMS) value of a set of data provides an overall value that can be representative as the "energy" of that set of data. In many cases, it provides more relevant information than does the mean or standard deviation and is easier to use as a diagnostic parameter. In many cases, the RMS value of a set of collected engine vibration data can be compared to a pre-determined threshold value to be used as pass/fail criteria. If the RMS value exceeds that of the threshold value, then it is apparent that there is some form of malfunction with that component or area being measured. This is beneficial in indicating a potential area or component that may be faulty in the early stages of diagnosis of engine defects. It is calculated as follows:

$$x_{RMS} = \sqrt{\frac{1}{S} \sum_{i=1}^S x_i^2} \quad (5.6)$$

5.4.4 RMS Comparison Ratio (CR)

In order to observe the effect of the channel RMS value to the overall RMS value of a dataset, a comparison ratio can be tabulated for each channel RMS value. The comparison ratio is determined as follows:

$$CR = \frac{RMS_{channel}}{RMS_{overall}} \quad (5.7)$$

This ratio represents the RMS response at each transducer location compared to the average RMS response of the whole engine. It shows if any one area of the engine is responding differently than the rest of the engine. This would be the case if a defect were present in one region of the engine where a particular transducer was mounted. In the case where an engine is defect-free, the response at each measurement point selected on the engine should be relatively similar in form and in amplitude to the overall response of the engine. Therefore, the theoretical target value for the CR of each channel of data is 1.

5.5 Frequency Domain Analysis

In many cases, data analyzed in the time/position domain doesn't provide the required diagnostic information regarding the vibration signals collected. For this reason, it is necessary to analyze this data in the frequency domain in order to extract the desired information. There are many software packages and signal analyzers available that have the capability to perform frequency-domain manipulation as well as representation of

data. Moreover, there are a number of methods available to analyze data in the frequency domain. The following sections describe the methods that were used in the study.

5.5.1 Fourier Transform

A frequency analysis method that has been used extensively since its discovery in a variety of applications is Fourier Analysis. The basis for this method is that the signal being investigated is composed of a number of sine and cosine functions with a given amplitude and phase at varying frequencies, which can be decomposed into its frequency components through mathematical manipulation. The Fourier transform can take many forms depending on the manner in which the analysis is to be conducted as described in detail by Randall [43]. The fundamental form of the Fourier transform is the Integral transform, which assumes an infinite and continuous manner in both the time and frequency domain. It is represented by the following Fourier transform pair shown below:

$$G(f) = \int_{-\infty}^{\infty} g(t)e^{-j2\pi ft} dt \quad (5.8)$$

$$g(t) = \int_{-\infty}^{\infty} G(f)e^{j2\pi ft} df \quad (5.9)$$

The Fourier series is composed of a periodic time domain signal but results in discrete components in the frequency domain. For sampled time functions, the time domain is in a discrete form, which then results in a continuous and periodic frequency spectrum. The most useful form of the transform when used with real, digitally sampled data is the Discrete Fourier Transform, which results from data that is sampled in both the time and

frequency domains. This form of the Fourier transform was used in the study and will be discussed in the following section.

5.5.2 Discrete Fourier Transform

As mentioned above, the most useful form of the Fourier transform for digitally sampled data is the Discrete Fourier Transform (DFT). Essentially, it replaces the Integral transform equation with a finite version. The forward and inverse transform pair is shown below:

$$G(k) = \frac{1}{N} \sum_{n=0}^{N-1} g(n) e^{-j \frac{2\pi kn}{N}} \quad (5.10)$$

$$g(n) = \sum_{k=0}^{N-1} G(k) e^{j \frac{2\pi kn}{N}} \quad (5.11)$$

When applying the DFT to data collected in the time-domain, it is necessary to compute a large number of complex multiplications in order to generate a useful frequency spectrum. This is a computationally exhaustive process and not practical when performing real-time analysis. For this reason, an algorithm has been developed that greatly reduces the number of computations to be performed. This calculation procedure is known as the Fast Fourier Transform and is the most commonly used frequency analysis tool found in industry today.

5.5.3 Fast Fourier Transform

As stated in the previous section, computation of the DFT is quite extensive and contains a large number of arithmetic operations. The Fast Fourier Transform (FFT) is an

algorithm that results in a DFT with a greatly reduced number of computations in comparison with the direct evaluation of the DFT. The FFT is possibly the most widely implemented signal analysis technique used for data analysis in industry today.

In using the FFT, the number of data samples must be of the order 2^n where $n = 0, 1, 2, \dots, n$, due to the nature of the algorithm itself. It is shown by Randall [43] that the FFT algorithm produces the identical result to the direct application of the DFT with the added advantage of a greatly reduced amount of calculations.

5.5.4 Auto Power Spectrum

A useful form of the computed FFT frequency spectrum is the Auto Power spectrum. This spectrum is generated by adding the negative frequency components of the FFT spectrum to the positive ones, essentially doubling them in the process. The result is a 1-sided spectrum of values that have units of input signal units rms squared. The Auto Power spectrum is defined in the following manner:

$$\text{Auto Power Spectrum}(x) = \frac{FFT(x)FFT^*(x)}{n^2} \quad (5.12)$$

where x is the input time-domain data signal and n (a power of two) is the number of points in the signal.

The Auto Power spectrum is very helpful in identifying key frequency components in the resulting spectrum. However, since all "imaginary" components have been removed and the spectrum is composed of entirely "real" amplitudes, phase information is lost and the original time signal cannot be recreated. An Auto Power spectrum generated from a "good" engine is shown in the following figure.

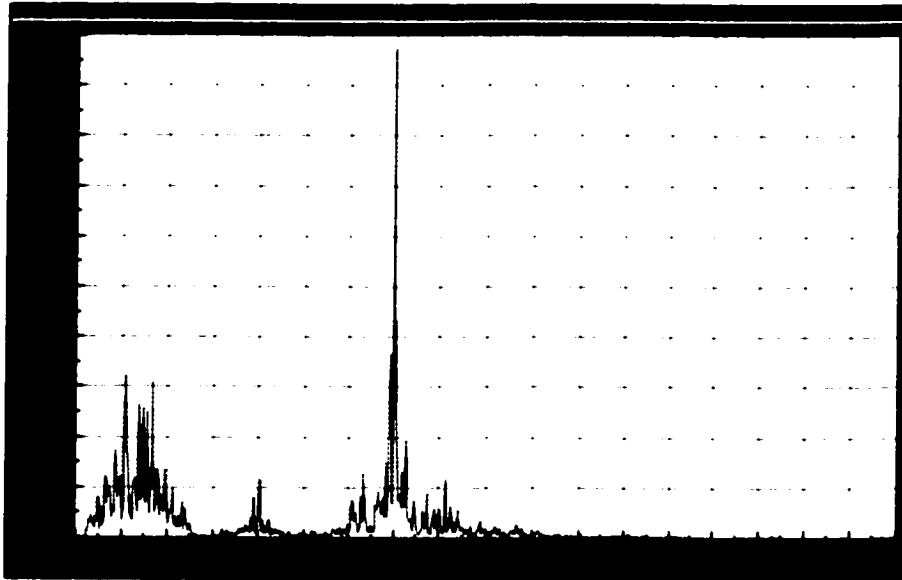


Figure 5.6 An auto power spectrum of block vibration from a "good" engine. There are 3 noticeable frequency components. Note: unit of frequency is in Order as opposed to Hz.

5.5.5 Order Analysis

Order analysis is another frequency analysis technique that is generally performed on noise or vibration data collected from mechanisms with rotating components (i.e. internal combustion engines). The main difference between order analysis and conventional frequency analysis is that the resulting spectrums are a function of order (harmonics of the rotational speed) as opposed to a function of frequency (i.e. Hz).

The main concept behind order analysis is to lock the sampling locations to constant shaft angles so that even if the speed changes, the sampling locations will still occur at the same shaft angles and the frequency content of the signal will be a function of order, independent of the rotational speed.

There are two methods of obtaining a vibration signal sampled at constant shaft positions. The first is to use external sampling, such as an external trigger, consisting of a di-magnetic pickup creating a trigger pulse from a toothed wheel attached to the crankshaft

of an engine. A second method would be to collect data in the time-domain and then digitally resample the data to constant shaft positions. Once the data is in such a form, applying an FFT on the data then transforms the position (angular) domain into the order domain. This is analogous to an FFT transforming the time domain into the frequency domain. The resulting spectral lines represent constant orders as opposed to constant frequencies.

Two important relationships that exist in the order domain are shown below:

$$o_{\max} = \frac{o_s}{2} \quad (5.13)$$

where o_s is the angular sampling frequency.

$$\Delta o = \frac{1}{R} = \frac{o_s}{N} \quad (5.14)$$

where R is the total number of revolutions and N is the FFT block size.

5.6 Mahalanobis-Taguchi System

A modern pattern recognition method currently used in many areas of research and industry is the Mahalanobis-Taguchi System (MTS). This method uses a factor known as the Mahalanobis distance (MD), which is used to distinguish the pattern of a certain group from other groups. For a "normal" group, the MD should be close to 1 for each element in the group. This distance will increase as the elements become more deviant from the norm. The accuracy of the MD distance against the measured variables is known as the Signal-to-Noise (SN) ratio, which helps in determining which variables are more sensitive to changes in the data.

The systematic steps of the method provided by Taguchi are parameter design, the selection of the "normal" group and selection of the data's variables using an orthogonal array and the SN ratio. This method is both applicable in the area of diagnosis and forecasting of abnormal groups of data.

The MTS method uses a series of matrix manipulations to arrive at decisions regarding data in the groups. This method has the ability to distinguish an abnormal test result from a normal test result granted a known reference group has been established. The mathematical procedure to determine the MD is shown in Appendix C.

CHAPTER 6.

RESULTS AND DISCUSSION

This chapter will present the experimental results of the tests conducted for the purpose of detecting engine defects on-line through the analysis of engine noise and vibration signatures. The areas covered in this chapter include investigation of the validity of the transducers selected, their locations for the test setup as well as the validity of the data collection sampling methods being used. Experimental results will be presented for both good and defective engines that were tested at the cold test station. The use of various analysis methods will then be presented to determine which defects are detectable, which methods are feasible to use and what, if any, transducers are redundant. Finally, a performance matrix will be presented showing the optimal test setup required to efficiently detect a large number of engine defects.

6.1 Cold Test Transducer Feasibility

One of the main goals of this study is to use appropriate transducers at optimal locations to detect engine noise and vibration on-line in an industrial environment. Testing in an industrial environment is somewhat different than testing in a laboratory environment. Many factors are introduced once a test system is implemented on-line, such as meeting cycle time, differentiating factory noise and vibration from that of the engine, dealing with uncontrollable climate conditions and ensuring that tests aren't influenced by on-line personnel. For this reason, not all transducers are feasible to use in such an environment.

This section discusses the transducer selection method used in the study including the reasons why certain transducers weren't used due to constraints imposed by the factors mentioned above.

6.1.1 Accelerometers

The most commonly used transducer for the acquisition of engine vibration signals in industry today is the accelerometer. Due to its size, relative low cost, simplicity, performance and availability, it has been a popular transducer choice for many years.

The B & K Type 4366 charge mode accelerometer is the optimal transducer for this study, since it is relatively small and can withstand the harsh factory conditions while providing a good vibration signal. It is capable of accurately measuring surface-borne vibration off of various surface types. The following figures show results from measurements taken from a cast iron block and a cam cover bolt head.

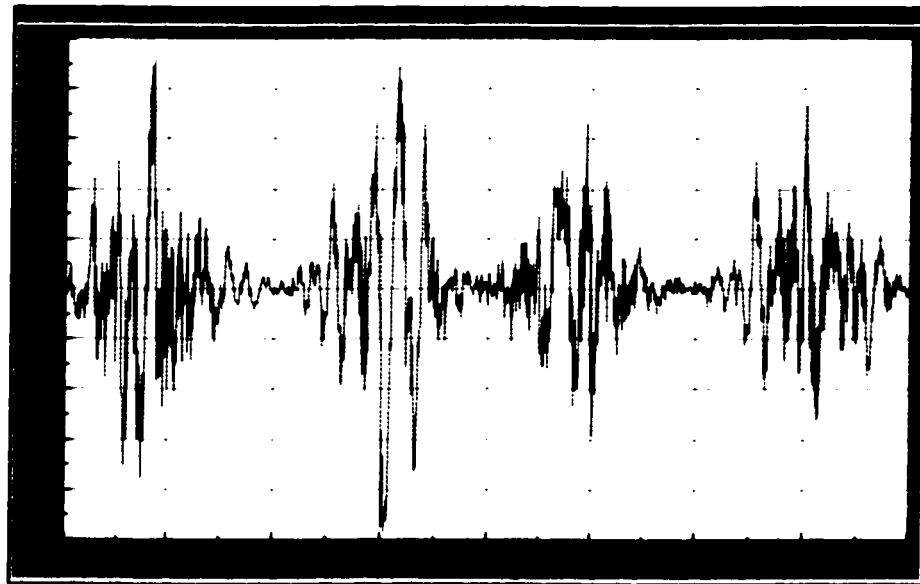


Figure 6.1 Accelerometer vibration signal captured from the valley area of a cast iron cylinder block in the detection of a non-machined cylinder bore surface.

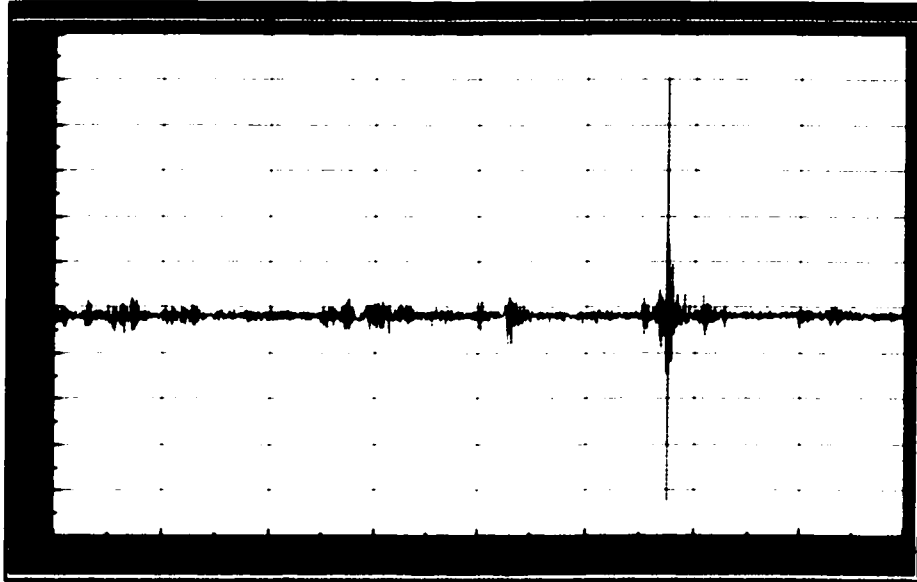


Figure 6.2 Accelerometer vibration signal captured from a cam cover bolt head on a 4.6L 4-valve engine to detect a gross valve tick.

The figures easily show the vibration detection capabilities of accelerometers when mounted on either the cylinder block or cam cover of the engine. For this reason, accelerometers will be used to capture vibration signals in the on-line testing process for the purpose of engine defect detection.

6.1.2 Laser Vibrometer

In the study, a Polytec IVS 200 laser Doppler vibrometer was used to capture vibration levels from a variety of engines. Measurement locations used included the locating lugs, the cylinder block walls and the cam covers. Due to the nature of the test surface and its perpendicularity to the test signal, the locating lugs were found to be the optimal location in order to achieve a strong vibration signal with a high signal-to-noise ratio from the laser vibrometer. The following figure demonstrates the capability of the laser

vibrometer to detect a non-cleanup cylinder bore when measuring surface velocity off of a locating lug.

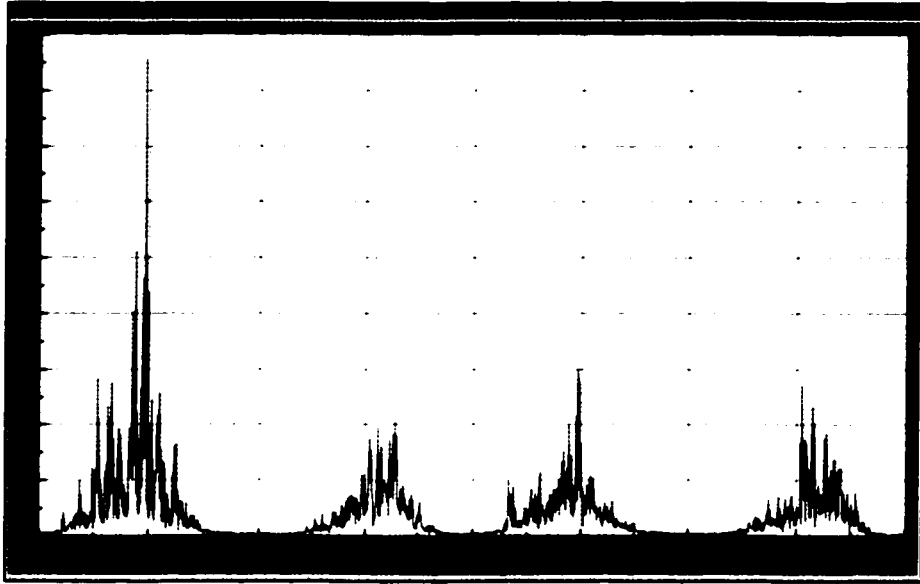


Figure 6.3 Laser vibration variance signal captured from the left front locating lug at cold test while detecting a non-machined cylinder bore.

It is apparent that the laser vibrometer is a good choice of transducer to use for acquiring vibration signals. However, it appears as though there are a number of limitations involved in using the laser vibrometer at the cold test station. The laser lens has an optimal stand-off distance in order to acquire a strong, clean signal. This would result in the laser vibrometer(s) being set back a certain distance and possibly interfering in the work-path of the cold test personnel. With the laser being quite sensitive to movement or interference, this may not be a feasible choice. Moreover, either four laser vibrometers would be required to capture a signal from each of the locating lugs on the engine or a complex mirror-laser system would have to be implemented to do so.

The feasibility of using the laser vibrometer as a defect detection transducer in a production setting will be investigated in the study.

6.1.3 Microphones

Microphones are one of the ideal transducers to use in order to detect abnormal noise emanating from devices such as internal combustion engines when operating in a controlled lab environment. However, the effective use of microphones in an industrial setting, in which the plant noise level is comparable with the noise level of the measured component, is more difficult to achieve. Sound pressure measurements were taken from running engines at the cold test station and were compared with normal plant sound pressure measurements. The following figure shows the comparison between both the sound pressure and the sound pressure level (SPL) of the two:

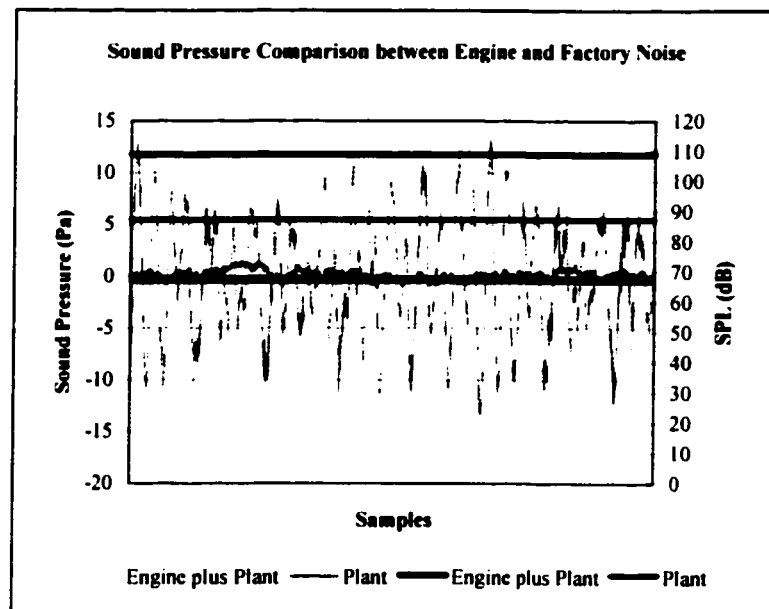


Figure 6.4 Comparison of noise measurements between engine and plant noise.

As can be seen in the previous figure, the sound pressure level of the engine and the plant (~108 dB) greatly exceeds that of the plant alone (~87 dB) by approximately 21 dB. Therefore, the contribution of the plant noise to the engine noise measurements appears to be minimal and thus, should have little effect on their outcome. For this reason, it should be feasible to acquire noise signals from the engine at the cold test station granted the microphones are mounted at an appropriate distance, only robust industrial design microphones are used and there is no interference from station personnel. These requirements will be met in the study in order to achieve feasible results.

6.1.4 Pressure Transducers

Detection of engine defects through the monitoring of pressure pulsations with the use of pressure transducers is usually a good method to use, if one has easy access to mounting locations in the engine. However, in many cases, this requirement is not met. Such is the case when considering the use of pressure transducers for engine defect detection at the cold test station.

There are a number of reasons why it isn't feasible to use pressure transducers at the cold test station:

1. If considering the use of in-cylinder pressure transducers:
 - a. An engine is fully assembled when tested at cold test, meaning all spark plugs would have to be removed in order to accommodate the pressure transducers. This process would not meet cycle time and is thus, not feasible.

- b. Combustion is required when measuring defects such as spark knock. The cold test station operates without the use of fuel and thus, no combustion occurs in-cylinder. Therefore, it would be ineffective to monitor in-cylinder pressures without combustion.
 - c. Prior to the fully assembled engine reaching cold test, an in-cylinder compression test is performed on a partially assembled engine using pressure transducers mounted in the spark plug holes. This test is used to detect missing components or incorrectly timed engines. With no combustion process present, the compression test essentially monitors what an in-cylinder pressure test would monitor at cold test, making it a redundant test.
2. If considering the use of pressure transducers mounted in other engine galleries or ports:
- a. Cycle time would not be met if hole plugs had to be taken out prior to the test and then re-installed once the test was complete.
 - b. The current system has a variety of test stations, prior to cold testing, that monitor pressures and leak rates in the oil and coolant cavities. It would be inefficient to perform the same test again at the cold test station.

For the reasons mentioned above, pressure transducers will not be used in the study for the on-line detection of engine defects. Their usage is more suitable, but not limited to, a laboratory environment in which cycle time is not a factor, the combustion process is present and transducer locations can be modified without affecting the entire test system.

6.1.5 Knock Sensor

Acquiring the knock sensor signal of an engine can be valuable if vibration occurs in the vicinity of the engine block. In general, the knock sensor is used as a means to monitor vibration due to spark knock. However, being that there is no combustion occurring when an engine runs at cold test, the knock sensor would be used in monitoring vibration resulting from mechanical impacts rather than combustion knock. It's defect detection capabilities will be investigated in the study. The following figure shows a knock sensor vibration signal acquired at the cold test station.

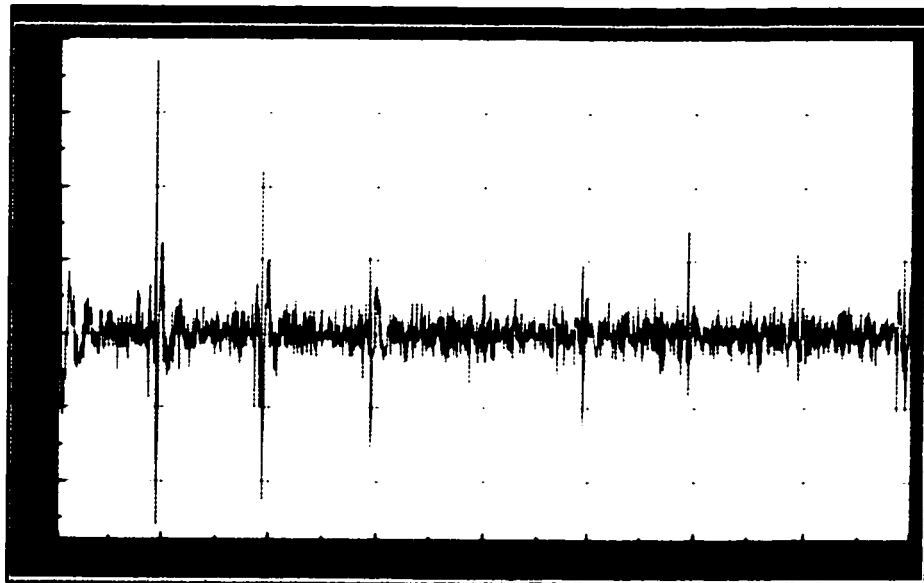


Figure 6.5 Vibration signal captured from the knock sensor at cold test.

6.1.6 Transducer Locations

As was explained above, the transducers to be used for the study are charge mode accelerometers, a laser Doppler vibrometer, microphones and a knock sensor. The transducer setup at cold test was as is shown in Figure 6.6. As can be seen in the figure,

an accelerometer was mounted on each of the 4 lugs of the engine, the laser was mounted in 4 separate locations so that the laser beam was directed at each lug, the two microphones were located in the vicinity of the front and rear lugs and the knock sensor was mounted in the valley portion of the cylinder block.

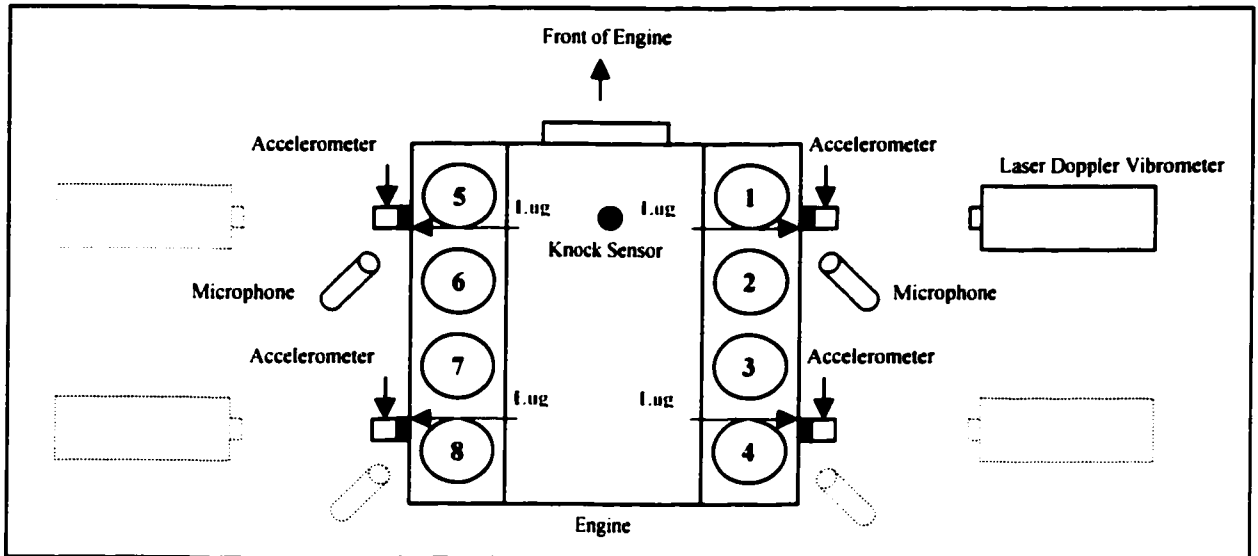


Figure 6.6 Transducer setup used at the cold test station as seen from the top view of the engine.

6.2 Triggering Method Validity and Data Positioning

In the preliminary testing conducted in the dynamometer test cells, an external trigger (diamagnetic pickup and 720-tooth flywheel) was used to sample data so that all measurements taken were with respect to crankshaft position, not time. The reference point for all measurements was the crankshaft angle at which the piston of cylinder #1 was at top dead center (TDC) on the power (firing) stroke. The reference position was determined from the Camshaft Identification signal that was obtained from the CID sensor located on the left-side cam sprocket attached to the camshaft. The CID signal generates a discontinuous sine wave once per engine cycle and appears as follows:

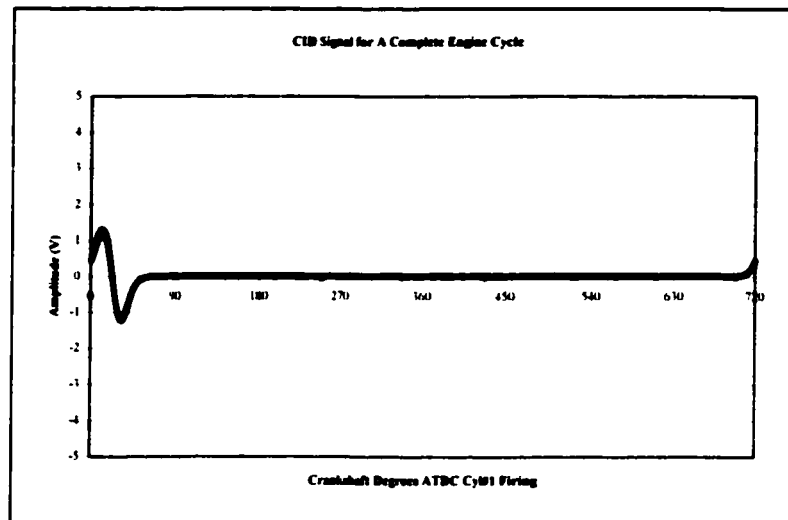


Figure 6.7 Camshaft identification signal acquired from CID sensor.

As a design parameter of the engine, the sine wave zero-crossing of the CID signal occurs exactly 22° after top dead center of cylinder #1 on the power stroke. Therefore, by simultaneously collecting the CID signal with the vibration signals and then offsetting all of the data with respect to TDC of cylinder #1 on the power stroke, a consistent reference position was established so that valid comparisons were made from test to test.

For the case of the on-line tests conducted, an internal triggering method based on time was utilized to collect the required data. For the study, all measurements taken were to be analyzed in the position domain in order to link defects with crankshaft angle. In order to accomplish this, all data was sampled based on time and then re-sampled into the position domain using a custom built post-processing application.

The application requires both the CID signal and the CPS (Crankshaft Position Sensor) signal to properly re-sample the data into the position domain. The CPS signal is generated from a variable reluctance sensor that magnetically detects the rise and fall of teeth on a toothed wheel attached to the crankshaft. There are 36-minus-1 (1 missing

tooth) equally spaced teeth on the wheel and for every tooth detected, the sensor outputs a sine wave with an amplitude that is proportional to the speed of the engine. Since the toothed wheel is attached to the crankshaft, for one complete engine cycle the toothed wheel revolves twice and as a result, the missing tooth is detected twice and represents a reference point from TDC of cylinder 1 for both the intake and power strokes. The CPS signal is required in the re-sampling process to increase the accuracy of conversion from the time to position domain. The relative appearance of both the CID and CPS signals are shown in Figure 6.8.

To test the validity of the re-sampling process, an engine with vibration spikes in known positions was tested using both the external triggering method and the internal triggering method with adaptive re-sampling to see if both provided the same results. Figures 6.9 and 6.10 show the resulting vibration signals acquired using both methods.

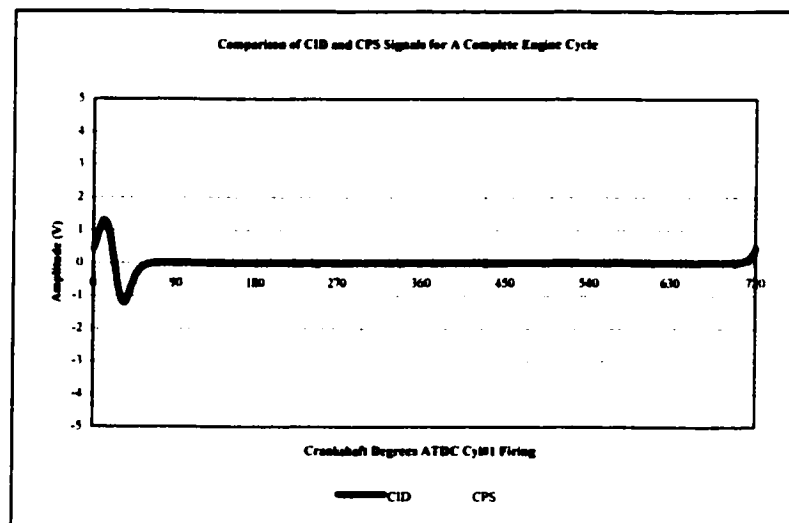


Figure 6.8 Comparison of the CID and CPS signals relative positions over one engine cycle.

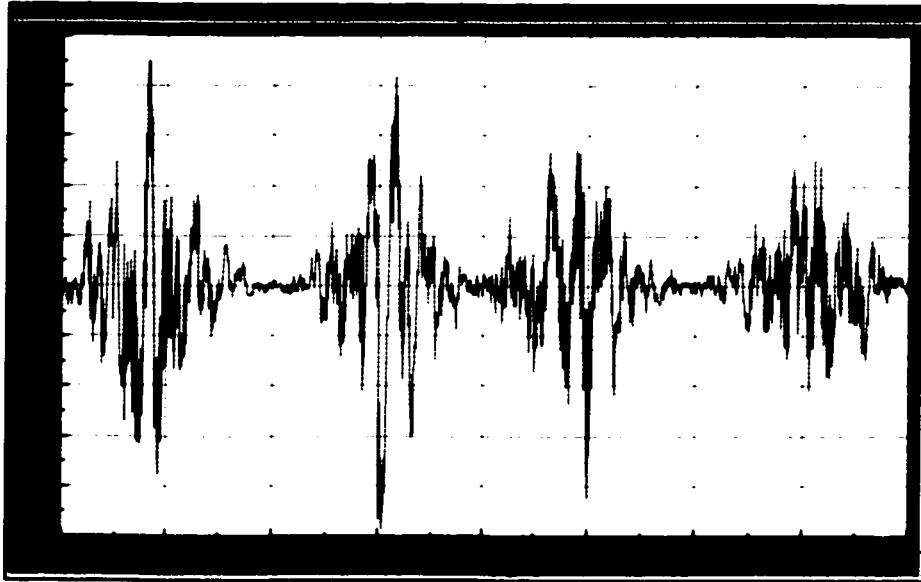


Figure 6.9 Vibration signature from external triggering method.

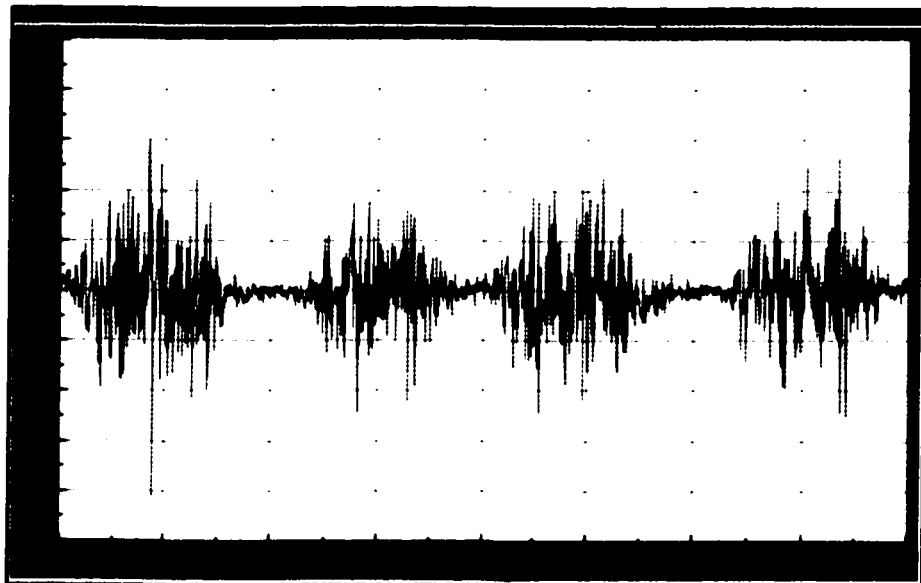


Figure 6.10 Vibration signature from adaptive re-sampling method.

As can be seen in Figures 6.9 and 6.10, the vibration signals are quite similar with the spikes occurring at the same crankshaft positions. It is important to note that since these

vibration signatures were captured at different measurement locations, engine speeds and test setups, their amplitudes are dissimilar and their appearance is slightly altered. However, their vibration spikes occur at coincident crankshaft angles. Therefore, this validates the use of the adaptive re-sampling technique that was used for all data acquired on-line at the cold test station.

6.3 Baseline Measurement Results

In order to use vibration measurements as a basis for engine defect detection, the vibration measurement patterns of suspected "good" engines were determined. Once established, proper limits were then set to baseline the acceptable vibration levels that an engine can exhibit. In doing so, 30 engine vibration signatures were captured from the cold test station and analyzed.

6.3.1 Mahalanobis Distance

In order to establish a group of engines that represented the normal or "good" engine case, the Mahalanobis Distance (MD) method was utilized for this purpose. This method has the capability of determining whether or not the suspected "good" engines fit the vibration patterns of the other engines in the "good" group. It is necessary to use a statistical method for this purpose so that baseline signatures can be established accurately. This was accomplished by acquiring the RMS vibration values from each transducer location for each of the 30 engines while being run at the cold test station. The resulting matrix of observations (RMS values) appeared as follows:

Engine	Channel Overall RMS Values (g)			
	Channel 1 (Cyl 1,2)	Channel 2 (Cyl 3,4)	Channel 3 (Cyl 5,6)	Channel 4 (Cyl 7,8)
Good Engine 1	0.45	0.35	0.34	0.31
Good Engine 2	0.44	0.34	0.35	0.29
Good Engine 3	0.44	0.34	0.32	0.29
Good Engine 4	0.42	0.35	0.32	0.28
Good Engine 5	0.36	0.36	0.33	0.24
Good Engine 6	0.35	0.35	0.32	0.23
Good Engine 7	0.35	0.34	0.32	0.22
Good Engine 8	0.37	0.33	0.32	0.23
Good Engine 9	0.45	0.36	0.35	0.31
Good Engine 10	0.45	0.38	0.35	0.30
Good Engine 11	0.44	0.36	0.34	0.29
Good Engine 12	0.51	0.39	0.33	0.35
Good Engine 13	0.50	0.40	0.33	0.35
Good Engine 14	0.50	0.39	0.32	0.35
Good Engine 15	0.49	0.39	0.31	0.35
Good Engine 16	0.50	0.39	0.33	0.35
Good Engine 17	0.41	0.38	0.35	0.30
Good Engine 18	0.42	0.39	0.33	0.30
Good Engine 19	0.41	0.37	0.34	0.29
Good Engine 20	0.46	0.39	0.33	0.32
Good Engine 21	0.41	0.34	0.35	0.27
Good Engine 22	0.41	0.36	0.37	0.28
Good Engine 23	0.36	0.35	0.36	0.24
Good Engine 24	0.42	0.39	0.34	0.29
Good Engine 25	0.41	0.39	0.32	0.28
Good Engine 26	0.41	0.36	0.31	0.27
Good Engine 27	0.41	0.36	0.31	0.26
Good Engine 28	0.40	0.34	0.31	0.26
Good Engine 29	0.36	0.36	0.36	0.24
Good Engine 30	0.39	0.35	0.34	0.27
Average	0.42	0.36	0.33	0.29
Std. Deviation	0.05	0.02	0.02	0.04
3 Sigma	0.14	0.06	0.05	0.11
Upper Limit ($\mu + 3\sigma$)	0.56	0.42	0.38	0.40

Table 6.1 Matrix of observations (channel RMS values) for each baseline engine.

By performing a series of matrix manipulations on the observational data (as is shown in Appendix C), the resulting Mahalanobis Distances were determined and are shown in the following figure:

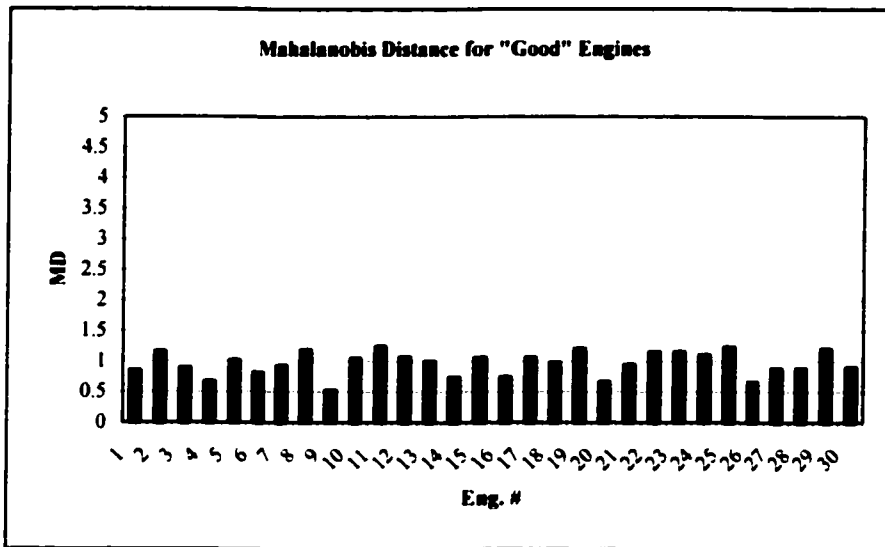


Figure 6.11 MD for each of 30 engines tested as part of the baseline "good" group.

For this study, if the MD value for each engine lies in the proximity of 1, then it will be classified as a member of the "good" group. In general, a MD value of 1 or less is usually the requirement for observations to fit the pattern of the "good" group well. However, in this study, due to the inherent variability that exists between different engine types tested, MD values close to 1 will be acceptable. Therefore, as can be seen above, the 30 engines tested have quite similar patterns since all of the MD values are close to a value of 1 and thus, they will be used as the baseline group for the study.

A variability study was conducted to observe the trends that exist for the vibration levels at each transducer location as well as the vibration level variability from channel to channel. In doing so, one can set the appropriate upper and lower limits by which all acceptable engine data should lie within. The following figure shows the RMS acceleration values at each transducer location for each of the 30 engines tested.

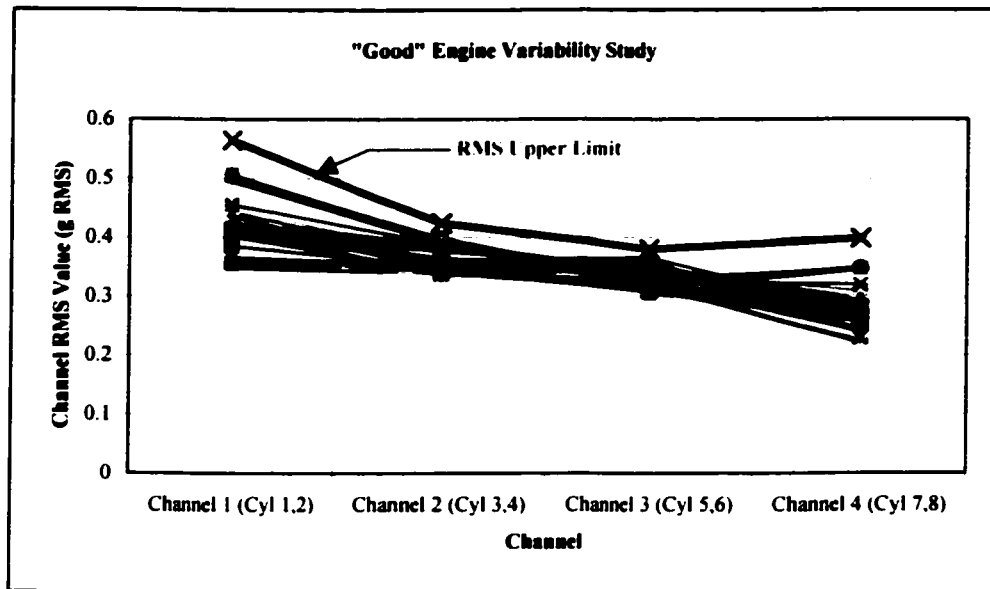


Figure 6.12 RMS acceleration values for each transducer for each of 30 baseline engines tested.

As can be seen from the above figure, there exists little variation between engines when considering the vibration levels from each transducer. However, it is apparent that there is some variability when comparing the vibration levels from channel to channel. This is due to the inherent differences in vibration response that various areas of the cylinder block (transducer locations) will have. Since the variability is quite small, the baseline values are quite acceptable and will be used with confidence as the values by which all other engine vibration will be measured against.

The upper limits of each channel were determined as the channel average value plus three times the channel standard deviation (3 sigma). The upper limits established above will be used in the study as a preliminary check to indicate whether the vibration level of a particular channel exceeds that of the baseline group. They will be used in conjunction with other defined limits to detect and diagnose defective engines.

6.3.2 RMS Comparison Ratio (CR) Results

For the 30 baseline engines tested, the average comparison ratio (CR) was determined for each and is shown in Figure 6.13.

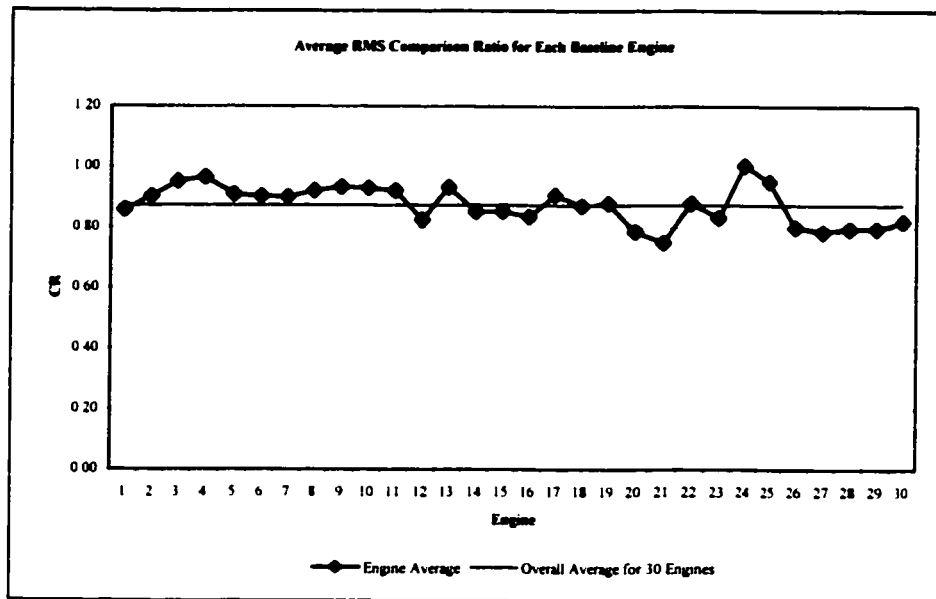


Figure 6.13 RMS Comparison Ratio for each of 30 baseline engines tested.

As can be seen in the figure, the comparison ratio for each engine generally lies in the range of 0.8 to 1.0. This is expected since all of the engines tested are defect-free, meaning that the response from each transducer location should be consistent with the overall response of the engine.

The RMS comparison ratio (CR) will be used in the study as a diagnostic tool in identifying regions of the engine that may have defects based upon the vibration response from that particular region of the engine.

Based on the comparison ratio results from the baseline engines, the overall average of all engine CR values was found to be 0.873. As a result, an upper limit of 0.9 will be used in

the study to identify engines with potential faults. This limit will be used in conjunction with other diagnostic tools in order to establish if a defect is present, where the defect is located and what the nature of the defect is.

6.4 Fault Diagnosis Using NVH Attributes

In general, engine vibration signals have certain attributes that will be relatively consistent from engine to engine. It is due to these attributes that threshold limits can be established in order to develop a fault diagnosis method. The attributes for vibration signals acquired at cold test are as follows:

1. Defect-free engines will have a consistent low amplitude distribution with no distinctive vibration spikes present as is shown in Figure 6.14.
2. Vibration signatures from defective engines will contain spikes occurring at least once to twice per revolution of the crankshaft for mechanical impacts. These vibration spikes will have amplitudes much greater than those from a defect-free engine. An example of such a signal is shown in Figure 6.15.
3. The duration of the vibration spike will be related to the nature of the mechanical impact or to the contact area of the defective components.

As explained in the previous sections, both the channel RMS and CR values will be used in the study as part of the defect detection process. However, using these values as diagnostic parameters can only give information regarding the condition of a certain region of the engine and not a specific location or a suspected defect. For this reason, variance signature analysis will also be used as a diagnostic parameter to help identify particular defects and where they occur in the engine.

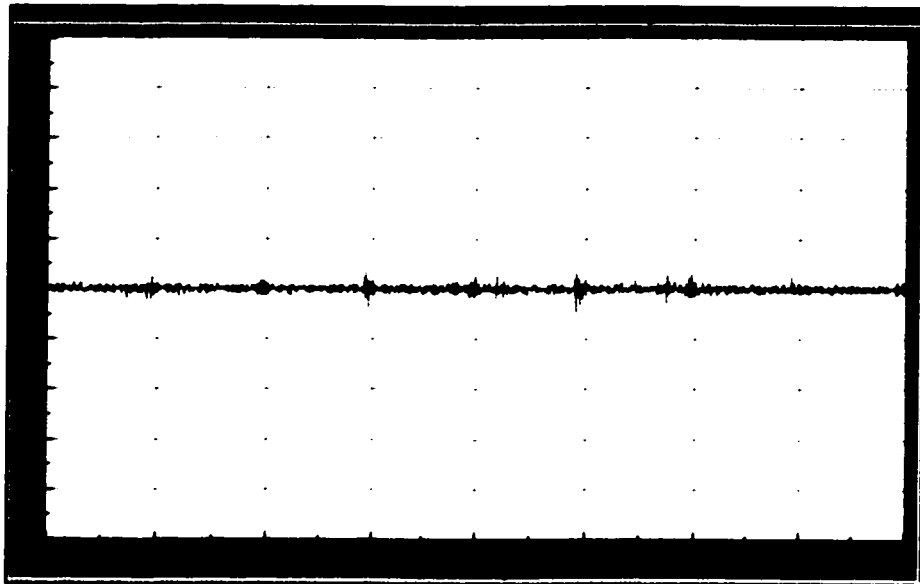


Figure 6.14 An average raw data trace captured by an accelerometer from the lug of a good engine.

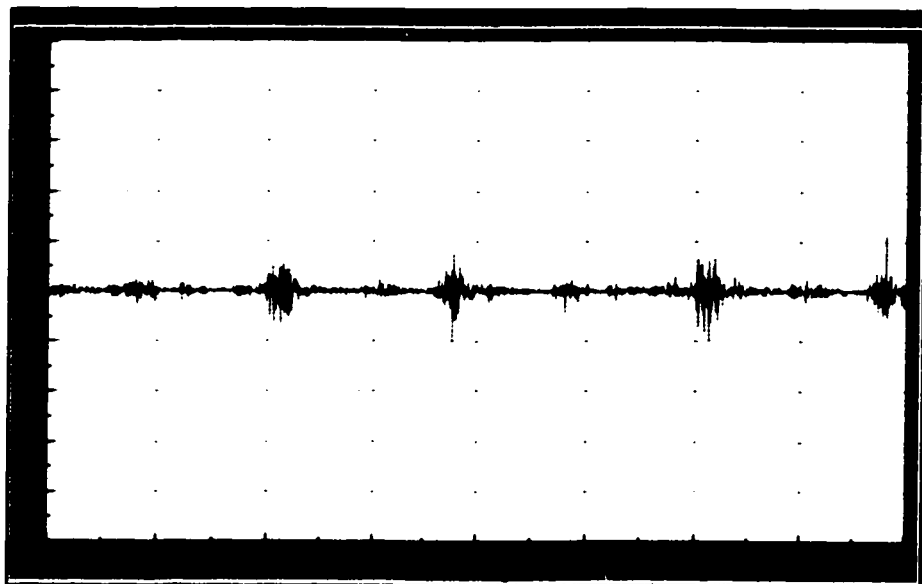


Figure 6.15 An average raw data trace captured by an accelerometer from the lug of a defective engine.

6.4.1 Variance Signature Analysis

Due to the cyclic operation of an internal combustion engine, vibration spikes should occur at relatively constant crankshaft positions from cycle to cycle. Moreover, where they occur and how many times per cycle will determine which cylinder the defect is related to and possibly identify the nature of the defect itself.

Variance analysis is a useful tool for extracting semi-periodic components from a set of data. This type of analysis is useful in attenuating amplitudes of normal occurring data values to a low level in order to better observe and exaggerate the semi-periodic components of the signal. As well, since the variance process squares all of the data, all data values are positive, which makes developing a diagnostic algorithm much easier.

In the study, the cyclic structure of the data was broken down into 8 bands each covering 90° of the total 720° of a cycle as is shown in Figure 6.16. In each band, the maximum variance value over the 90° period was compared to adjacent maximum values to observe if the distance between them and their relative amplitudes were within the acceptable limits.

Since measurements were taken primarily on the locating lugs of the engine, each of the 4 locations will account for information regarding 2 cylinders. For this reason, it was necessary to consider not only the relative amplitudes and distances between spikes but also to consider the actual bands into which the spikes fall. This was an essential part in identifying the cylinder in which the defect was present as well as the nature of the defect.

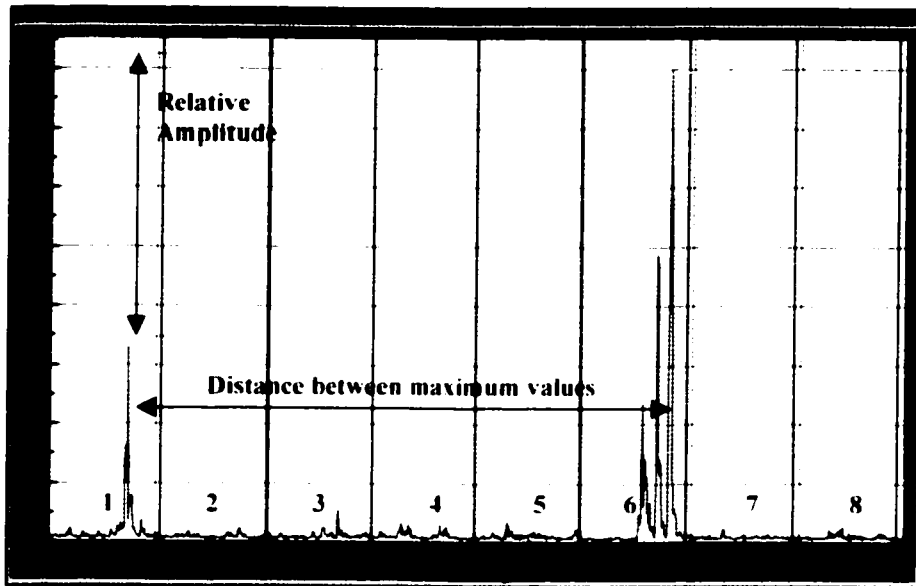


Figure 6.16 Fault diagnosis method that includes 90° bands of data, relative amplitude values and distance between band maximum values.

6.4.2 RMS, CR Threshold Levels

As established from the baseline test results, defect-free engines exhibit certain patterns regarding their RMS values as well as their comparison ratio (CR) values. Threshold limits have been established for each parameter based on the baseline results of 30 engines.

In general, if an engine defect is present and is to be detected, its vibration amplitude must exceed the threshold limits established for both the RMS level and the CR. Therefore, in the study, in order for a full fault diagnosis to take place, the initial criteria that both the acceptable RMS levels and CR levels must be exceeded. Once this is the case, then there is a need to identify if and where a defect is present through the use of the variance signature analysis method described in the previous section.

6.5 Cold Test Fault Diagnosis Results

The on-line cold test station was used to conduct the NVH tests for all of the baseline and defective engines. The engines were driven by an electric motor without fuel (i.e. no combustion) at a constant speed of 600 RPM for a duration of 18 seconds. Data was time sampled for the entire test period and then re-sampled into the position domain for a period of at least 40 cycles.

Vibration measurements were taken using a charge mode accelerometer mounted on each of the 4 locating lugs of the engine, a knock sensor mounted in the valley portion of the cylinder block and a laser Doppler vibrometer directed at each of the 4 locating lugs of the engine.

Noise measurements were taken using robust internally amplified microphones located just below the locating lugs of the engine.

A variety of data analysis methods were investigated in order to determine their applicability for the detection of engine defects. Variance analysis, position domain averaging, (FFT) fast Fourier transform and statistical indicators such as RMS values were the analysis methods used in the study.

The defective engines chosen for the study were both vehicle assembly plant returns and dealership returns. These were engines that had component defects that were not detected at the assembly stage and therefore, were assumed as good engines and initially shipped out before eventually being returned for abnormal operation. These engines were chosen since they were undetectable by the current in-process testing system. Therefore, if NVH testing can detect these defects, it will be a great cost and effort savings for the automotive engine production facility.

Engines with both known defects and reported defects were used in the study in order to verify customer complaints of engine noise and vibration. The engines tested had the following reported defects:

1. Non-machined #6 cylinder bore
2. Deep grooves in both cylinder #1 and #8
3. Lower-end rod knock due to excessive rod-to-pin clearance
4. Abnormal engine noise

Each of these engines were monitored for noise and vibration, the cold test results are shown in the following sections.

6.5.1 Detection of a Non-machined Cylinder Bore

A common defect that causes both engine noise and vibration is a non-machined cylinder bore, which is when a cylinder block machining process is either missed or due to a complication in the machining process, the surface of a cylinder bore is left rough and unfinished. The finish of a cylinder bore must be extremely smooth so that friction between the piston rings and bore is minimal and the piston rings do not make abnormal contact with the rough surface that would lead to ring degradation and wear. The surface borne noise and vibration is a result of the piston rings making contact with the rough areas of the bore for each stroke of the engine cycle.

Figure 6.17 shows the resulting averaged raw vibration signature from an engine with a non-machined #6 cylinder bore as collected by an accelerometer on the #3 lug of the engine. As can be seen in the figure, the areas in which the piston rings contact the non-machined areas of the cylinder bore stand out in the vibration trace as regions with large

amplitudes that are repeated from cycle to cycle. The vibration pulses occur in regions where the crankshaft angle is at 90°, 270°, 450° and 630° after top-dead-center of cylinder #1.

Data traces from the laser, microphone and knock sensor are shown in Figures 6.18, 6.19 and 6.20, respectively. As can be seen from the variance analysis of the laser data in Figure 6.18, it is apparent that the vibration spikes are easily visible. However, in both Figures 6.19 and 6.20, the signals acquired from both the microphone and knock sensor show no traces of any spikes present from the non-cleanup. The low-amplitude pulses present in the knock sensor signature can be attributed to the impacts associated with in-cylinder peak pressures when the piston in each cylinder is approaching top-dead-center. The location of the knock sensor is optimal for detecting such pulses or those related to combustion.

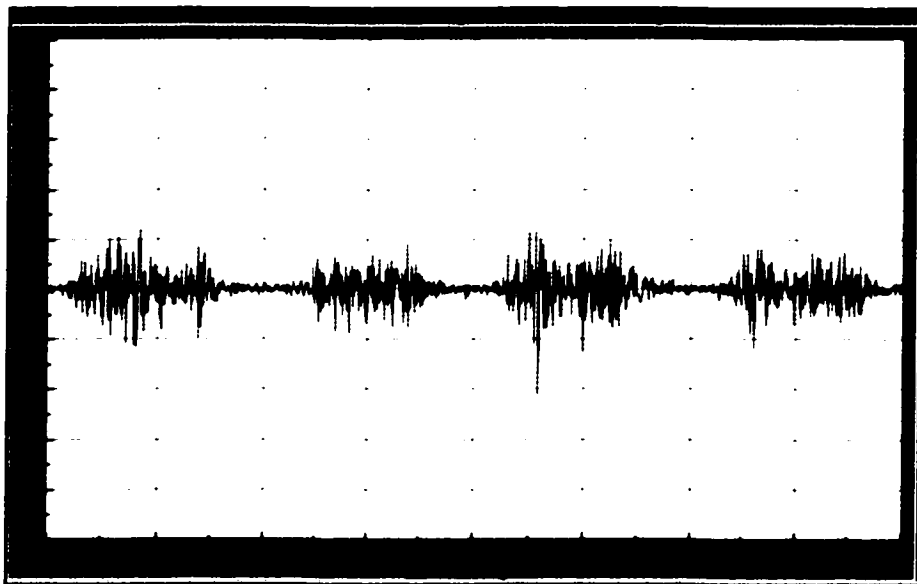


Figure 6.17 A 40-cycle average of raw data captured by an accelerometer from the #3 lug.

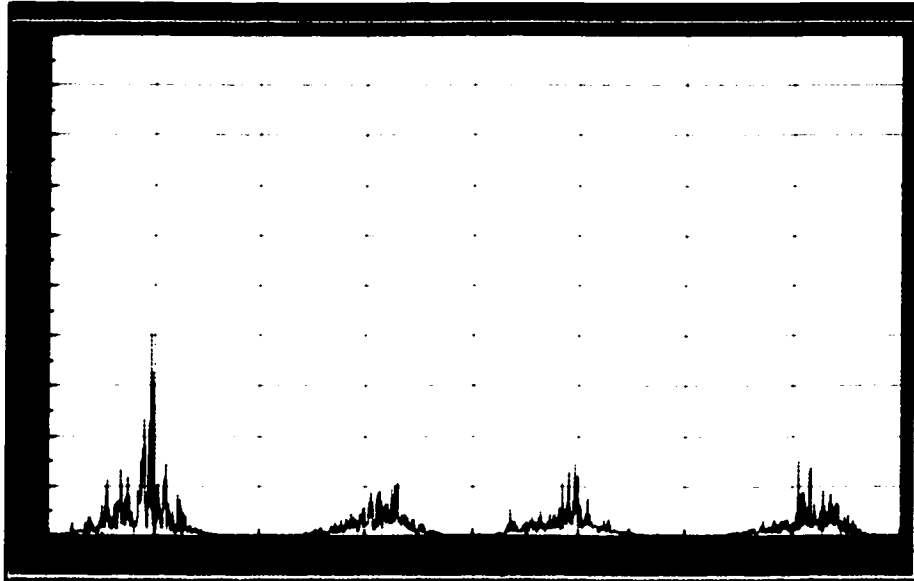


Figure 6.18 A 40-cycle average of variance data captured by the laser from the #3 lug.

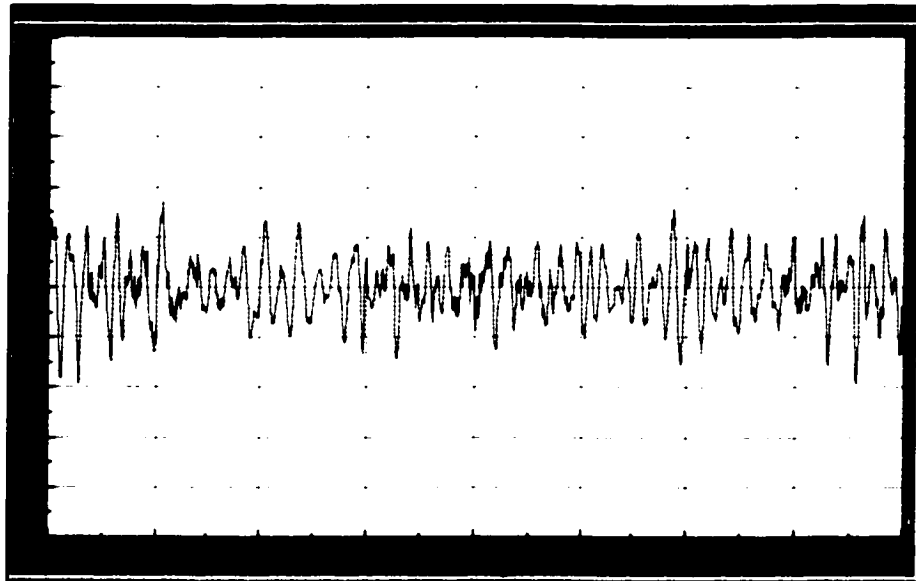


Figure 6.19 A 40-cycle averaged overall level captured by a microphone in the area of the #3 lug.

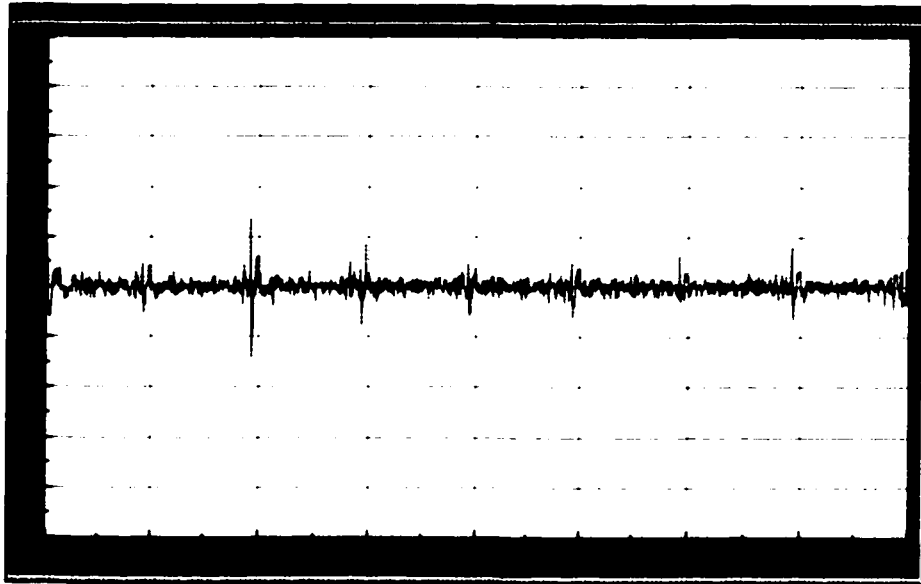


Figure 6.20 A 40-cycle average of raw data captured by the knock sensor in attempt to detect the non-cleanup of cylinder bore #6.

Using the algorithm developed for the study with the threshold limits set as described in previous sections, an attempt was made to detect the non-cleanup using the collected accelerometer data. The diagnosis was a success with the algorithm correctly identifying which cylinder, what portion of the cylinder and what the suspected defect was. A screen shot of the diagnosis form as well as the defect report are shown in Figure 6.21 and 6.22. As can be seen in Figure 6.21, both the channel RMS and CR values were exceeded for lug #3 (cylinder 5 and 6) and the relative amplitude and locations of the variance spikes fell within the proper limits in order to diagnose the defect to cylinder #6. The defect report found in Figure 6.22 gives a listing of the possible defects associated with such a signature. It is clear from the analysis that such a defect is detectable with the use of an accelerometer or laser vibrometer in conjunction with the diagnostic method developed in the study. A performance matrix is shown in Table 6.2.

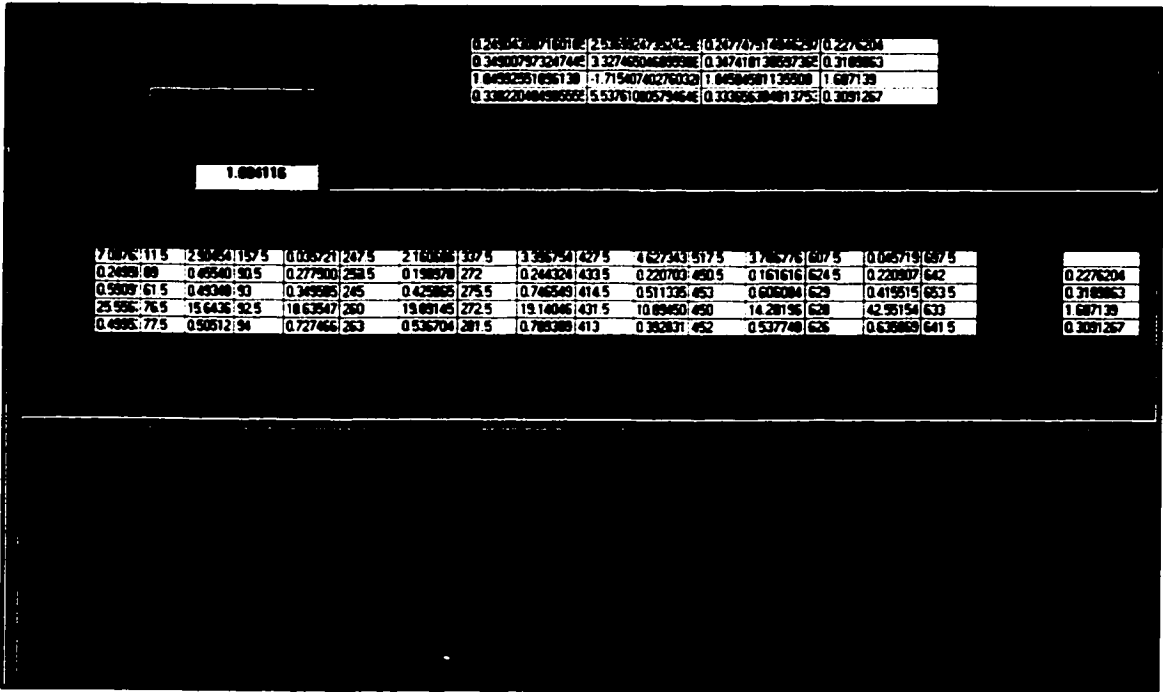


Figure 6.21 Diagnosis results from analysis of accelerometer data.

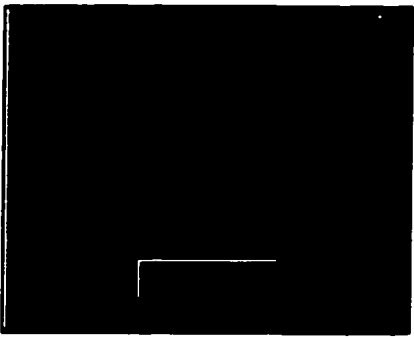


Figure 6.22 Defect report of diagnosis results.

Measurement Location	NVH Signature Characteristics			
	Accelerometer	Laser Vibrometer	Microphone	Knock Sensor
Lug 1 (Cyl 1,2)	N	N	N	N/A
Lug 2 (Cyl 3,4)	N	N	N	N/A
Lug 3 (Cyl 5,6)	A	A	N	N/A
Lug 4 (Cyl 7,8)	N	N	N	N/A
Block Valley	N/A	N/A	N/A	N

N – NVH signature exhibits normal characteristics, no defect detected

A – NVH signature exhibits abnormal characteristics, defect detected

N/A – Not Applicable

Table 6.2 Performance matrix of cylinder non-cleanup detection.

6.5.2 Detection of a Deep Groove in a Cylinder Bore

A defect that is similar in nature to a non-machined cylinder bore is a scored cylinder bore that results in a deep groove. This can result from a missed machining process or an incorrectly machined cylinder bore. One difference between this engine and the engine with the non-cleanup was that the deep groove appeared as a constant circumferential ring in both cylinder #1 and #8, whereas the non-cleanup appeared as a rough surface finish covering only a certain area of the bore and wasn't constant throughout its circumference. This was apparent from the signatures collected from the engine with a deep groove in both cylinder #1 and cylinder #8.

Figure 6.23 and 6.24 are the resulting variance plots of accelerometer data measured from lug #1 and lug #4, respectively. As can be seen, vibration spikes are identifiable, but due to the difference in their amplitudes, it is apparent that the defects vary in terms of severity. The amplitudes of the vibration spikes from lug #1 are a magnitude of 10 greater than those acquired from lug #4. However, all spikes exceed the acceptable limits for vibration amplitudes.

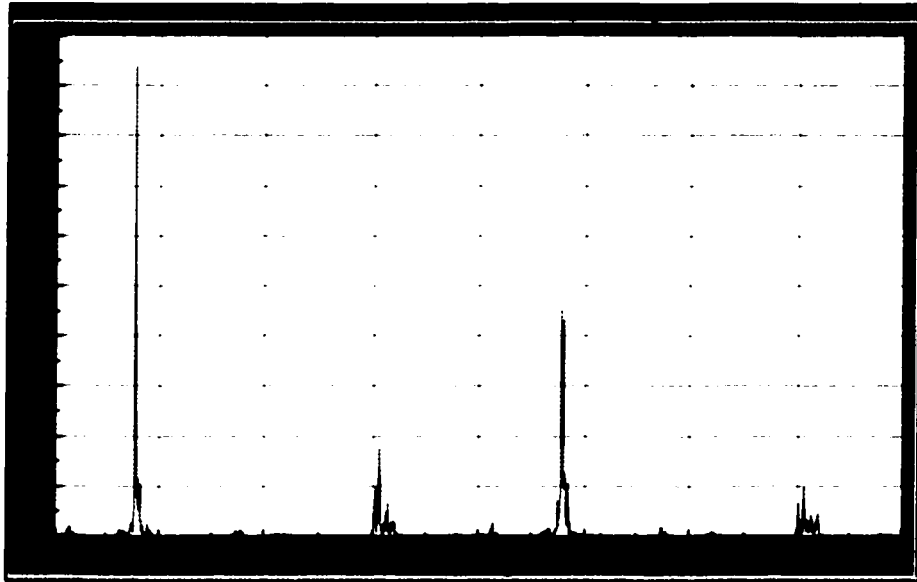


Figure 6.23 A 40-cycle average of variance data captured by an accelerometer from the #1 lug.

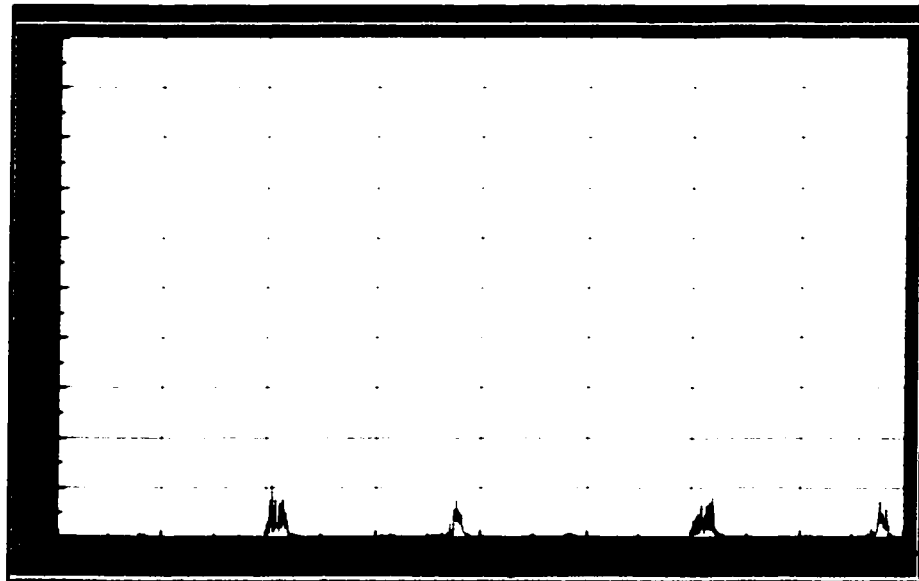


Figure 6.24 A 40-cycle average of variance data captured by an accelerometer from the #4 lug.

Figure 6.25 shows the raw data waterfall plot for 40 cycles of laser data collected at lug #1 of the engine. It is quite clear that vibration spikes are present and their location is in agreement with the data collected from the accelerometer.

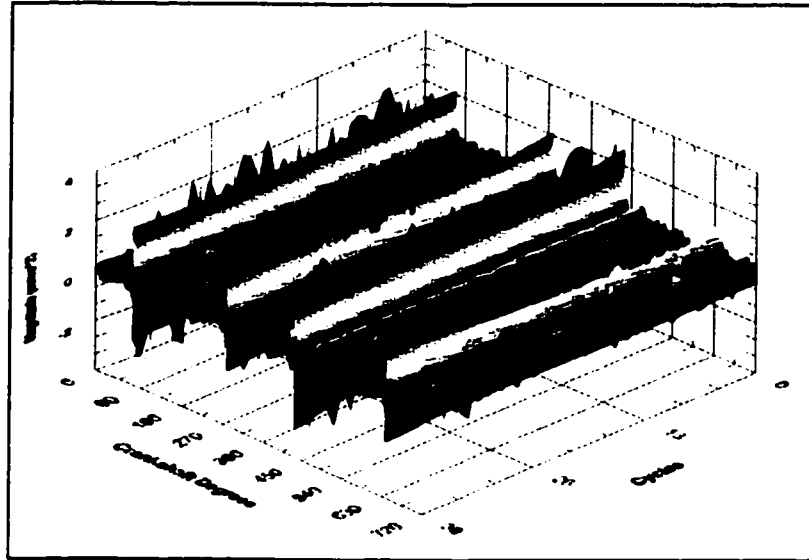


Figure 6.25 Waterfall plot for 40-cycles of raw data as collected by the laser vibrometer from lug #1.

The overall levels of noise collected from the microphones at each location once again provided no information regarding the defects present. Figure 6.26 shows an auto-power spectrum of the noise data collected from lug #1, shown in the order domain.

It appears as though there are visible components at a number of orders that may possibly be related to the deep grooves in the cylinder bore. However, upon inspection of the auto-power spectrum obtained from a defect-free engine, as shown in Figure 6.27, there is little difference that can be observed between the two spectrums. The frequency spectrum of data collected from these locations seems to provide no useful information regarding the detection of the defects present. It is apparent that the air borne noise due

to the defects under consideration is not as detectable as the direct surface borne vibration of the cylinder block.

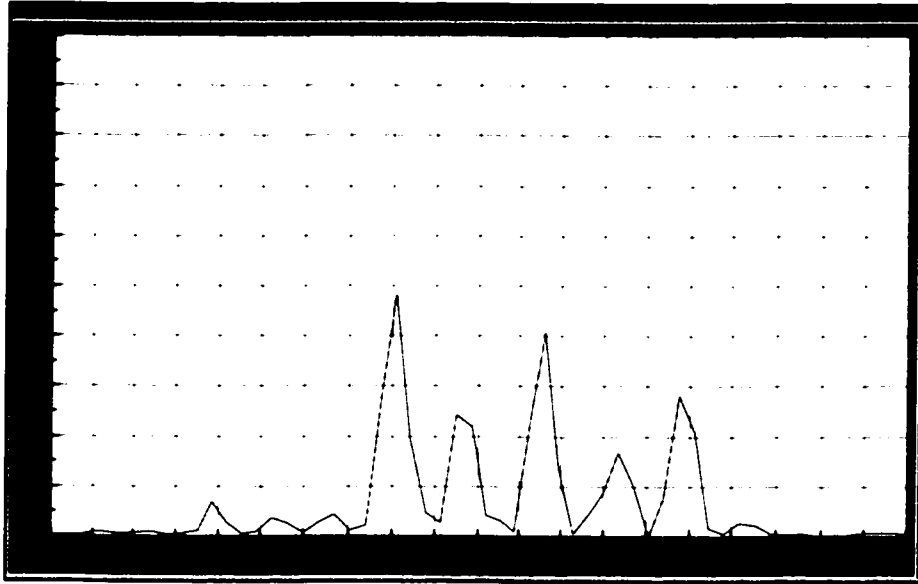


Figure 6.26 Auto-power spectrum of noise data collected from lug #1 of engine with deep groove in cylinder #1 and #8 (frequency shown in orders).

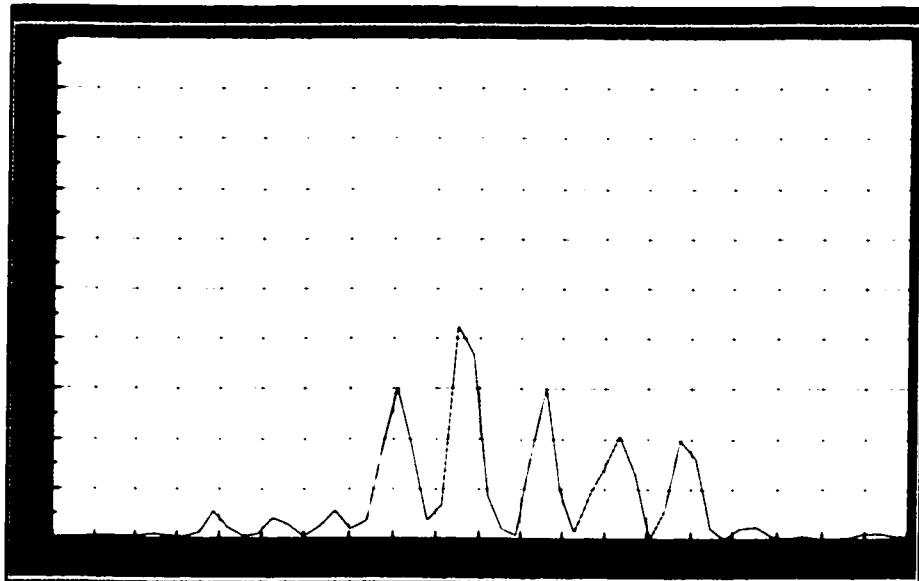


Figure 6.27 Auto-power spectrum of noise data collected from lug #1 of defect-free engine (frequency shown in orders).

Data collected from the knock sensor showed no signs of vibration spikes present to identify abnormal engine operation in the vicinity of the cylinder block. The only vibration pulses that were present were those from the impacts involved when each piston approached top-dead-center and peak in-cylinder pressures were achieved, as is shown in Figure 6.28.

Using the fault diagnosis algorithm developed for the study, the deep grooves in both cylinders were detected successfully. Based on the crankshaft angles at which the vibration spikes occurred and the relative amplitudes of the spikes, the algorithm correctly determined that the defects were in cylinder #1 and #8. Figure 6.29 shows a screen shot of the diagnosis form after analysis of the accelerometer data taken from the lugs of the engine. Notice that both lug 1 and lug 4 data were found to be unacceptable. Figure 6.30 shows the two defect reports resulting from the analysis of the vibration data.

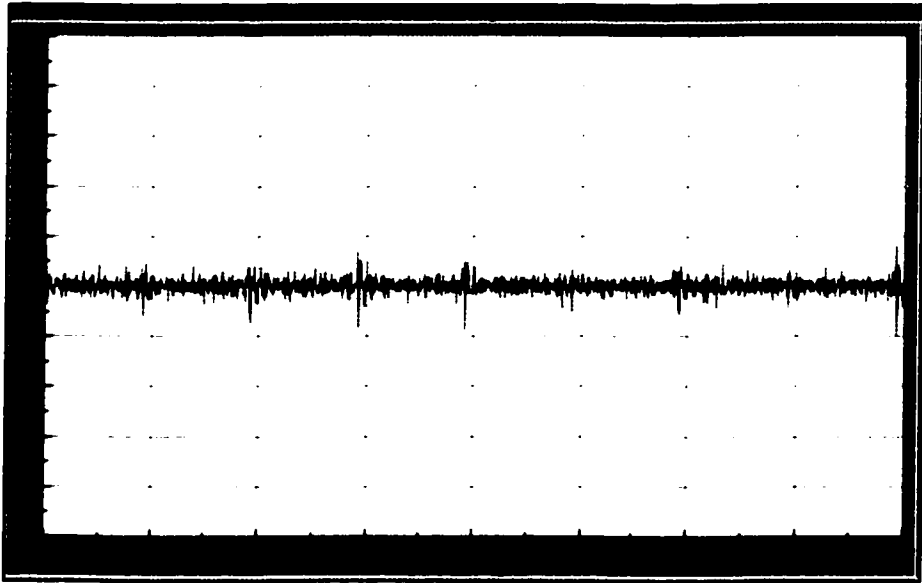


Figure 6.28 A 40-cycle average of raw data captured by the knock sensor in attempt to detect the deep grooves in cylinder #1 and #8.

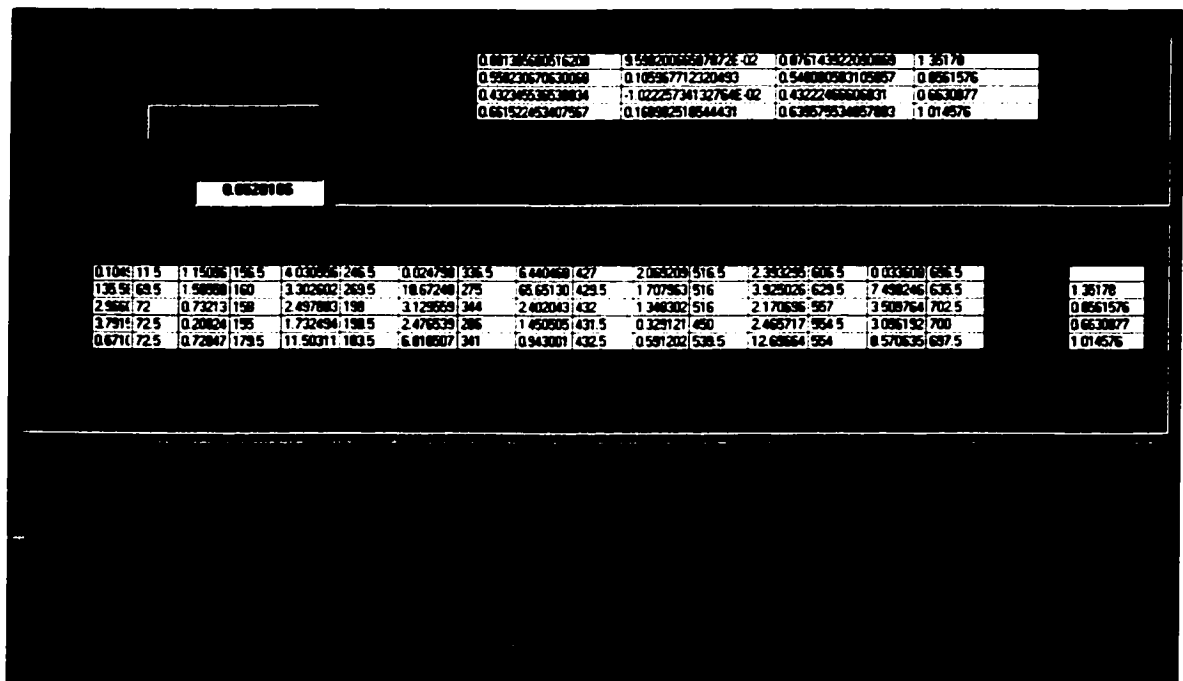


Figure 6.29 Diagnosis results from analysis of accelerometer data.



Figure 6.30 Defect reports of diagnosis results.

After analysis of the data, the transducers of choice for the detection of a deep groove are the accelerometer and the laser vibrometer. The microphone and knock sensor signatures failed to detect the deep groove in either cylinder. The fault diagnosis algorithm once again was successful in detecting the defects and their location, whereas the frequency

analysis provided no useful diagnostic information. The analysis findings for this engine are summarized in the performance matrix found in Table 6.3.

Measurement Location	NVH Signature Characteristics			
	Accelerometer	Laser Vibrometer	Microphone	Knock Sensor
Lug 1 (Cyl 1,2)	A	A	N	N/A
Lug 2 (Cyl 3,4)	N	N	N	N/A
Lug 3 (Cyl 5,6)	N	N	N	N/A
Lug 4 (Cyl 7,8)	A	A	N	N/A
Block Valley	N/A	N/A	N/A	N

N – NVH signature exhibits normal characteristics, no defect detected

A – NVH signature exhibits abnormal characteristics, defect detected

N/A – Not Applicable

Table 6.3 Performance matrix of deep groove in cylinder detection.

6.5.3 Detection of Connecting Rod Knock

The next engine encountered in the study had a number of problems related to it as discovered after a teardown analysis of the engine was conducted. Due to missing thrust bearings in the engine, there was excessive "chuck" movement of the crankshaft as well as blockage in the oil passage to one of the crankshaft pin journals that in turn led to premature wearing of the connecting rod bearings. Once the bearings were worn down, there was excessive clearance between the connecting rod and crankshaft pin journal for cylinders #1 and #5 resulting in a knocking condition between the two during certain stages of the engine cycle.

Figure 6.31 shows an averaged raw data trace from lug #1 showing distinct vibration spikes occurring at a crankshaft angle of 180° and smaller vibration spikes approximately

occurring at both 450° and 700°. The variance plot of the same data, shown in Figure 6.32, allows one to observe the positions at which the spikes are most prominent. In this case, the vibration spikes at 180° definitely stand out as the greatest contributor of engine vibration while the appearance of the smaller vibration components greatly diminishes.

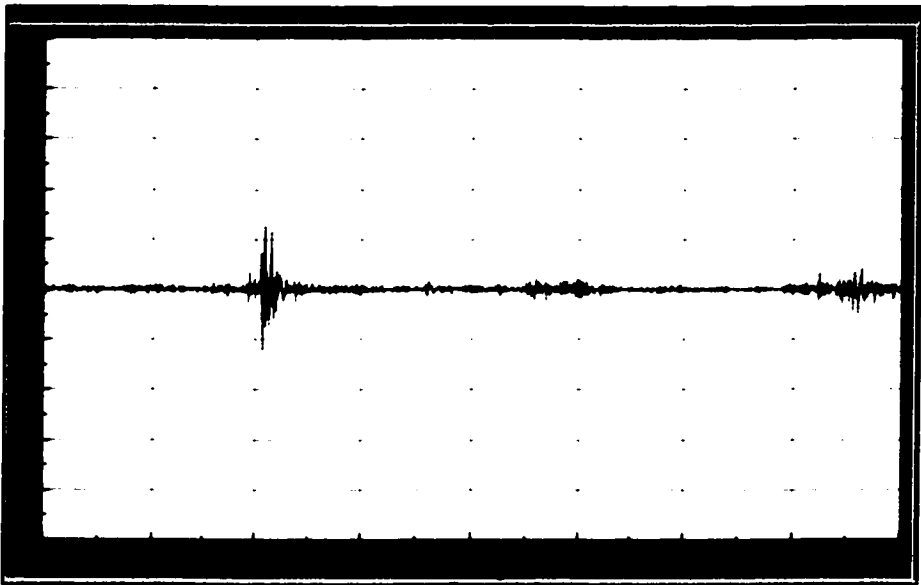


Figure 6.31 A 40-cycle average of raw data captured by an accelerometer from the #1 lug.

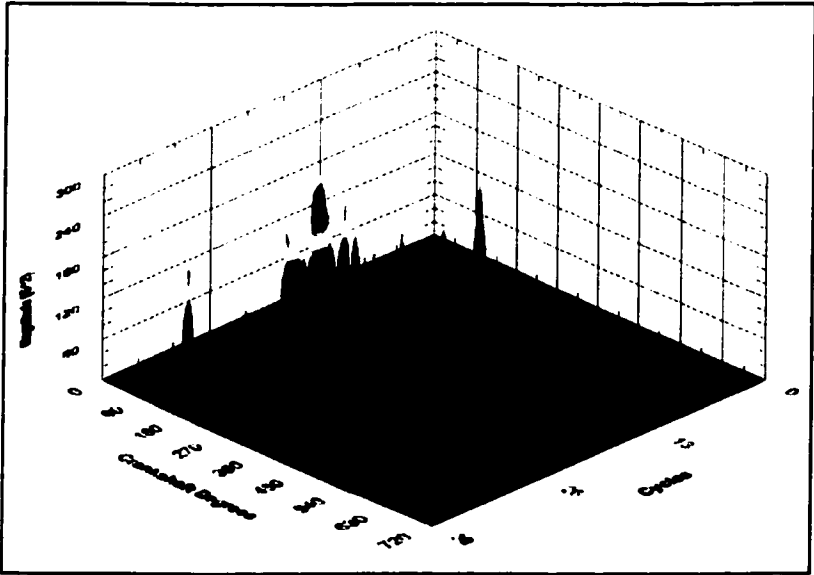


Figure 6.32 A 40-cycle waterfall plot of variance data captured by an accelerometer from the #1 lug.

Figure 6.33 and 6.34 show the averaged raw data trace and the variance waterfall plot of the accelerometer data collected from lug #3, respectively. Again, the benefit of using a variance plot is shown from its ability to decipher semi-periodic vibration components from those that normally occur from cycle to cycle.

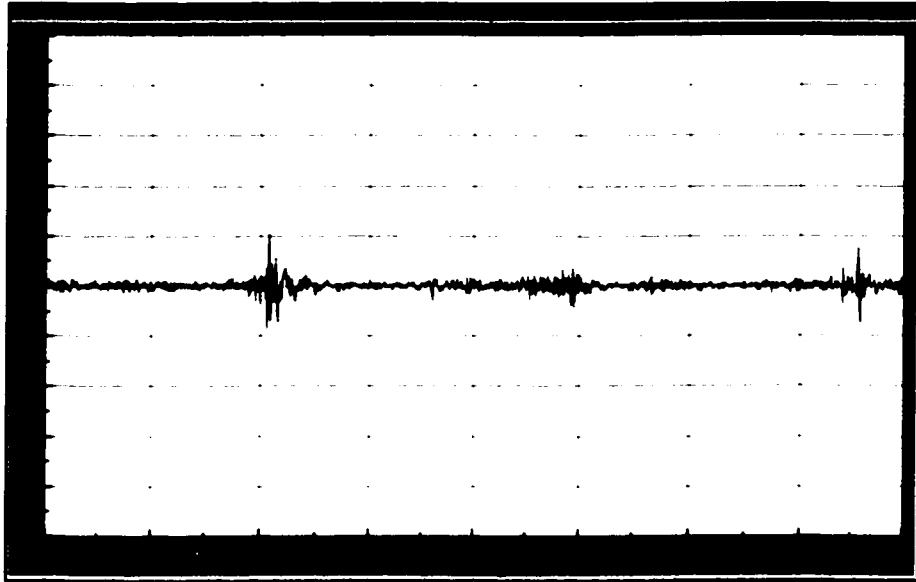


Figure 6.33 A 40-cycle average of raw data captured by an accelerometer from the #3 lug.

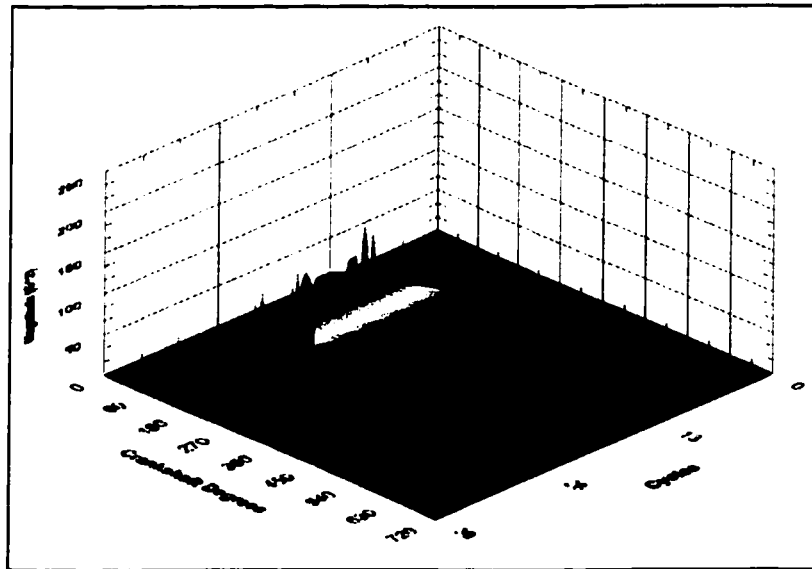


Figure 6.34 A 40-cycle waterfall plot of variance data captured by an accelerometer from the #3 lug.

Figures 6.35 and 6.36 show noise traces collected by the internally amplified microphones from the lug #1 and lug #3 areas, respectively. By comparing the signatures from the microphones and accelerometers, it can be seen that they are in agreement with one another. For this case, the microphones were able to detect the knock occurring within the engine. This is due to the nature of the defect and the severity of the knock. For the case of the non-cleanup or deep groove, a heavy mechanical knock was not occurring and was therefore, not as easily audible, but rather was detected through surface borne vibration. For this engine, collection of microphone data proved to be useful due to the severe audible knock present.

Laser vibrometer data was once again collected and analyzed. Figure 6.37 shows the averaged signature captured from lug #3 of the engine. This signature is in agreement with both the accelerometer data and the microphone data. The vibrometer has once again proven to be capable of detecting surface borne vibration through the monitoring of the surface velocity of the cylinder block.

Figure 6.38 shows the averaged raw data signal acquired from the knock sensor. The vibration components detectable by every other transducer were undetectable by the knock sensor. However, the ability of the knock sensor to detect vibration due to the piston at top-dead-center is quite good, but is of no use in the study and is therefore, not required.

Using the fault diagnosis algorithm developed for the study, defects were detected in the vicinity of lugs 1 and 3 since RMS, CR and variance levels from these locations exceeded the acceptable limits established in the study. However, due to the nature of the signatures collected, the diagnostic method only predicted the quarters of the engine that

contained the defects and not the specific cylinders. As can be seen in the fault diagnosis screen shot found in Figure 6.39 and the reports found in 6.40, the defects were suspected to be in either cylinder 1 or 2 and cylinder 5 or 6. From the teardown analysis results, the defects were linked to cylinders 1 and 5 as discussed earlier. Therefore, the algorithm successfully determined the areas of the engine containing the defects. The results from testing and analysis of this engine are shown in Table 6.4.

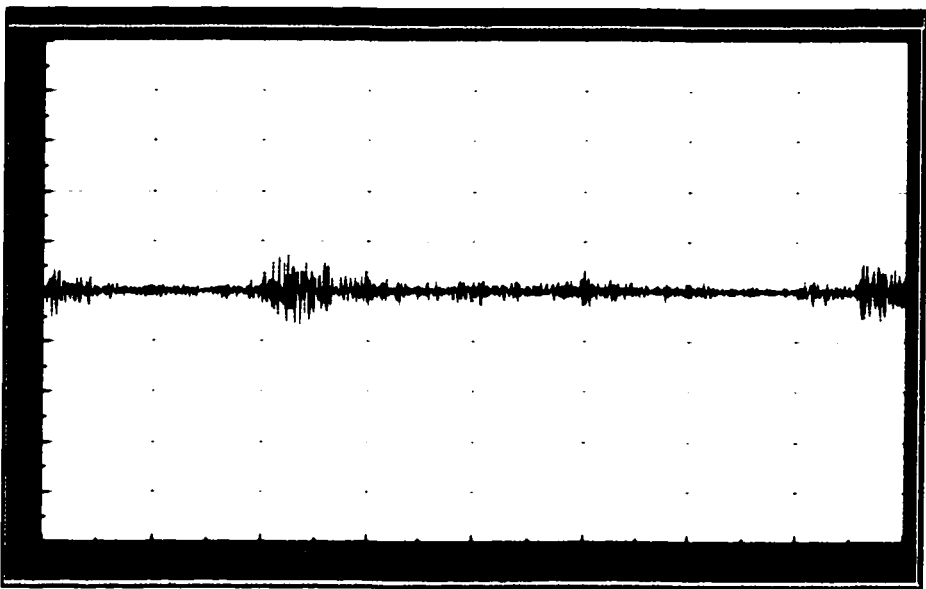


Figure 6.35 An averaged overall level of raw data captured by a microphone from the area of lug #1.

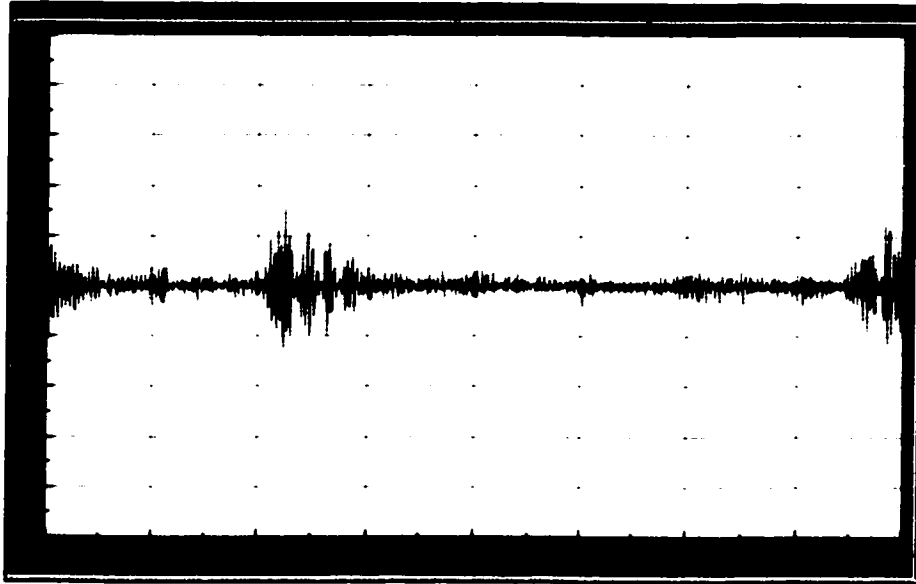


Figure 6.36 An averaged overall level of raw data captured by a microphone from the area of lug #3.

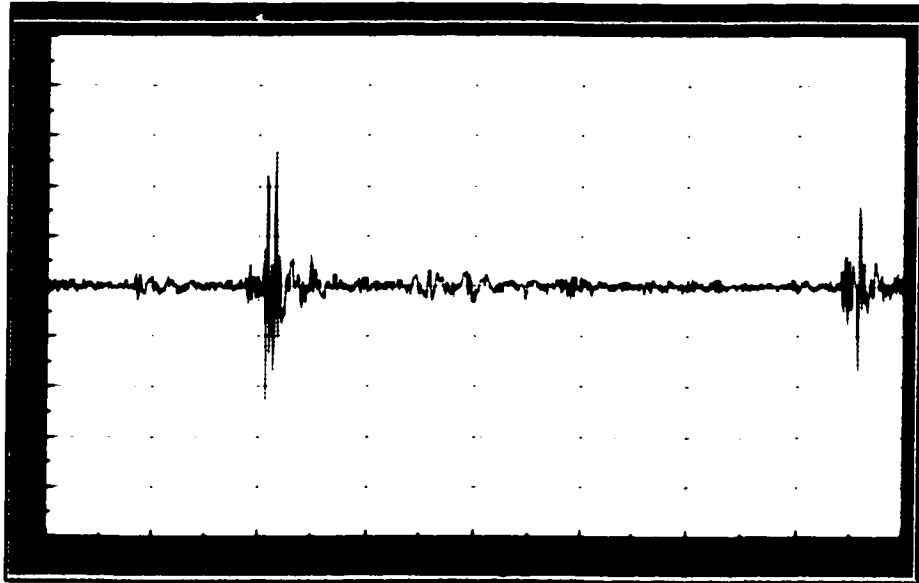


Figure 6.37 A 40-cycle average of raw data captured by the laser vibrometer from the #3 lug.

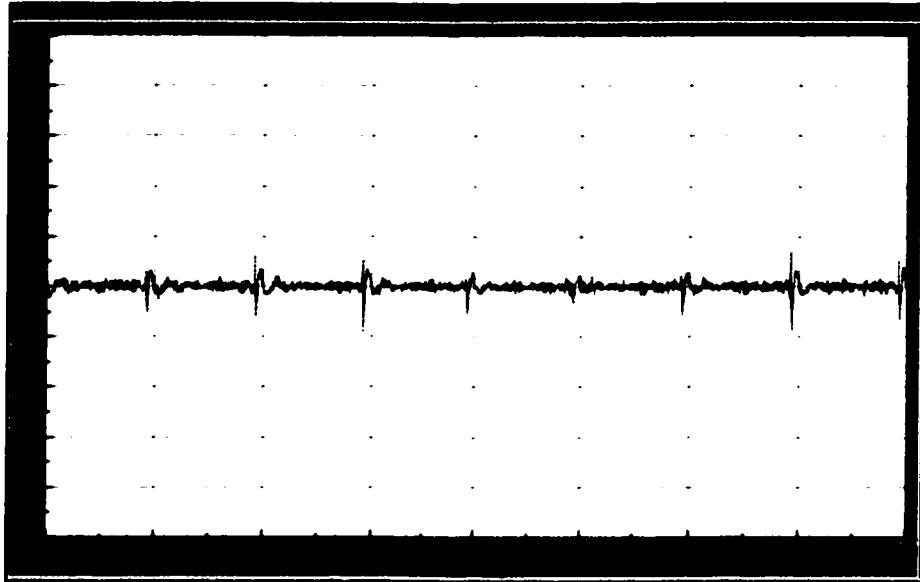


Figure 6.38 A 40-cycle average of raw data captured by the knock sensor.

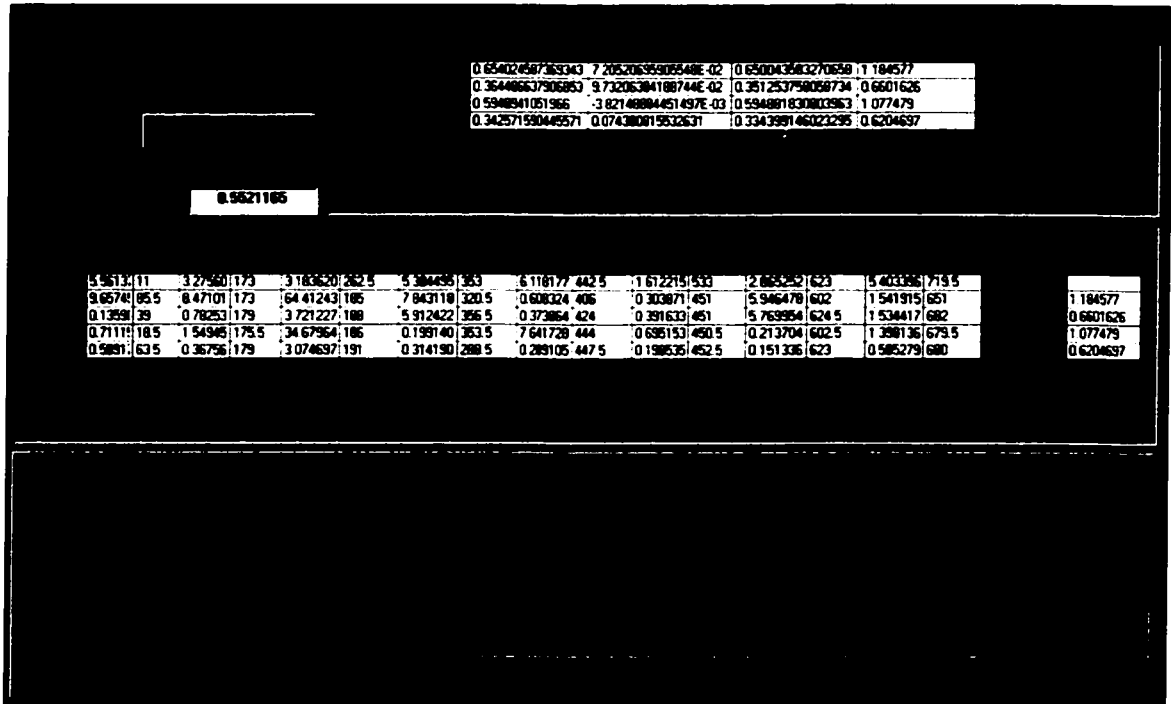


Figure 6.39 Diagnosis results from analysis of accelerometer data.

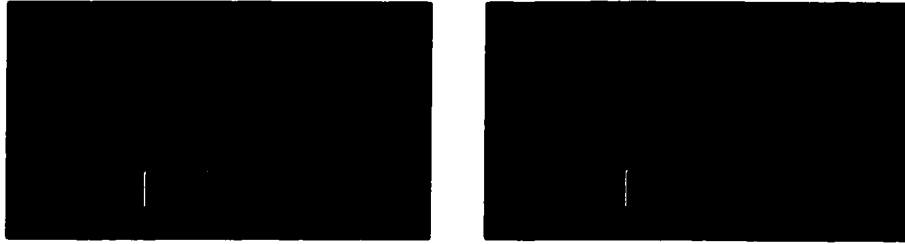


Figure 6.40 Defect reports of diagnosis results.

Measurement Location	NVH Signature Characteristics			
	Accelerometer	Laser Vibrometer	Microphone	Knock Sensor
Lug 1 (Cyl 1,2)	A	A	A	N/A
Lug 2 (Cyl 3,4)	N	N	N	N/A
Lug 3 (Cyl 5,6)	A	A	A	N/A
Lug 4 (Cyl 7,8)	N	N	N	N/A
Block Valley	N/A	N/A	N/A	N

N – NVH signature exhibits normal characteristics, no defect detected

A – NVH signature exhibits abnormal characteristics, defect detected

N/A – Not Applicable

Table 6.4 Performance matrix of connecting rod knock detection.

6.5.4 Detection of Abnormal Engine Noise

The engine under consideration in this portion of the study was reported to have an abnormal noise and was returned from a dealership for this reason. The engine was subjected to the same NVH tests as the other engines and diagnosed with the algorithm developed. Upon analysis of the data collected, there was no sign of abnormal NVH characteristics found and the algorithm was unsuccessful in identifying any irregularities concerning the variance data.

Figure 6.41 is the averaged raw data trace for the accelerometer data collected. As can be seen in the figure, there is no sign of abnormal vibration pulses present and the amplitudes are consistently low. This was the case for each measurement location on the engine.

Figure 6.42 shows the resulting auto power spectrum of the microphone data collected from the area of lug #1. When compared to the resulting spectrum from a good engine, the frequency components fall along the same orders. Therefore, based on the data analysis, there was no indication that this engine had any defective components.

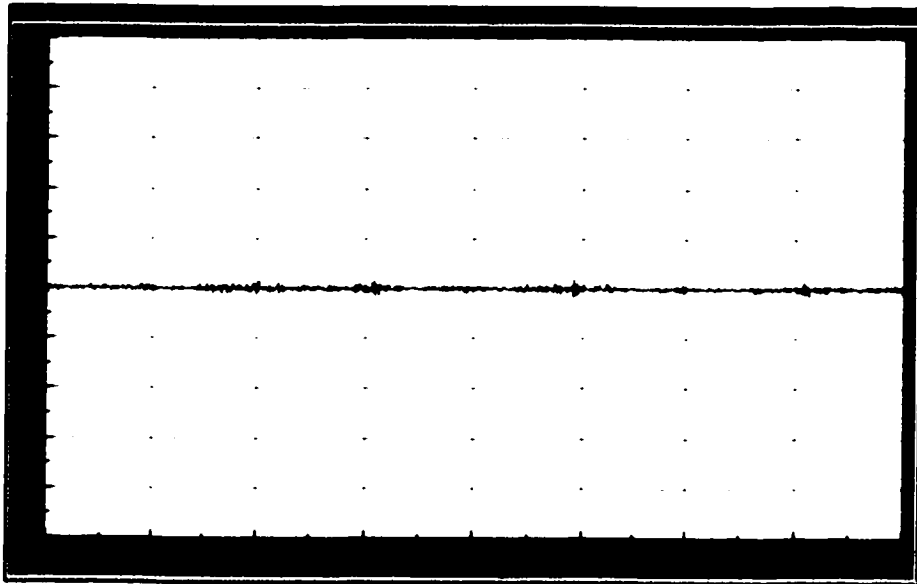


Figure 6.41 A 40-cycle average of raw data captured by an accelerometer from the #1 lug.

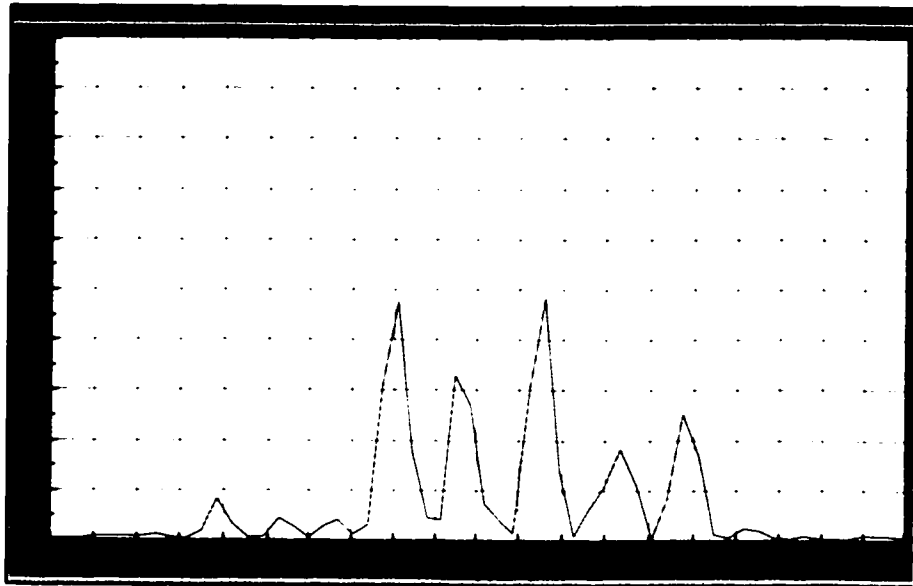


Figure 6.42 Auto-power spectrum of noise data collected from lug #1 of engine with reported noise.

Once again, the fault diagnosis algorithm was used to try and identify any defects present in the engine. As can be seen in Figure 6.43, the diagnosis found the engine to be defect-free with no suspected trouble areas. In terms of the statistical parameters calculated, all channel RMS values were much lower than the channel upper limits, however, all CR values were greater than the threshold value of 0.9. All variance amplitudes were quite low and within the acceptable limits as well. Since only 1 parameter exceeded the acceptable limits and all others were within the appropriate range, the engine was diagnosed as defect-free. Therefore, based on NVH indicators, if a defect was present in this engine, it was undetectable through these means.

A teardown was performed for this engine and all clearances and components were within the design specifications and no indications of any defects were found in the analysis. This correlates with the findings of the NVH tests conducted at cold test.

Table 6.5 provides a summary of the data collected from this engine. All measurements taken from each transducer were found to have normal NVH characteristics.

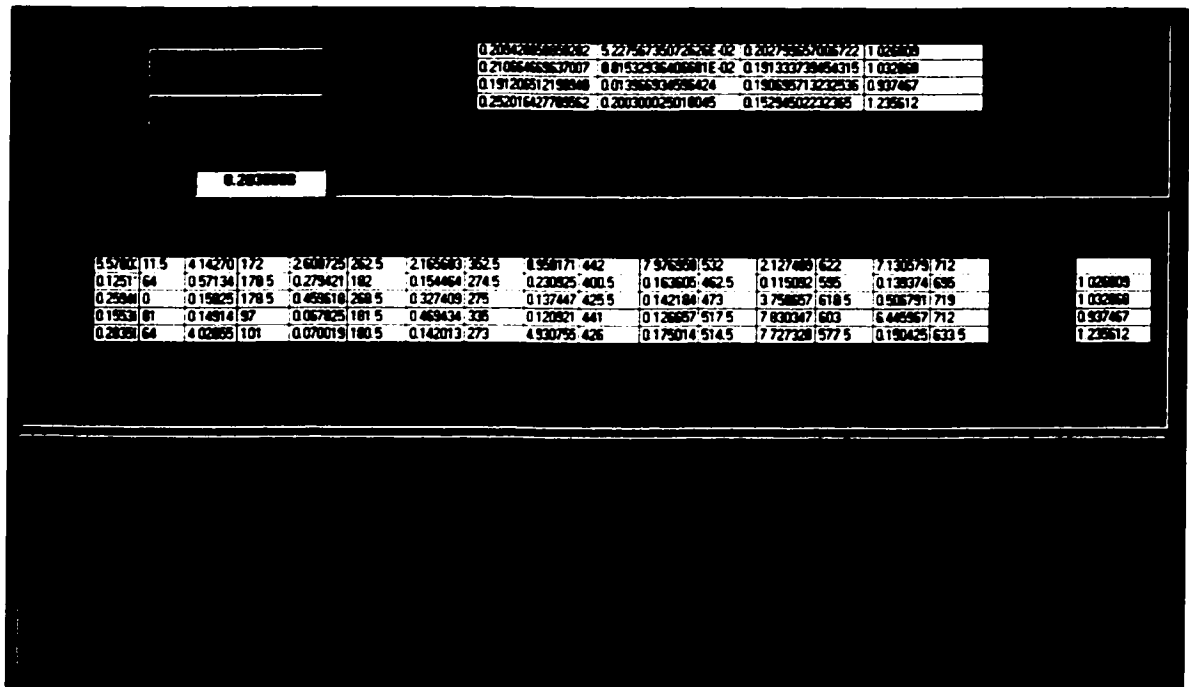


Figure 6.43 Diagnosis results from analysis of accelerometer data.

Measurement Location	NVH Signature Characteristics			
	Accelerometer	Laser Vibrometer	Microphone	Knock Sensor
Lug 1 (Cyl 1,2)	N	N	N	N/A
Lug 2 (Cyl 3,4)	N	N	N	N/A
Lug 3 (Cyl 5,6)	N	N	N	N/A
Lug 4 (Cyl 7,8)	N	N	N	N/A
Block Valley	N/A	N/A	N/A	N

N – NVH signature exhibits normal characteristics, no defect detected

A – NVH signature exhibits abnormal characteristics, defect detected

N/A – Not Applicable

Table 6.5 Performance matrix of defect detection of engine with reported abnormal noise.

6.5.5 Cold Test Fault Diagnosis Summary

The following table summarizes the ability of the transducers investigated to detect the specific defects chosen from the given measurement locations using the analysis of the NVH signatures and the developed fault diagnosis algorithm.

Defect	Transducer			
	Accelerometer	Laser Vibrometer	Microphone	Knock Sensor
Non-cleanup of cylinder #6	F	F	U	U
Deep grooves in cylinder #1 and #8	F	F	U	U
Connecting rod knock	F	F	F	U
Abnormal engine noise	U	U	U	U

F – feasible transducer for detection of noise or vibration resulting from the defect(s) specified

U – transducer unable to detect noise or vibration resulting from the defect(s) specified

Table 6.6 Overall performance matrix of engine defect detection using NVH indicators.

CHAPTER 7.

CONCLUSIONS & RECOMMENDATIONS

7.1 Conclusions

After a detailed analysis of the experimental results obtained, the following conclusions have been reached:

1. For the on-line monitoring of lower-end engine vibration, the most reliable and consistent transducers were the accelerometer and laser Doppler vibrometer. Microphones were found to yield inconsistent results and the knock sensor was unable to detect the defects investigated.
2. Optimal measurement locations for the on-line detection of lower-end engine defects were found to be the 4 locating lugs of the engine. These locations were easily accessible, had excellent vibration response characteristics and were positioned so that each lug represented a quarter of the engine (i.e. two cylinders).
3. The Cold Test station was an ideal test station to use when conducting engine condition monitoring using NVH indicators. This was due to its ability to motor the engine at an adequate speed, test each engine under consistent operating conditions and allow for additional transducers to be installed without interfering with its current setup.
4. Signature analysis of position domain averaged raw data and variance data provided an excellent indication of the condition of the engine in terms of noise

and vibration levels. In this study, frequency analysis methods provided no additional information to assist in the detection of lower-end engine defects.

As well, the use of statistical indicators such as the RMS and CR values as upper limits (threshold values) provided a consistent standard by which all measurement amplitudes were compared to in order to be classified as defect-free.

5. The fault diagnosis algorithm developed, incorporating both variance signature analysis and statistical analysis, was successful in identifying all of the known defects including the non-machined cylinder bore, deep-grooved cylinder bores and the severe connecting-rod knock. The algorithm was also successful in identifying all of the engines that were defect-free.
6. The main objective of this study has been met. Through the successful development of various in-process engine defect detection methods, the future implementation of a fully functional NVH test system, that uses these methods for engine condition monitoring, is completely feasible.

7.2 Recommendations

The following recommendations will provide possible future improvements to on-line NVH diagnostic testing used in industry.

1. Use the information and findings from this investigation to implement fully functional on-line NVH monitoring systems into applicable manufacturing and assembly plants that can use NVH parameters as indicators of component condition.

- 2. Investigate the use of innovative technology and equipment to further enhance the defect monitoring system in order to allow for the detection of more defects, not only limited to lower-end components.**
- 3. Utilize more complex analysis techniques, such as wavelet analysis, to better refine the fault diagnosis algorithm so that an in-depth analysis can be performed that may lead to a more specific identification of engine defects and their respective locations.**
- 4. Reinvestigate the use of microphones and the knock sensor on-line and attempt to develop a method by which data collected from these transducers can be used for engine fault diagnosis.**

REFERENCES

1. Antoni, J., Danier, J., El Badaoui, M., Guillet, F., "Some New Diagnostic Parameters for Reciprocating Engines", SAE Paper 1999-01-1714, 1999, 6 pages.
2. Aust, V., "In Cylinder Diagnosis by Laser Tomography", SAE Paper 981381, 1998, 12 pages.
3. Balasubramanian, M., Dong, B., Duncan, A.E., Goetchius, G.M., Gogate, S.D., "Process to Achieve NVH Goals: Subsystem Targets via Digital Prototype Simulations", SAE Paper 1999-01-1692, 1999, 15 pages.
4. Ball, A.D., Gu, F., Li, W., "The Condition Monitoring of Diesel Engines using Acoustic Measurements Part 2: Fault Detection and Diagnosis", SAE Paper 2000-01-0368, 2000, 10 pages.
5. Beidl, C.V., Rasser, M., Rust, A., "Key Steps and Methods in the Design and Development of Low Noise Engines", SAE Paper 1999-01-1745, 1999, 11 pages.
6. Beidl, C.V., Hargreaves, N.M., Stucklschwaiger, W., "NVH Considerations to Make Modern Diesel Engines an Attractive Alternative for SUV Powertrains", SAE Paper 1999-01-1772, 1999, 9 pages.
7. Bell, D.H., Bell, L.H., "Industrial Noise Control-Fundamentals and Applications: Second Edition, Revised and Expanded", Marcel Dekker, 1994, pages 37-63, 67-80, 135-165.
8. Ben-Ari, J., deBotton, G., Itzhaki, R., Sher, E., "Vibration Signature Analysis as a Fault Detection Method for SI Engines", SAE Paper 980115, 1998, 8 pages.
9. Ben-Ari, J., deBotton, G., Itzhaki, R., Sher, E., "Fault Detection in Internal Combustion Engines by the Vibration Analysis Method", SAE Paper 1999-01-1223, 1999, 9 pages.
10. Bernard, L., Loibnegger, B., Micelli, D., Rainer, G., Turino, G., "An Integrated Numerical Tool for Engine Noise and Vibration Simulation", SAE Paper 971992, 1997, 10 pages.
11. Blough, J.R., Dexter, M., Evensen, H., Van Karsen, C., "Extraction/Filtration of Transients Embedded in Stationary Signals Using Wavelets; Focus on Extraction of Frequency Response Functions", SAE Paper 1999-01-1824, 1999, 8 pages.
12. Blough, J.R., Gwaltney, G.D., "Summary and Characteristics of Rotating Machinery Digital Signal Processing Methods", SAE Paper 1999-01-2818, 1999, 16 pages.

13. Broatch, A., Desantes, J.M., Torregrosa, A.J., "Wavelet Transform applies to Combustion Noise Analysis in High-speed DI Diesel Engines", SAE Paper 2001-01-1545, 2000, 11 pages.
14. Broch, J.T., "Mechanical Vibration and Shock Measurements", Bruel & Kjaer Publication, 1984, pages 20-71.
15. Bryzik, W., Henein, N.A., Nichols, A., Taylor, C., "Dynamic Parameters for Engine Diagnostics: Effect of Sampling", SAE Paper 932411, 1993, 18 pages.
16. Cheng, Z., "Analysis of Automobile Crash Responses Using Wavelets", SAE Paper 2002-01-0183, 2002, 7 pages.
17. Clement, V., Weinstein, J., "Free Field Simulation in Anechoic Chambers", SAE Paper 2001-01-1492, 2001, 11 pages.
18. Chowdhury, S., Taguchi, G., Wu, Y., "The Mahalanobis-Taguchi System", McGraw-Hill, 2001, pages 1-22.
19. Discenzo, F.M., Loparo, A., Lou, X., Twarowski, A., Yoo, J., "A Wavelet-Based Technique for Bearing Diagnostics", US Office of Naval Research, 1998, 4 pages.
20. Duffield, T.L., "Current Sensor Applications in Engine Diagnostic Systems", SAE Paper 870292, 1987, 8 pages.
21. Durfy, J.L., "Investigation of Damping Treatments for Propeller Shaft Vibration", M.A.Sc. Thesis, University of Windsor, 2000.
22. Eovaldi, D., Stene, R.L., Westbrook, J., "Analyzing Vibrations in an IC Engine Valve Train", SAE Paper 980570, 1998, 10 pages.
23. Evenson, H.A., Gatley, W.S., Lord, H.W., "Noise Control for Engineers", Krieger Publishing Company, 1987, pages 103-118.
24. Gerges, S.N.Y., Gustavo, D.P.S., Soeiro, N.S., "Vibration Characteristics of an Engine Block by Modal Analysis and Sound Intensity Techniques", SAE Paper 973044, 1997, 7 pages.
25. Gerges, S.N.Y., Lalor, N., de Luca, J.C., "Development of a Model for Piston Slap Noise Prediction in Reciprocating Internal Combustion Engines", SAE Paper 973056, 1997, 7 pages.
26. Ghosh, B., Vora, K.C., "Vibration Due to Piston Slap and Combustion in Gasoline and Diesel Engines", SAE Paper 911060, 1991, 11 pages.

27. Goetz, T.G., Meier Jr., R.C., "Cost-Effective Engine Diagnostics for Production Engine Hot Test", SAE Paper 851564, 1985, 9 pages.
28. Greenup, J.E., Ward, S.H., Zablocki, E.G., "Noncontact Sensors for Automotive Testing", SAE Paper 860403, 1986, 11 pages.
29. Heisler, H., "Advanced Engine Technology", Society of Automotive Engineers, 1995, pages 152-178.
30. Heywood, J.B., "Internal Combustion Engine Fundamentals", McGraw-Hill, 1988, pages 9-19.
31. Hulls, L.R., Welch, J.R., "Engine Vibration Signals as an Aid to Fault Diagnosis", SAE Paper 670872, 1967, 9 pages.
32. Inman, D.J., "Engineering Vibration", Prentice-Hall, 1996, pages 60-72.
33. Iwahara, M., Sakai, T., Tanak, T., "The Optimization of Engine Vibration Reduction by Simulation Analysis", SAE Paper 962203, 1996, 9 pages.
34. Joerres, M., Jonuscheit, H., Strama, O., "NVH Testing of Engines in the Production Line", MEDAV Technical Paper, 2000, 14 pages.
35. Jonuscheit, H., "Acoustic Tests on Combustion Engines in Production", MEDAV Technical Paper, 2000, 27 pages.
36. Licht, T.R., Serridge, M., "Piezoelectric Accelerometers and Vibration Preamplifier Handbook", Bruel & Kjaer Publication, 1987, pages 12-37.
37. LMS N. America, Introduction to CADA-X Technical and Lecture Notes.
38. LMS N. America, Digital Signal Processing Technical and Lecture Notes.
39. Mercer, C., "Frequency, Hertz & Orders: An Examination of the Relationship between Frequency and Orders", www.prosig.com/signal-processing/frequencyhzorders.html, 2002, 7 pages.
40. Nefske, D.J., Sung, S.H., "Engine Vibration and Noise Reduction using a Crank-Block System Model", SAE Paper 891129, 1989, 7 pages.
41. PCB Piezotronics, "Introduction to Signal Condition for ICP & Charge Piezoelectric Sensors", www.pcb.com/tech_signal.html, 1999, 19 pages.
42. Polytec Laser Doppler Vibrometer Technical Notes.

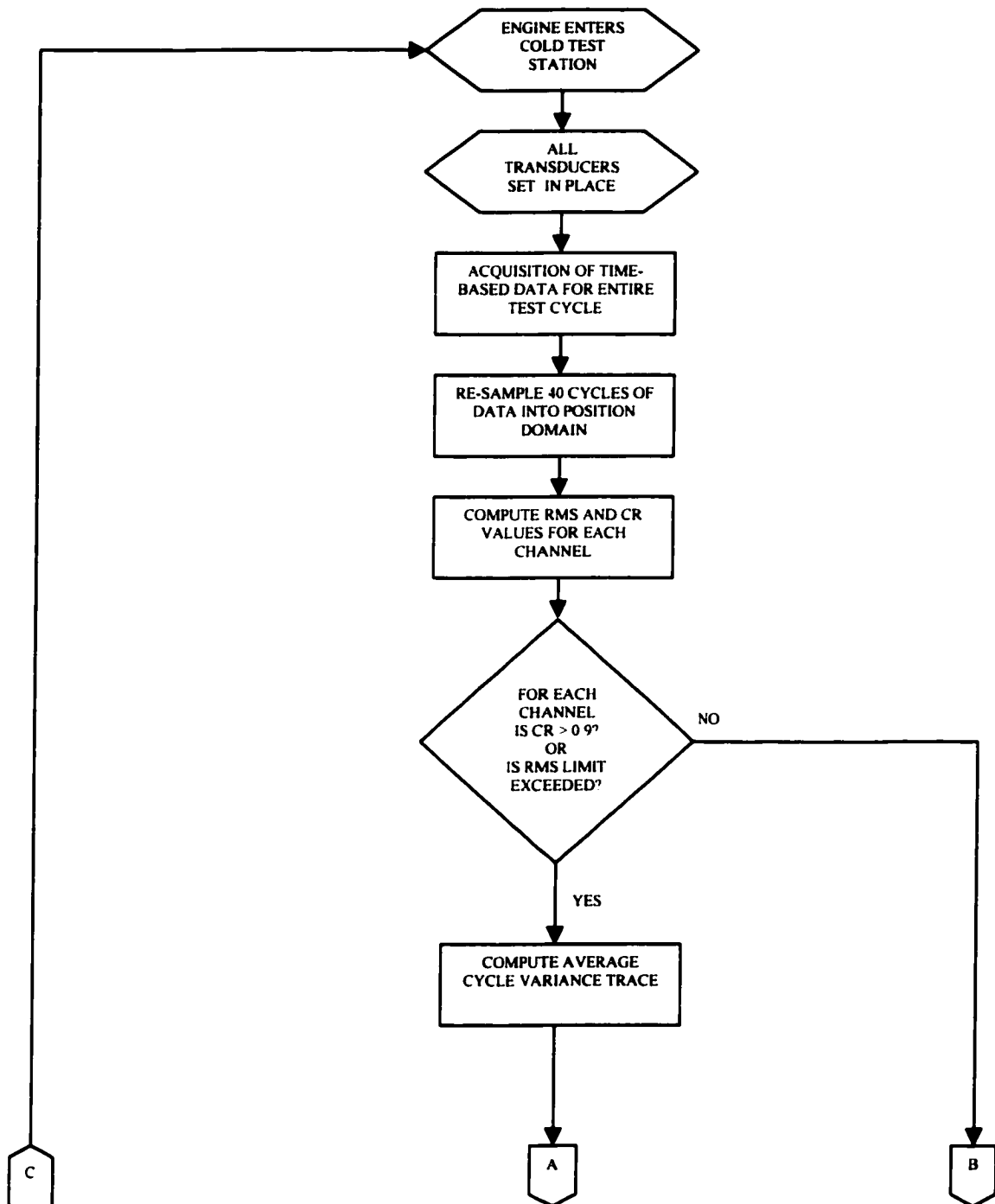
43. Randall, R.B., "Frequency Analysis", Bruel & Kjaer Publication, 1987, pages 211-226.
44. Stone, R., "Introduction to Internal Combustion Engines: Third Edition", Society of Automotive Engineers, 1999, pages 1-12.
45. Stout, J.L., "Valvetrain Unbalance and its Effects on Powertrain NVH", SAE Paper 971993, 1997, 8 pages.
46. Summers, C.E., "Measurement of Engine Vibration Phenomena", SAE Paper 250005, 1925, 32 pages.
47. Tjong, J.S-Y., "Engine Dynamic Signal Monitoring and Diagnostics", Ph.D. Dissertation, University of Windsor, 1992.
48. Tomota, E., Zhang, Z., "A New Diagnostic Method of Knocking in a Spark-Ignition Engine using the Wavelet Transform", SAE Paper 2000-01-1801, 2000, 10 pages.

APPENDICES

APPENDIX A

A. FAULT DIAGNOSIS FLOWCHART

The process by which a defect is detected at cold test is through an algorithm developed for the study that is shown in the flow chart below.



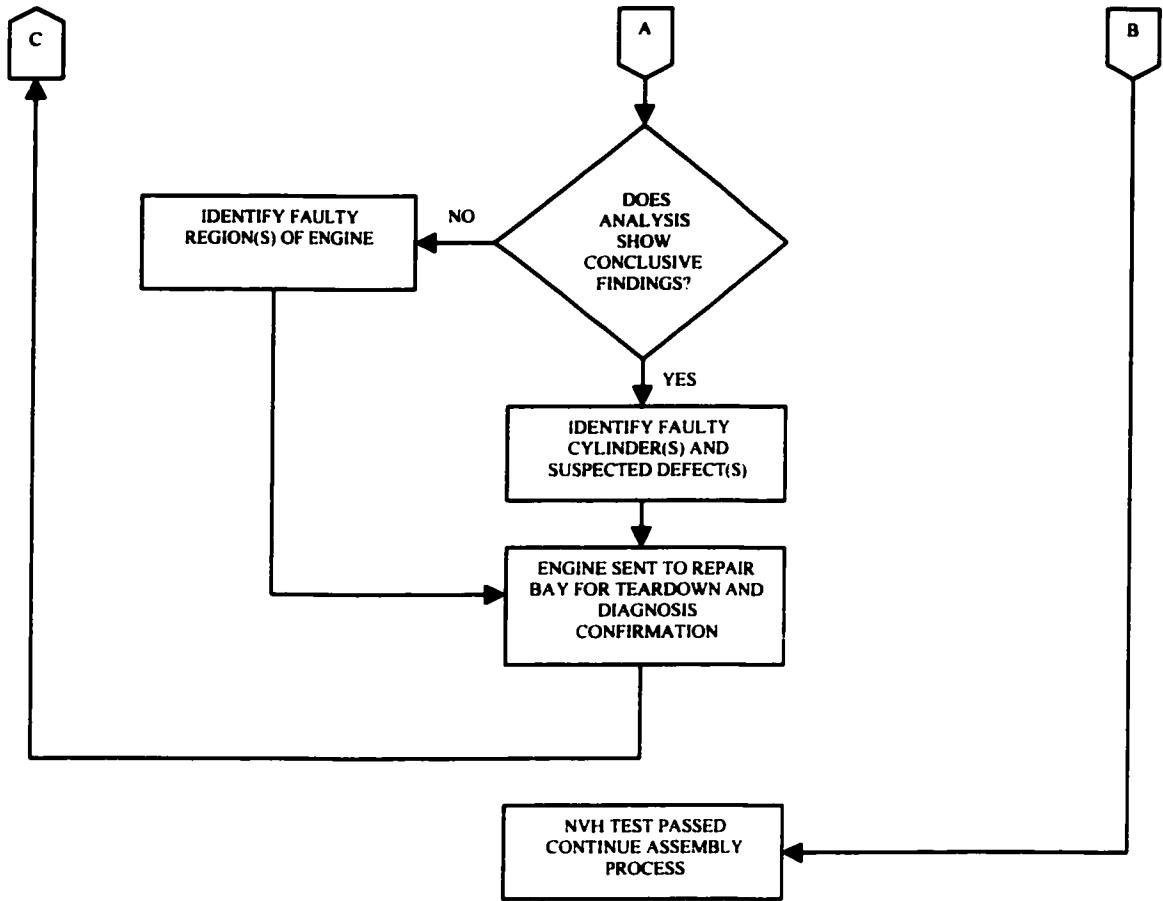


Figure A.1 Flow chart showing the fault diagnosis methodology used by the algorithm.

APPENDIX B

B. EXPERIMENTAL EQUIPMENT SPECIFICATIONS

Electro Corporation Digital-Magnetic Pickup Type 58413		
Specification	Unit	Value
Supply Voltage	V DC	5.0 to 15
Operating temperature range	°C	-40 to 107
Housing material		400 Stainless Steel
Frequency Response	kHz	380
Thread length	in, mm	0.8, 20
Overall length	in, mm	1.1, 28
Weight	grams	14

Figure B.1 Specifications for the Electro Corporation Type 58413 Digital-Magnetic Pickup.

Bruel & Kjaer Accelerometer Type 4366		
Specification	Unit	Value
Weight	grams	30
Charge Sensitivity	pC/g	47 ± 2%
	pC/ms ⁻²	5 ± 2%
Voltage Sensitivity	mV/g	40
	mV/ ms ⁻²	4
Mounted Resonance	kHz	26
Frequency Range	Hz	0.2-3500
Capacitance	pF	1167
Max. Transverse Sensitivity	%	1.7
Piezoelectric Material		PZ23
Construction		Delta Shear
Base Strain Sensitivity	ms ⁻² /με	0.006
	g/με	0.0006
Temperature Transient Sensitivity	ms ⁻² /°C	0.1
	g/°F	0.0047
Magnetic Sensitivity	ms ⁻² /T	3
	g/kgauss	0.03
Ambient Temperature Range	°C	-74 to 250
Max. Operational Shock (± Peak)	kms ⁻²	50
	g	5000
Max. Operational Continuous Sinusoidal Acceleration	kms ⁻²	20
	g	2000
(Peak)Base Material		Stainless Steel

Figure B.2 Specifications for the Bruel & Kjaer Type 4366 Charge Mode Accelerometer.

PCB Charge Amplifier Model 462A		
Specification	Unit	Value
Ranges	Units/V	50 to 100,000
Range Tolerance	± %	1.0
Transducer Sensitivity Dial	pC/V	0.1 to 1.1
Calibration Input	pC/V	1,000
Low Frequency (-3 dB)	Hz	0.16/TC
Frequency Response (± 5%)	Hz/kHz	DC to 100
Time Constant:		
Short	sec	Range x 0.001
Medium	sec	Range x 0.1
Long	sec	Range x 100
Linearity (to ± 10V)	± %	0.1
DC Drift	± mV, 8 hours	1.0
Threshold Noise	mV, rms	0.1
Noise, Input (per 1000 pF source capacitance)	pC, rms	0.1
Output Voltage	± V	10
Output Current	± mA	50
Output Impedance	ohms	2.0
Overload Recovery	μ sec	10
Temperature Range	°F, °C	+30 to +130, -1.11 to +54.4
Power Required (50 to 400 Hz)	V	105 to 125
Size (h x w x d)	in, mm	5.0 x 2.0 x 10.50, 127 x 50.8 x 266.7
Weight	lb, kg	4, 1.814
Connectors, All	type	Off Ground BNC Jack

Figure B.3 Specifications for the PCB Model 462A Charge Amplifier.

Bruel & Kjaer Calibration Exciter Type 4294		
Specification	Unit	Value
Frequency	Hz	159.2
Acceleration	ms ⁻² (rms)	10
Velocity	mms ⁻¹ (rms)	10
Displacement	μm (rms)	10
Transverse Amplitude	% of amplitude	<5
Signal Duration	sec	103
Maximum Load	grams	70
Power Source (battery)	V	9
Dimensions (l x D)	in, mm	6.1 x 2.05, 155 x 52
Weight	grams	500

Figure B.4 Specifications for the Bruel & Kjaer Type 4294 Calibration Exciter.

PCB Accelerometer Model 359B15		
Specification	Unit	Value
Amplifier		ICP
Sensitivity ($\pm 10\%$)	mV/g	10
Measurement Range	g (peak)	± 500
Frequency Range ($\pm 5\%$)	Hz	1 to 10000
Resonant Frequency	kHz	>70
Broadband Resolution	g rms	0.005
Non-Linearity	%	<1
Transverse Sensitivity	%	<5
Overload Limit (Shock)	g (peak)	± 10000
Temperature Range (Operating)	$^{\circ}\text{C}$	-54 to 121
Base Strain Sensitivity	g/ $\mu\epsilon$	<0.002
Excitation Voltage	V DC	18 to 30
Constant Current Excitation	mA	2 to 20 mA
Output Impedance	ohms	<100
Output Bias Voltage	V DC	8 to 12
Discharge Time Constant	sec	0.5 to 2.0
Settling Time	sec	<5
Size (D x h)	mm	7.9 x 10.9
Weight	grams	2.0
Housing Material		Titanium
Sensing Element		Quartz
Sensing Geometry		Shear

Figure B.5 Specifications for the PCB Model 359B15 Accelerometer.

PCB Signal Conditioner Model 480E09		
Specification	Unit	Value
Channels		1
Excitation Voltage	V DC	27
Constant Current Excitation	MA	2
Time Constant	Sec	11
Low Frequency Response (-5%)	Hz	0.15
High Frequency Response (-5%)	Hz	100 000
Voltage Gain		x1, x10, x100
Noise Broadband (gain x 100) -1 Hz to 10 kHz	μV	430
Output Range	V	± 10
Power Required	V/mA	18 to 28 / 8
Input/Output Connectors		BNC
Dimensions (l x w x h)	mm	73.7 x 38.1 x 101.6
Weight	kg	0.34
Temperature Range	$^{\circ}\text{F}$, $^{\circ}\text{C}$	32 to +120, 0 to 50

Figure B.6 Specifications for the PCB Model 480E09 Signal Conditioner.

Polytec Laser Doppler Vibrometer Model IVS 200		
Specification	Unit	Value
Supply Voltage	V DC	11 to 14.5
Current consumption	A	1
Protection rating		IP64
Operating temperature	°C	+5 to +40
Storage temperature	°C	+5 to +60
Relative humidity (max)	%	80
Output Swing	V	± 4
Output Impedance	Ohms	50
Min. load resistance	Kohms	10
DC Offset (max)	mV	± 10
Spurious free dynamic range	dB	>80
Harmonic Distortions	% THD	<1
Measurement Range (scaling factor)	(mm/s)/V	25
Full scale (peak to peak)	mm/s	200
Resolution	µm/s	1
Bandwidth (-3 dB)	Hz	0.5 to 25000
Maximum acceleration	G	1600
Amplitude frequency response	Hz	2 to 20000

Figure B.7 Specifications for the Polytec Model IVS 200 Laser Doppler Vibrometer.

TMS Microphone Type 130C10		
Specification	Unit	Value
Response		Free-field
Amplifier		ICP
Nominal Sensitivity	mV/Pa	25
Frequency Range	Hz	10 to 15000 Hz
Noise Floor	dB SPL	15
Linearity	dB SPL	128
Saturation Point	dB SPL	132
Directivity		Omnidirectional
Temperature Range	°C	-20 to 65

Figure B.8 Specifications for the TMS Type 130C10 Microphone.

Bosch Knock Sensor		
Specification	Unit	Value
Sensitivity	mV/g	30
Capacitance	pF	1240
Maximum Operating Frequency	Hz	18000
Impedance	Ohms	4.9

Figure B.9 Specifications for the Bosch Knock Sensor.

APPENDIX C

C. MAHALANOBIS DISTANCE METHOD

The Mahalanobis Distance method involves performing many matrix manipulations with a set of data as shown below. In this case, there were 30 test engines with the RMS values from each of the 4 transducer locations representing the characteristics. Table C.1 shows the matrix of RMS values as was calculated from the measurements of the "good" engines. In order for the data to be compared on the same scale, it was standardized using the statistics relationship shown below. The resulting standardized matrix is found in Table C.2.

$$Z_{ij} = \frac{x_{ij} - \mu_j}{\sigma_j} \quad (C.1)$$

where μ is the column mean and σ is the column standard deviation.

0.45	0.35	0.34	0.31
0.44	0.34	0.35	0.29
0.44	0.34	0.32	0.29
0.42	0.35	0.32	0.28
0.36	0.36	0.33	0.24
0.35	0.35	0.32	0.23
0.35	0.34	0.32	0.22
0.37	0.33	0.32	0.23
0.45	0.36	0.35	0.31
0.45	0.38	0.35	0.30
0.44	0.36	0.34	0.29
0.51	0.39	0.33	0.35
0.50	0.40	0.33	0.35
0.50	0.39	0.32	0.35
0.49	0.39	0.31	0.35
0.49	0.39	0.33	0.35
0.41	0.38	0.35	0.30
0.42	0.39	0.33	0.30
0.41	0.37	0.34	0.29
0.46	0.39	0.33	0.32
0.41	0.34	0.35	0.27
0.41	0.36	0.37	0.28
0.36	0.35	0.36	0.24
0.42	0.39	0.34	0.29
0.41	0.39	0.32	0.28
0.41	0.36	0.31	0.27
0.41	0.36	0.31	0.26
0.40	0.34	0.31	0.26
0.36	0.36	0.36	0.24
0.39	0.35	0.34	0.27

Table C.1 Original matrix of RMS values.

0.60	-0.73	0.50	0.53
0.28	-1.14	0.94	0.21
0.28	-1.04	-1.01	-0.07
-0.02	-0.73	-1.01	-0.09
-1.45	-0.07	-0.32	-1.21
-1.51	-0.94	-0.70	-1.61
-1.62	-1.35	-0.82	-1.74
-1.21	-1.55	-0.89	-1.58
0.62	-0.12	1.01	0.61
0.58	0.55	1.01	0.42
0.41	-0.32	0.44	0.02
1.79	1.32	-0.00	1.62
1.73	1.73	-0.38	1.68
1.67	1.22	-0.51	1.60
1.52	1.32	-1.07	1.60
1.54	1.27	-0.38	1.62
-0.19	0.55	1.20	0.26
-0.06	1.27	-0.38	0.26
-0.23	0.04	0.50	0.18
0.68	1.27	-0.38	0.93
-0.21	-1.40	0.88	-0.35
-0.38	-0.17	2.14	-0.19
-1.26	-0.73	1.76	-1.16
0.00	1.22	0.63	0.07
-0.23	1.06	-0.57	-0.27
-0.36	-0.17	-1.39	-0.35
-0.26	-0.32	-1.52	-0.57
-0.45	-1.09	-1.45	-0.76
-1.43	-0.22	1.51	-1.18
-0.81	-0.73	0.25	-0.54

Table C.2 Standardized matrix [Z].

The next step in the process is to find the correlation matrix [R] from the standardized matrix [Z]. The correlation coefficient of each pair of characteristics can be calculated using the following equation:

$$r_{ij} = \frac{(\sum x_{it} \times x_{jt})}{n} \quad (C.2)$$

where x_{it} and x_{jt} are the standardized values at the given indices and n is the number of observations (i.e. 30).

From these results, their correlation matrix [R] is constructed and should have dimensions of $k \times k$, where k is the number of characteristics (i.e. 4). The matrix is shown below.

1.00	0.66	-0.09	0.98
0.66	1.00	-0.02	0.75
-0.09	-0.02	1.00	0.00
0.98	0.75	0.00	1.00

Table C.3 Correlation matrix [R].

From the correlation matrix, its inverse matrix, denoted by [A] can be constructed and is shown below.

31.97	4.93	3.06	-34.85
4.93	3.03	0.52	-7.06
3.06	0.52	1.29	-3.38
-34.85	-7.06	-3.38	40.25

Table C.4 Inverse of the correlation matrix [A].

The next step in the process is to find the product matrix of the standardized matrix [Z] and the correlation inverse [A]. The resulting matrix is shown below.

-1.33	-2.73	0.32	3.87
-1.05	-3.05	0.78	3.51
0.92	-2.25	-0.98	0.78
-4.32	-2.23	-1.46	5.78
-5.48	1.04	-0.80	3.36
1.00	0.73	-0.58	-3.13
-0.16	-0.16	-0.84	-1.47
6.01	0.05	-0.33	-7.48
1.12	-1.07	1.09	0.31
9.56	2.06	1.93	-10.44
12.05	1.12	1.58	-12.56
7.21	1.35	0.69	-6.41
4.16	1.69	0.04	-3.64
2.00	0.33	-0.32	-0.60
-4.01	-0.39	-1.46	5.80
-2.39	-0.27	-0.61	4.15
-8.82	-0.50	0.37	9.23
-6.03	1.48	-0.90	5.03
-12.04	-2.05	-0.66	13.45
-5.44	0.44	-0.88	5.91
1.37	-2.31	0.96	0.03
0.24	0.09	2.17	-0.50
1.88	0.68	1.96	-3.50
5.38	3.49	1.20	-7.78
5.56	3.70	0.03	-8.46
-4.30	-0.51	-1.80	4.22
5.42	0.99	-0.99	-6.59
2.22	-0.92	-1.27	-2.22
-0.89	1.45	1.46	-1.40
-9.85	-2.25	-0.71	10.74

Table C.5 Standardized matrix [Z] multiplied by inverse of the correlation matrix [A].

The next matrix manipulation involves multiplying the above matrix with the transpose of the standardized matrix and dividing each matrix coefficient by the number of characteristics (i.e. 4). The resulting matrix has dimensions of 30 x 30 in this case. Due to the large size of this matrix, it will be omitted from the report.

The importance of this matrix is that the diagonal coefficients represent the Mahalanobis Distance for each observation (engine). The diagonal coefficients are shown in Table C.6. According to Mahalanobis' Law, if all of the engines are defect-free, the average of

the MD values should be approximately equal to 1. In the case of this study, the average of the MD values is equal to 0.967, which is extremely close to 1. Moreover, the MD value for each engine was close to 1, indicating that all of the engines had similar characteristics. As a result, these engines were deemed to be defect-free and thus, belonged to the "good" group of engines. These engines were then used to establish appropriate NVH measurement baselines that were used in the study.

1	0.85
2	1.16
3	0.89
4	0.67
5	1.02
6	0.81
7	0.93
8	1.19
9	0.53
10	1.05
11	1.25
12	1.07
13	1.00
14	0.74
15	1.06
16	0.74
17	1.07
18	0.98
19	1.21
20	0.66
21	0.94
22	1.16
23	1.16
24	1.11
25	1.23
26	0.66
27	0.89
28	0.88
29	1.21
30	0.91

Table C.6 Mahalanobis Distances calculated for each of the 30 test engines.

VITA AUCTORIS

Eric R. Leitzinger was born on March 23, 1977 in Windsor, Ontario. He graduated from Holy Names High School in 1996. He attended the University of Windsor, Ontario where he received the degree of Bachelor of Applied Science in Mechanical Engineering with Automotive Option in 2000. Upon completion of his undergraduate degree, Eric became a member of the Powertrain Research and Development Group at the Ford Essex Engine Plant. He is currently a candidate for the degree of Master's of Applied Science in Mechanical Engineering at the University of Windsor and is expected to fulfill his requirements for this degree in September of 2002.